DARK-BRIGHT SOLITONS IN BOSE-EINSTEIN CONDENSATES: DYNAMICS, SCATTERING, AND OSCILLATION

by

Majed O. D. Alotaibi

A thesis submitted to the Faculty and the Board of Trustees of the Colorado School of Mines in partial fulfillment of the requirements for the degree of Doctor of Philosophy (Physical Science).

Golden, Colorado

Date _____

Signed: _____
Majed O. D. Alotaibi

Signed: _____
Prof. Lincoln Carr
Thesis Advisor

Golden, Colorado

Date _____

Signed: _____
Prof. Uwe Greife
Professor and Head
Department of Physics

ABSTRACT

In this thesis, we have studied the behavior of two-component dark-bright solitons in multicomponent Bose-Einstein condensates (BECs) analytically and numerically in different situations. We utilized various analytical methods including the variational method and perturbation theory. By imprinting a linear phase on the bright component only, we were able to impart a velocity relative to the dark component and thereby we obtain an internal oscillation between the two components. We find that there are two modes of the oscillation of the dark-bright soliton. The first one is the famous Goldstone mode. This mode represents a moving dark-bright soliton without internal oscillation and is related to the continuous translational symmetry of the underlying equations of motion in the uniform potential. The second mode is the oscillation of the two components relative to each other. We compared the results obtained from the variational method with numerical simulations and found that the oscillation frequency range is 90 to 405 Hz and therefore observable in multicomponent Bose-Einstein condensate experiments. Also, we studied the binding energy and found a critical value for the breakup of the dark-bright soliton. Building on these results, we have studied another situation where we have the dark-bright soliton oscillate in a harmonic potential. We found for weak trapping the internal modes are nearly independent of center of mass motion of the dark-bright soliton. In contrast, in tighter traps the internal modes couple strongly to the center of mass motion, showing that for dark-bright solitons in a harmonic potential the center of mass and relative degrees of freedom are not independent. We found this result is robust against noise in the initial condition and should, therefore, be experimentally observable. In addition, we have studied the interaction between a moving dark-bright soliton in a uniform background with internal oscillation and a fixed impurity, modeled by a delta function potential. The interaction excites different modes in the system. Our analytical model capture two of these modes: the relative oscillation between the two

components, as well as the in-sync oscillation of the widths. The numerical simulations allow further internal modes like out-of-sync oscillations of the soliton widths and even shape deformations of various kinds. We identify regions in parameter space for the transmission, reflection and inelastic scattering of the dark-bright soliton by the potential barrier. We have studied the velocity of dark-bright solitons described with an ansatz that uses one center of mass variable to represent the position of the two components. We found for a dark-bright soliton the maximum velocity is limited by the relative number of atoms in the bright component as compared to the size of the hole or density notch created by the dark component. Above this critical velocity the dark-bright soliton develops internal oscillations, and eventually unbinds and breaks apart.

TABLE OF CONTENTS

LIST OF FIGURES

LIST OF TABLES

LIST OF SYMBOLS

Wave function ..... ψ

Planck's constant ..... $\hbar$

Number of atoms in the system ..... N

s-wave scattering length ..... a_s

Healing length ..... ξ

Transverse trapping frequency ..... ω_z

Inter-atomic interaction ..... g

Intra-atomic interaction ..... g_1, g_2

Kinetic energy ..... E_k

Intracomponent mean-field energy ..... E_{MF}

Speed of sound in a Bose-Einstein condensate ..... c_s

Delta function ..... $\delta(x)$

Rubidium–87 ..... $^{87}\mathrm{Rb}$

Atomic mass ..... m

LIST OF ABBREVIATIONS

Bose–Einstein condensates ..... BECs

Nonlinear Schrödinger equation ..... NLSE

Gross-Pitaevskii equation ..... GPE

Ordinary differential equations ..... ODE

Partial differential equations ..... PDE

Korteweg and deVries ..... KdV

Inverse scattering transform ..... IST

Imaginary time propagation ..... ITP

Dark-bright soliton ..... DB soliton

Equations of motion ..... EOM

ACKNOWLEDGMENTS

First I would like to thank my advisor Lincoln Carr for his passion and enthusiasm for research and his dedication to his students. I appreciate the high level of support that Lincoln shows toward me in my time in the Colorado School of Mines. Also, I'm very grateful for Lincoln's help and care for my family life over the progress of my degree.

I would also like to thank my committee, Paul Martin, Jim Bernard, Timothy Ohno and David Wood for their encouragement and their advice. In addition, I thank the faculty of the Physics Department at the Colorado School of Mines for their tireless efforts and dedication to students like myself.

I'm thankful for all the members of the Carr Theoretical Physics Research Group for their help and support through my time in CSM. I would like to send a special thank-you to Diego Alcala, Justin Anderson, Daniel Jaschke, Gavriil Shchedrin for all the support and help.

Most importantly, I am grateful for and would not be here without my family. My parents have continually encouraged me throughout all the hard times. I would not be where I am today if not for their sacrifice and hard work. Finally, I thank my wife for enduring the stresses associated with graduate school and my daughter for being in my life.

I dedicate this thesis

to my mother and father,

my wife and my daughter,

my brothers, and my sister.

CHAPTER 1

HISTORY AND FUNDAMENTAL CONCEPTS OF SOLITONS IN BOSE-EINSTEIN CONDENSATES

A soliton is a self-supporting solitary wave that propagates without changing its shape or velocity. It is also a solution to nonlinear partial differential equations (PDEs). Waves that propagate according to linear PDEs encounter a known effect called dispersion of the wave packets which cause a spreading of the wave. A wave packet is an envelope of different waves with different frequencies that form a unit. Each component of the wave packet propagates with different velocity due to the fact that the wave velocity depends on the frequency. Therefore, we see the dispersion effect in linear systems. In nonlinear systems, other effects can reverse the spread of the wave packets and therefore produce a cancelation of this action. The balance between the nonlinear and dispersive effects produce a solitary wave. In the literature, the term soliton is reserved for solitary waves that survive collisions. That is, a solitary wave emerges without changing shape or velocity after interacting with another solitary wave. Also, a soliton is known to be a nonlinear wave, that is, a solution of nonlinear PDEs.

Nonlinear waves have been a fascinating subject since the discovery of the solitary wave in 1834 by John Scott Russell in the Union Canal in Scotland where he observed the great wave of translation as he called it [1]. The discovery is described here in his own words [2]:

I was observing the motion of a boat which was rapidly drawn along a narrow channel by a pair of horses, when the boat suddenly stopped, not so the mass of water in the channel which it had put in motion; it accumulated round the prow of the vessel in a state of violent agitation, then suddenly leaving it behind, rolled forward with great velocity, assuming the form of a large solitary elevation, a rounded, smooth and well-defined heap of water, which

continued its course along the channel apparently without change of form or diminution of speed. I followed it on horseback and overtook it still rolling on at the rate of some eight or nine miles an hour, preserving its figure some thirty feet long and a foot to a foot and a half in height. Its height gradually diminished and after a chase of one or two miles, I lost it in the windings of the channel. Such, in August 1834, was my first chance interview with that singular and beautiful phenomenon.

Russell's works on solitary waves opened the doors for more theoretical investigations of nonlinear waves. Essential studies conducted by Stokes, Boussinesq, and Korteweg and deVries (KdV) shed light on the mathematical models describing solitary waves [1]. The well known KdV equation illustrates the propagation of solitary waves in shallow water surfaces. It is considered to be the first soliton equation by experts in the field of nonlinear waves [2]. It is also an integrable equation, a criterion that implies a system has an infinite number of degrees of freedom and therefore it exhibits an infinite number of conserved quantities such as energy, momentum, number of particles, etc. This equation was the starting point for renewed interest in the theory of nonlinear waves in the twentieth century when Enrico Fermi, John Pasta, Stanislaw Ulam, and Mary Tsingou conducted computer simulations of a vibrating string that included a nonlinear term which is well known as the FPUT experiment [2]. In this experiment an initial mode of vibration on one end of the string did not fade away after many iterations, a process known as thermalization. Instead the system exhibits a quasi-periodic behavior. The continuum limit of the mathematical model used in FPUT experiment is the KdV equation. Another milestone in the theory of solitons is when Kruskal and Zabusky revisited the FPUT experiment and performed a numerical simulation for collisions of two solitary waves. The result was that the two solitons were not affected by the collision and they only gained a phase shift. Kruskal and Zabusky invented the word *soliton* to describe these solitary waves [2]. A few years later Gardner, Greene, Kruskal, and Miura discovered the Inverse scattering transform (IST) method to obtain a solution

to the KdV equation. This technique also used to find soliton solutions to the nonlinear Schrodinger equation (NLSE) by Zakharov and Shabat [2].

The NLSE has been the focus of many theoretical and experimental studies since Zakharov and Shabat published their work in 1972. Although the NLSE is a nonlinear variation of the Schrodinger equation, it is a classical field equation that is used to describe the evolution of a classical complex wave function [1]. It had been studied in the context of optical systems at that time to explain the propagation of light in nonlinear optical fibers and other optical systems. Hasegawa suggested, in 1973, that the realization of a solitary wave is possible in fiber optics when a pulse-narrowing nonlinear effect balances the effect of dispersive spreading of the light pulse [3]. His work led to the first experimental observation of solitons in optical fibers in 1980 by Mollenhauer, Stolen, and Gordon [4]. Another important discovery in the story of the theory of solitons was in 1988 when Weiner and Heritage demonstrated for the first time the creation of dark solitons in optical fibers [5].

In the second half of the nineties, solitary waves entered a new era with the discovery of the Bose–Einstein condensate (BEC). Since in this thesis, we work mainly with the NLSE, in the context of BEC we use the name Gross–Pitaevskii equation (GPE), which is the NLSE when we add a potential trap. To study the interaction between two types of soliton solutions in a two–component BEC it is useful to introduce the concept of BEC first before illustrating significant discoveries in soliton theory in BEC systems.

BEC was predicted theoretically by Satyendra Nath Bose and Albert Einstein in 1925 and created experimentally by Eric Cornell, Carl Wieman, Randy Hulet and Wolfgang Ketterle in 1995 [6]. It is a state of matter made of a dilute gas of bosons cooled to a temperature that is very close to absolute zero. A significant fraction of bosons at this temperature occupy the lowest single-particle state (ground state of the system). Consequently, microscopic quantum phenomena become manifest. These gases are typically 10-100 μm in size with a number of atoms ranging from 10^3 to 10^9 and the temperature range is 1 to 100nK. Usually the BEC experiments are conducted with ^{87}Rb and ^{23}Na atoms, in addition to many other atomic

species.

The development of laser cooling and magnetic trapping allowed for the creation of the BEC. Laser cooling, developed in the 1980s, used a well-known phenomenon called the Doppler effect [7] where a moving atom toward a light source (i.e., a laser beam) experiences a change in the frequency of the light beam and thereby absorbs a photon which places the atom in an excited state. When the atom releases the photon, it usually does so in the direction of the light beam: it loses momentum in the direction of the beam, and therefore slows down. Applying laser beams in the three perpendicular directions will slow down the velocity of the atoms in all direction and consequently cools the gas significantly. This method alone is not enough to cool down the gas below the critical temperature needed to observe the BEC.

An evaporation technique is used to allow a small fraction of the excited atoms to escape the trap in order to form a condensate with a very low temperature. In the early days of the creation of BEC, harmonic potentials were used to hold the condensate gases but nowadays different trap shapes can be designed to sustain and study trap BECs [6]. For example, box-like or double-well traps are regularly formulated to explore various features of the condensate gases. As mentioned above, magnetic traps are one way to hold the condensates [6]. There are other types of traps that can be used to hold the condensate like optical traps. The advantage of optical traps is that we can study the particle spin since in magnetic traps the spin is locked up due to the interaction with the magnetic field of the trap. This advancement in modifying the shape, strength, and type of the trap allows probing of the condensate properties with a high degree of flexibility. Also, by choosing the trap type, one can select some particular internal degrees of freedom of the particles as one wishes. BECs can also be formed from multiple components with different atomic species or different atomic hyperfine states for the same particle type, where the angular momentum of the hyperfine state for the usual alkali metal atoms being Bose condensed is composed of a sum between the unpaired electron spin outside the closed shell and the nuclear spin [6].

In multiple component BEC systems, the mutual interaction between the particles in different components adds more interesting phenomena. In one component there is only one scattering length variable, a quantity used in atomic physics to characterize the interactions of atoms in the low–energy limit. Whereas in multiple components we have $\frac{1}{2}n(n+1)$ scattering lengths for n mixed components. For example, when we have two-component BECs, like the case we are exploring in this thesis, there are three scattering lengths that describe the interactions: the scattering length between the same particles in one component (a_{11} and a_{22}), and the scattering length between the different components, a_{12}, where $a_{12} = a_{21}$. Examples of two-component BECs include ^{87}Rb–^{23}Na, different isotopes such as ^{87}Rb–^{85}Rb, or different hyperfine states of the same particles such as (F=2,m_F =2) and (F=1,m_F=1) states of ^{87}Rb.

In BECs, one can control to a high accuracy the interaction between the particles through a phenomenon known as Feshbach resonance. Also, by using this technique, we can change the sign of the interaction from repulsive to attractive interaction. Another significant aspect of low density dilute gases is the nature of the interaction between particles. At low temperature, the dominant interaction is of binary type, and therefore one can approximate the interaction potential to be represented by a delta function. This means that the interaction takes a nonlinear form. In chapter 2 we explain the role of the delta function and derive the associated nonlinear term. The fact that we can introduce and control a nonlinear effect in BECs allows us to create conditions to support the propagation of solitary waves. Indeed, by changing the interaction sign to be attractive between the particles in a BEC one can produce a bright soliton, a localized hump. In the case of a dark soliton, a localized dip on a continuous constant background, two conditions are needed. The first one is that the interaction should be of a repulsive type. The second is that there must be a π–phase difference between the two sides of the dark soliton. This can be done by shining light for a small time interval on one side of the condensate until it acquires the desired phase difference, and/or by digging a hole through removal of atoms with a laser, together with a quick phase imprint

on the condensate to one side of the hole. The latter technique is known as phase-density engineering [8].

These two types of soliton solutions are fundamentally different. One way to illustrate the difference between them is their maximum velocity. In the case of the dark soliton described by the GPE, there is a maximum limit of the velocity, the speed of sound in the BEC. Whereas in the case of the bright soliton, the velocity is not bounded by the sound speed, and has no upper limit. A moving dark soliton experiences two effects as it increases its speed. The width goes to infinity, and the depth goes to zero. Basically, we end up with plane wave for an accelerated dark soliton. It is noteworthy to mention that a moving dark soliton with a depth that is less than the maximum depth is called a gray soliton. Another aspect of the difference between the bright soliton and the dark one is that the bright soliton is the ground state of a system with an attractive interaction coefficient in the GPE. But the dark soliton is an excited state for a repulsively interacting system, orthogonal to the ground state as the dark soliton has a single node. One last piece of information needed to form a general picture of the basics of the soliton solution is how to move a soliton. We do this by applying a phase on the complex wave function solution of the GPE. This is done by multiplying the wave function by $e^{if(x)}$, where $f(x)$ is a real wave function with a step-like form smoothed out to avoid exciting additional phonons in the background BEC around the dark or grey soliton. The physics behind this is that in the hydrodynamics approach for the BEC the velocity of the condensate can be obtained by taking the gradient of the phase. Note that a Madelung transformation maps the complex wave function onto the density and phase of the condensate.

BECs are considered to be an ideal place to study the nonlinear excitations for the properties mentioned above [6, 9]. Many studies focus on exploring soliton dynamics in one or multiple component BECs. To model solitons in such systems, one needs to have a number of coupled scalar GPEs equal to the number of BEC components. These types of systems are called vector solitons where one can modify the interaction in each component

independently, and the equation governing them is known as the vector NLSE or vector GPE in our case. A particular structure of a coupled dark-bright vector soliton may exist in two-component BECs with repulsive interatomic interactions in all components, where a dark soliton in one component creates a potential well that traps a bright soliton in the second component [10–15]. Although a bright soliton does not exist in a scalar or single-component system with repulsive interactions [16], it can be supported in a binary two-component system due to the nonlinear interaction with the dark soliton component. These solitons can be referred to as symbiotic [17]. A dark-bright soliton is a bound state of a bright component with a positive kinetic energy and a dark component with a negative kinetic energy. A dark soliton is an excited state which when accelerated connects continuously to the ground state through the complex plane. Thus a dark soliton can be thought of as having a negative mass: as the velocity goes up, the energy goes down [18]. We can think of the exciton as an analogy to the dark-bright system where we have a bound state of an electron and a hole which are attracted to each other by the electrostatic Coulomb force. A similar possibility for such a mechanism was proposed early in the literature in terms of a Bose-Fermi mixture where bosons and fermions attract each other, but the interaction between the bosons themselves is repulsive [19]. Vector solitons also exist in fiber optics [20–22] including bright-bright vector solitons [23] and dark-bright vector solitons [24]. Different types of vector solitons in multi-component BECs, such as pseudo-spinor BECs or three- and higher-component spinor BECs [25, 26], can be created and transformed into each other by tuning the inter-component interaction via Feshbach resonances [14, 27, 28]. Examples of these vector solitons in two-component BECs include bright-bright vector solitons [29] and dark-dark vector solitons [15], which exhibit rich dynamical far-from-equilibrium phenomena such as beating dark-dark vector solitons [30]. Among the techniques to create dark-bright solitons in a binary mixture of BECs are phase imprinting [10] and counter-flowing of two binary BEC mixtures [31].

The theory of solitons has its own history when it comes to studying the nonlinear excitations in BECs. Since the early days of the discovery of BECs, there were intense efforts to create solitons. As mentioned above, the freedom to control the interaction between atoms in the condensate allows creating dark and bright solitons to be much easier. But there are always difficulties when dealing with attractive interactions in the BECs which is known as the collapse of the condensate when the number of atoms exceeds a critical value. The relative ease to work with a condensate where the interaction is repulsive manifest itself by creating the dark soliton first in the BECs. The pioneering work of Burger, *et al.* [32], in 1999, and Denschlag, *et al.* [33], in 2000, lead to the realization of dark solitons in BECs. Soon after, Strecker, *et al.* [34] and Khaykovich, *et al.* [35], in 2002, were able to overcome the difficulties with collapsing condensates for attractive interactions and create one or more bright solitons in BECs. Another breakthrough in the theory of soliton in BECs happened when Anderson, *et al.* [36], in 2000, constructed the first dark-bright soliton in two-component BECs following the theoretical work of Busch and Anglin, *et al.* [11].

In this Ph.D. thesis, consisting of three distinct projects, we investigate different aspects of the behavior of the dark-bright vector solitons. In the first project, we study the oscillations of the two components when we imprint a phase on one of the components, namely the bright soliton, and find the oscillation frequency. Our calculations explore observable eigenmodes, namely, the internal oscillation eigenmode and the Goldstone eigenmode. Also, we study the binding energy between the two components and obtain a critical value for the phase kick on the bright component that breaks the dark-bright solitons to its constituents. Both these studies were performed analytically and numerically.

Building on these results, we then implement the harmonic trap, investigating the internal oscillation of dark-bright (DB) solitons in employing the variational method. The oscillation of one component soliton has been investigated intensively in the literature. Many studies show that the one component bright soliton behaves as a classical particle and oscillate with the same frequency of the harmonic potential, ω. On the other hand, the oscillation of a

one-component dark soliton in a harmonic potential takes a universal value of $\omega/\sqrt{2}$. The next natural step is to investigate the behavior of a two-component dark-bright soliton in a harmonic potential and see if the universal behavior of the one component dark soliton oscillation in a harmonic potential will be affected by the presence of the bright component.

Finally, having addressed both the basic modes of oscillation, internal and external, of the dark-bright soliton, we turn to the question of scattering. The third project focuses on the behavior of dark-bright soliton when interacting with a delta potential barrier, modeling a fixed impurity. We study various aspects of the scattering process and interaction with the impurity, for example, the binding energy. The existence of the delta function modifies the background of the dark soliton, and therefore we need to include this effect where we utilize the perturbation method to do so. In this case, we use the well-known variational approach analytically but with a modified Euler-Lagrange equation to include the disturbance caused by the delta function. Also, we examine the velocity of the two components dark-bright soliton. It is well-known that the maximum velocity of the one component dark soliton is the speed of sound, c, where the depth of the dark soliton goes to zero, and the width goes to infinity as we get closer to c. We study the behavior of the dark soliton velocity when interacting with a bright soliton in the second component.

We end this chapter with a list of papers representing the main projects conducted in this thesis:

- "Dynamics of dark-bright vector solitons in Bose-Einstein condensates." M. O. D. Alotaibi and L. D. Carr, Physical Review A **96**, 13601 (2017).
- "Scattering of dark-bright soliton by an impurity." M. O. D. Alotaibi and L. D. Carr, under review, arXiv:1804.10339 (2018)
- "Internal Oscillations of a Dark-Bright Soliton in a Harmonic Potential." M. O. D. Alotaibi and L. D. Carr, under review, arXiv:1805.03339 (2018)

CHAPTER 2

MATHEMATICAL AND NUMERICAL NOTIONS OF DARK-BRIGHT SOLITONS IN BOSE-EINSTEIN CONDENSATES

This chapter is dedicated to the mathematical and numerical methods used in the soliton theory. In Sec. 2.1, we derive the GPE starting from the many-body Hamiltonian. In Sec. 2.2, we introduce the necessary methods to convert the 3D GPE to nondimensionalized 1D GPE. Sec. 2.3 is dedicated to explaining the imaginary time propagation (ITP) method where we show the procedures to obtain the ground state energy of one-component dark and bright solitons in addition to the ground state of the dark-bright soliton. In Sec. 2.4, we discuss the reasons behind choosing a specific ansatz and the role of this choice in the variational methods. Sec. 2.5 examine the techniques used to integrate the GPE numerically. Feshbach resonance method is explained in Sec. 2.6, and the Imaging techniques used to capture different aspects of the solitary waves experimentally is discussed in Sec. 2.7. We end the chapter with a general view of the experiments conducted so far on the dark-bright solitons in Sec. 2.8.

2.1 Derivation of Gross-Pitaevskii equation

The Gross-Pitaevskii equation describes the ground state of a Bose gas under BEC conditions. To derive this equation one starts from the full many-body Hamiltonian for interacting bosons,

$$\hat{H} = \int d^3\mathbf{r}\hat{\Psi}^\dagger(\mathbf{r})H_0\hat{\Psi}(\mathbf{r}) + \frac{1}{2}\int d^3\mathbf{r}\int d^3\mathbf{r}'\hat{\Psi}^\dagger(\mathbf{r})\hat{\Psi}^\dagger(\mathbf{r}')V_{\text{int}}(\mathbf{r},\mathbf{r}')\hat{\Psi}(\mathbf{r}')\hat{\Psi}(\mathbf{r}), \tag{2.1}$$

here $V_{\text{int}}(\mathbf{r},\mathbf{r}')$ represents the interaction potential term. The single particle Hamiltonian is $H_0 = (\hbar^2/2m)\nabla^2 + V_{\text{ext}}$, where V_{ext} is the external potential acting on the system. The field operators $\hat{\Psi}^\dagger(\mathbf{r})$ and $\hat{\Psi}(\mathbf{r})$ represent the creation and annihilation of a boson at positon $\mathbf{r}$, respectively. In the low energy BEC the dominant interaction between particles is a binary

interaction. Therefore, one can approximate the interaction potential, $V_{\text{int}}(\mathbf{r}, \mathbf{r}')$, to be of the following form,

$$V_{\text{int}}(\mathbf{r}, \mathbf{r}') = g\delta(\mathbf{r}' - \mathbf{r}), \tag{2.2}$$

where $g = 4\pi\hbar^2 N a_s/m$ governs the interaction strength between particles. The s–wave scattering length is a_s, the number of particles represented by N and m is the atomic mass. Using this potential in the above equation will integrate out r' and we are left with,

$$\hat{H} = \int d^3\mathbf{r}\hat{\Psi}^\dagger(\mathbf{r})H_0\hat{\Psi}(\mathbf{r}) + \frac{g}{2}\int d^3\mathbf{r}\hat{\Psi}^\dagger(\mathbf{r})\hat{\Psi}^\dagger(\mathbf{r})\hat{\Psi}(\mathbf{r})\hat{\Psi}(\mathbf{r}). \tag{2.3}$$

Applying the Heisenbergs time evolution equation, $i\hbar(\partial\hat{\Psi}(\mathbf{r})/\partial t) = [\hat{\Psi}(\mathbf{r}), \hat{H}]$, in order to evolve the field operator in time and using the bosonic commutation relations,

$$[\hat{\Psi}(\mathbf{r}), \hat{\Psi}^\dagger(\mathbf{r}')] = \delta(\mathbf{r}' - \mathbf{r}), \tag{2.4}$$

result in obtaining the equation of motion for the whole field,

$$i\hbar\frac{\partial}{\partial t}\hat{\Psi}(\mathbf{r}, t) = \left[-\frac{\hbar^2}{2m}\nabla^2 + V_{\text{ext}}(\mathbf{r})\right]\hat{\Psi}(\mathbf{r}, t) + g\hat{\Psi}^\dagger(\mathbf{r}, t)\hat{\Psi}(\mathbf{r}, t)\hat{\Psi}(\mathbf{r}, t). \tag{2.5}$$

We are interested in the equation of motion for the condensate alone. To this end, we split the field operator, $\hat{\Psi}$, into two parts representing an operator for the condensate part, $\hat{\Psi}_{\text{condensate}}$, and the non-condensate part, $\hat{\phi}$.

$$\hat{\Psi}(\mathbf{r}, t) = \hat{\Psi}_{\text{condensate}}(\mathbf{r}, t) + \hat{\phi}(\mathbf{r}, t). \tag{2.6}$$

The non-condensate part could represent thermally-excited atoms, quantum fluctuations, etc. Basically, any atoms that are not in the ground state. Therefore, one could ignore this part when considering a Bose gas under BEC conditions. The field operator for the condensate part can be approximated to represent a complex wavefunction when assuming a large number of particles in the condensate. This is a valid approximation since the operator acts on single particles. But when the particle number is large it will have no effect and we can consider the expectation value of the field operator to be of the following form,

$$\begin{aligned}\Psi_{\text{condensate}}(\mathbf{r}, t) &= \langle\hat{\Psi}_{\text{condensate}}(\mathbf{r}, t)\rangle, \\ \Psi^*_{\text{condensate}}(\mathbf{r}, t) &= \langle\hat{\Psi}^\dagger_{\text{condensate}}(\mathbf{r}, t)\rangle.\end{aligned} \tag{2.7}$$

By using Eq. (2.7) and Eq. (2.6) in Eq. (2.5), we obtain the Gross–Pitaevskii equation,

$$i\hbar\frac{\partial}{\partial t}\Psi(\mathbf{r},t)=\left[-\frac{\hbar^2}{2m}\nabla^2+V_{\text{ext}}(\mathbf{r})\right]\Psi(\mathbf{r},t)+g_{3D}\Psi^*(\mathbf{r},t)\Psi(\mathbf{r},t)\Psi(\mathbf{r},t), \tag{2.8}$$

where we dropped the subscript *condensate*. Equation (2.8) is the 3D GPE. In Sec. 2.2, we introduce the necessary steps to convert the dimensional 3D GPE to dimensionless 1D GPE.

2.2 Nondimensionalization and Dimensional Reduction for 3D Gross-Pitaevskii equation

Nondimensionalization is a method by which we partially (or entirely) remove physical units from an equation by a proper choice of variables. The result is often a dimensionless equation. Working with dimensionless equation has many benefits analytically and numerically. For example, solving a dimensionless equation numerically result in avoiding round-off due to manipulations with large or small numbers. Also, by working with a dimensionless equation analytically, we have insights into what parameters that could be small such that we can ignore or approximate.

The final form of the 3D GPE, Eq. (2.8) is,

$$i\hbar\frac{\partial}{\partial t}\Psi(\mathbf{x},t)=\left[-\frac{\hbar^2}{2m}\frac{\partial^2}{\partial\mathbf{x}^2}+V(\mathbf{x})+g_{3D}|\Psi(\mathbf{x},t)|^2\right]\Psi(\mathbf{x},t). \tag{2.9}$$

Here t is the time and $\mathbf{x}\in\mathbf{R}^3$ is the spatial coordinate in 3D. The wave function is $\Psi(\mathbf{x},t)$ and $V(\mathbf{x})$ represents harmonic potential. The 3D interaction coefficient is g_{3D}. To nondimensionlize Eq. (2.9) we multiply it by $\frac{1}{m\omega_x^2\sqrt{\ell}}$ and scale all quantities according to the following units:

$$\tilde{t}=\frac{t}{t_s},\ \tilde{\mathbf{x}}=\frac{\mathbf{x}}{\ell},\ \tilde{\Psi}(\tilde{\mathbf{x}},\tilde{t})=\ell^{\frac{3}{2}}\Psi(\mathbf{x},t). \tag{2.10}$$

The dimensionless version of Eq. (2.9) is,

$$i\frac{\partial}{\partial\tilde{t}}\tilde{\Psi}(\tilde{\mathbf{x}},\tilde{t})=\left[-\frac{1}{2}\frac{\partial^2}{\partial\tilde{\mathbf{x}}^2}+\tilde{V}(\tilde{\mathbf{x}})+\tilde{g}_{3D}|\tilde{\Psi}(\tilde{\mathbf{x}},\tilde{t})|^2\right]\tilde{\Psi}(\tilde{\mathbf{x}},\tilde{t}). \tag{2.11}$$

Here $\tilde{V}(\tilde{\mathbf{x}})=\frac{1}{2}\left(x^2+\gamma_y^2y^2+\gamma_z^2z^2\right)$, $\gamma_y^2=\frac{\omega_y}{\omega_x}$ and $\gamma_z^2=\frac{\omega_z}{\omega_x}$. The normalized interaction coefficient is $\tilde{g}_{3D}=\frac{4\pi aN}{\ell}$ where N is the number of particles and a is the scattering length.

In the following, we remove the tildes with the understanding that from now on we work mainly in dimensionless units. In the 1D limit we have $\omega_y \approx \omega_z >> \omega_x$. This lead to $\gamma_y^2 \approx \gamma_z^2 >> 1$. This means physically that we confine the condensates in y- and z-directions only such that we suppress any excitation other than the ones in the x-direction. In this way, we can factorize the wave function to the following expression,

$$\Psi(\mathbf{x}, t) = \Psi(x, y, z, t) = \psi(x, t)\, \phi(y, z)\,. \tag{2.12}$$

Here $\phi(y, z)$ is the wave function in the transverse direction (i.e. y and z directions). Since there are no excitations allowed in the transverse direction $\phi(y, z)$ is the ground state of the GPE and take the form of Gaussian wave function. Inserting Eq. (2.12) into Eq. (2.11) and multiply both side by $\phi^*(y, z)$ and integrate over the transverse direction result in the 1D GPE,

$$i\frac{\partial}{\partial t}\psi(x,t) = \left[-\frac{1}{2}\frac{\partial^2}{\partial x^2} + V(x) + g_{1D}|\psi(x,t)|^2\right]\psi(x,t), \tag{2.13}$$

with $g_{1D} = \frac{g_{3D}\sqrt{\gamma_y\gamma_z}}{2\pi}$. For a multiple-component system, we need an equation for each component. For example, the two-components GPEs take the form,

$$\begin{aligned} i\frac{\partial}{\partial t}u + \frac{1}{2}\frac{\partial^2}{\partial x^2}u - \left[g_1|u|^2 + g|v|^2\right]u = V(x)u, \\ i\frac{\partial}{\partial t}v + \frac{1}{2}\frac{\partial^2}{\partial x^2}v - \left[g_2|v|^2 + g|u|^2\right]v = V(x)v, \end{aligned} \tag{2.14}$$

where the wave function of component 1 is u and the wave function for component 2 is v. The interatomic interaction between the two components is g, and g_1 and g_2 represent the intra-atomic interaction for component 1 and component 2, respectively. The potential term is $V(x)$.

2.3 Imaginary time propagation

The ground state is by definition the lowest energy and the most stable state of the system. For this reason, it is preferable to use the ground state in numerical simulations. There are many numerical methods to obtain the ground state of a system [37, 38]. Here

we use a famous and reliable method, namely, the imaginary time propagation (ITP) [39]. The ITP is a mathematical trick used to numerically convert a random state to the ground state of a system. In the following, we highlight the main steps to illustrate the use of ITP to find the ground state of a system.

Expand a random wave function in terms of the system eigenfunctions,

$$\Psi(x,t) = \sum_{n=0}^{\infty} \psi_n(x)\, e^{-iE_n t}, \tag{2.15}$$

where each next eigenstate has higher energy than the previous one. That is, $E_n > E_{n-1}$. The next step is the one that gives the method its name where we substitute the real time by imaginary one (i.e $\tau = it$).

In this way, equation (2.15) becomes,

$$\Psi(x,\tau) = \sum_{n=0}^{\infty} \psi_n(x)\, e^{-E_n \tau} = \left(\psi_0 e^{-E_0\tau} + \psi_1 e^{-E_1\tau} + \psi_2 e^{-E_2\tau} + +\psi_3 e^{-E_3\tau} + ...\right). \tag{2.16}$$

We see that when we forward propagate τ, the exponentials with higher energy will decay faster than the those with the lower energy. As a result, for a long time propagation, we are left with the lowest energy state of the system (i.e. E_0). The choice of the initial random wave function affects the efficiency of the ITP method. It is favored to choose an initial wave function that is close to the shape of the desired one and not orthogonal to the ground state so that we minimize the time needed to find the ground state of a system. It is also better to choose a profile wave function with all Fourier components having a nonzero weight. The reason behind this fact is that when we propagate τ in time we want to include all the possible energy values otherwise the final result could be biased and will not reflect the real ground state of the system. In order to obtain the ground state energy of one component bright soliton we set the sign of g in Eq. (2.13) to be negative. In Figure 2.1 and Figure 2.2 we show the convergence of an arbitrary wave function to a bright soliton using the ITP.

The bright soliton solution in Figure 2.2 takes the form [40],

$$\psi_{BS}(x) = A\mathrm{sech}\left[A\sqrt{-g}\,(x - x_0 - vt)\right] e^{i\theta(x,t)}, \tag{2.17}$$

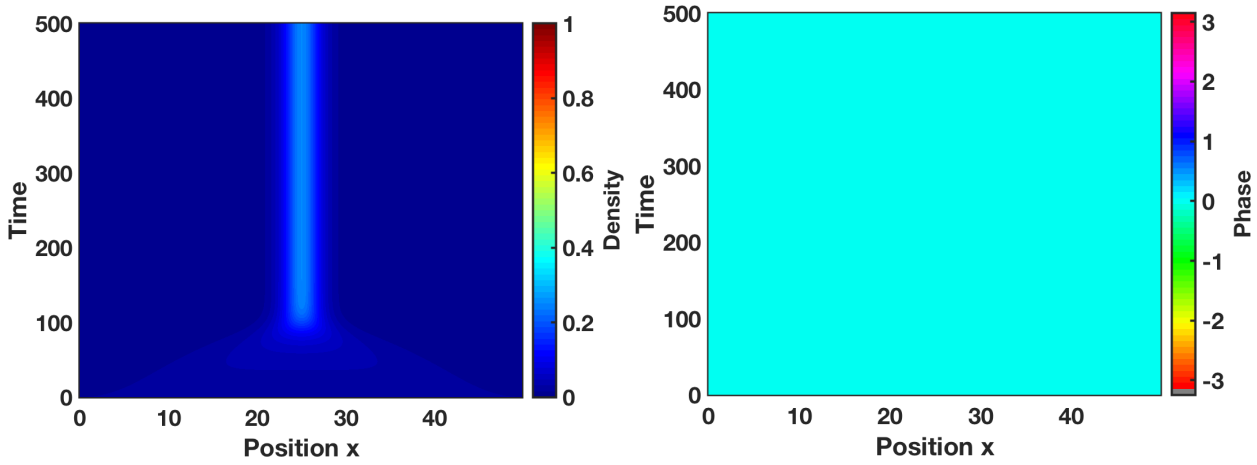

Figure 2.1 Convergence of arbitrary wave function to bright soliton. The left (right) panel shows the density (phase) of the propagation of bright soliton in ITP.

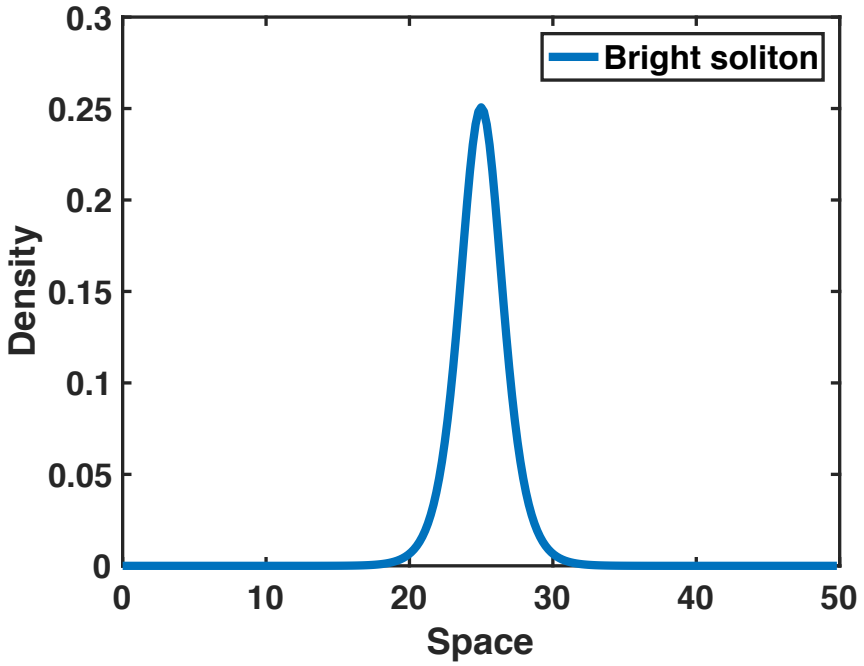

Figure 2.2 Bright soliton obtained by ITP. Final result of Figure 2.1.

where x_0 is the position of the soliton, v is the velocity, A is the amplitude and θ is the phase. We normalize the bright soliton in Figure 2.2 to one. Therefore, by compute the normalization of Eq. (2.17) to one we obtain the following expression,

$$\frac{2A}{\sqrt{-g}} = 1. \tag{2.18}$$

With $g = -1$ we find $A^2 = 0.25$ as shown in Figure 2.2.

ITP can also be used to obtain excited states like dark soliton. We do so by modifying the interaction coefficient to be repulsive (i.e., $g > 0$) then we imprint a π-phase on half of the condensate (i.e., $x > 0$) and allows the wave function to propagate in imaginary time until we get the desired result. The imprinting of a phase difference basically cut the condensates to two halves, and therefore we can think of this as a propagation of two constant backgrounds with an invisible barrier between them. Another way to see this is that when we first obtain the constant background, the phase through the condensate is constant and by applying a phase difference in a specific location we get a region where the phase is changing from 0 to π. Therefore, the particles in this part of the condensate will acquire a non-zero velocity, v, due to the well-known equation $v(x,t) = \frac{\hbar}{m}\nabla S(x,t)$, where $S(x,t)$ is the phase across the condensate. Hence, when we propagate the wave function in imaginary time, the particles in this region will move either to the right or left side, and a dark soliton will be created. Note that the absence of particles characterizes a dark soliton. In Figure 2.3 and Figure 2.4, we plot the result obtained from the ITP method.

In the case of the dark-bright soliton, we obtain the two-component wave function also by ITP. Here, we work mainly with repulsive interaction coefficients for all components (i.e., g_1, g_2 and $g > 0$). We only apply a phase difference on one component (i.e., component 1) such that we form a dark soliton in this component. The repulsive interaction between the particles in the two components force the particles in component 2 to cluster in the middle since there are no particles in this region in component 1 due to the presence of the dark soliton. Therefore, we obtain a bright soliton in the second component.

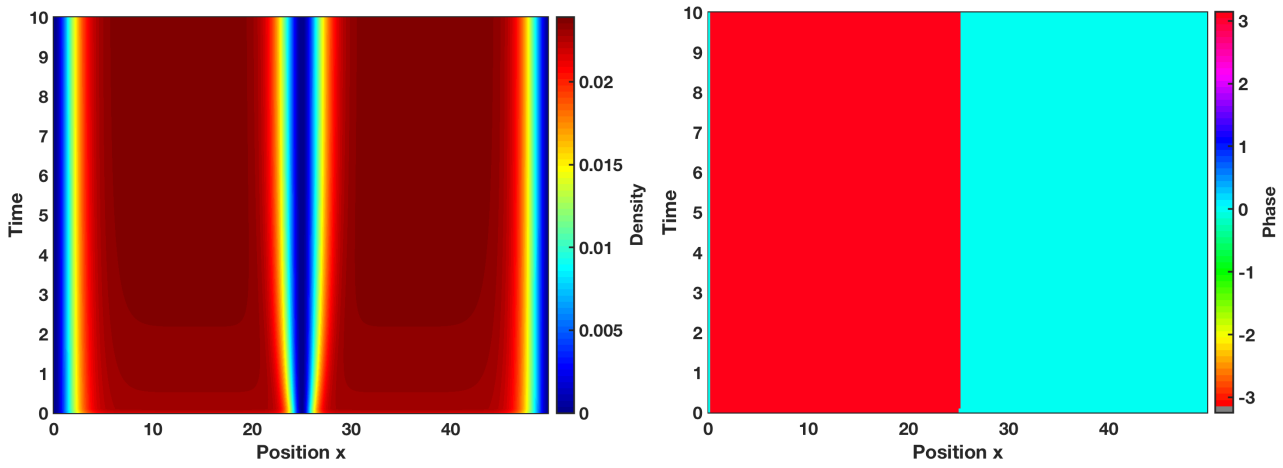

Figure 2.3 Convergence of arbitrary wave function to dark soliton. The left (right) panel shows the density (phase) of the propagation of dark soliton in ITP.

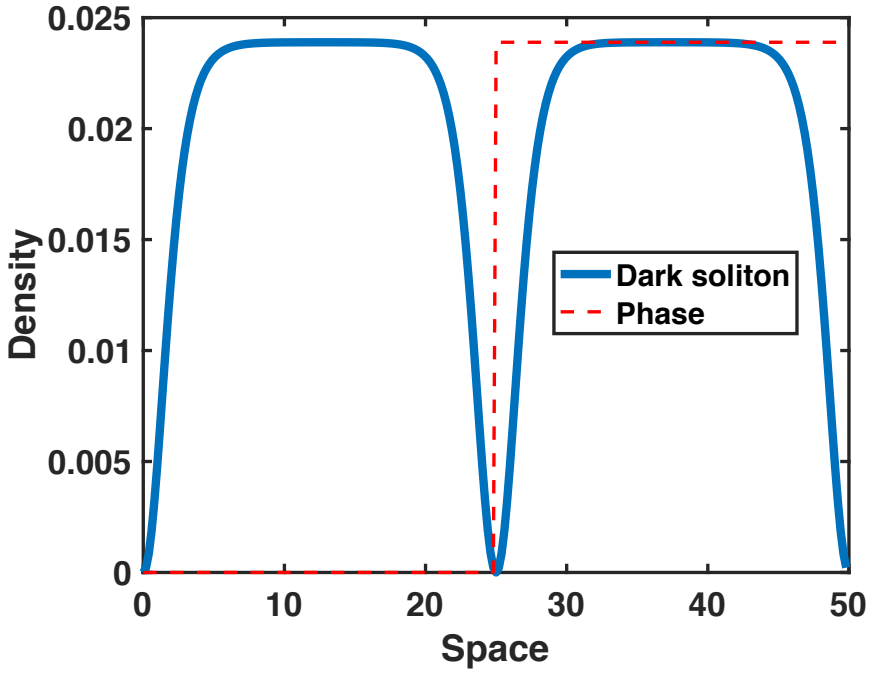

Figure 2.4 Dark soliton obtained by ITP. Final result of Figure 2.3.

In Figure 2.5 we plot the density and the phase of the dark component using the ITP and in Figure 2.6 we plot the density of the bright component using the ITP. Note that once we get a bright component, the dark component modifies its width to account for the existence of the bright soliton. Note that once we get a bright component, the dark component modifies its width to account for the existence of the bright soliton. An essential criterion that controls the shape of the dark-bright soliton is the miscible/immiscible condition [6],

$$g^2 > g_1 g_2, \tag{2.19}$$

where g is the interatomic interaction between the two components of the BEC and g_1 (g_2) represents the intra-atomic interaction for the dark (bright) component, respectively.

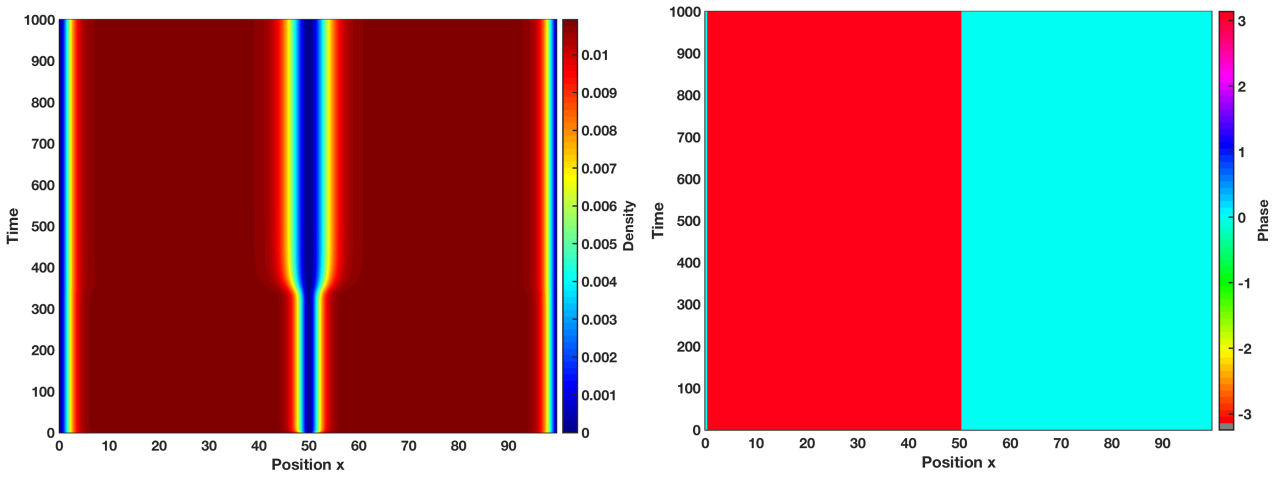

Figure 2.5 Dark soliton component in dark-bright soliton. The left (right) panel shows the density (phase) of the propagation of dark soliton component in ITP. Note that the creation of the bright component, Figure 2.6, modify the width of the dark component.

In Figure 2.7, we plot the final result obtained from the ITP for dark-bright wave function in two-component BEC.

2.4 History of ansatz

An essential step to obtain an accurate description of the dynamic of a solitary wave using the variational method is the choice of the ansatz. In the case of the bright soliton,

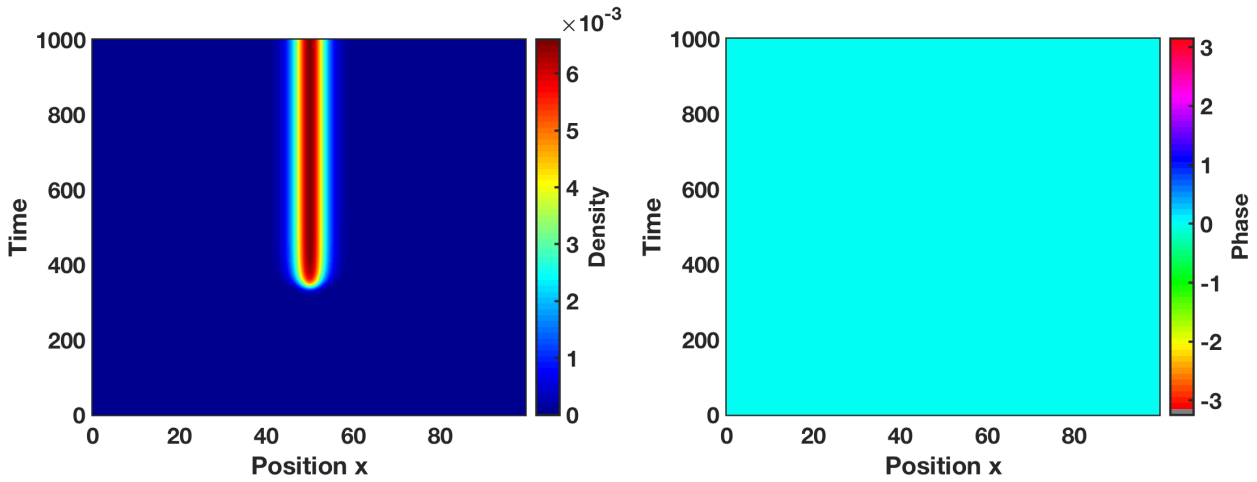

Figure 2.6 Bright soliton component in dark-bright soliton. The left (right) panel shows the density (phase) of the propagation of bright soliton component in ITP.

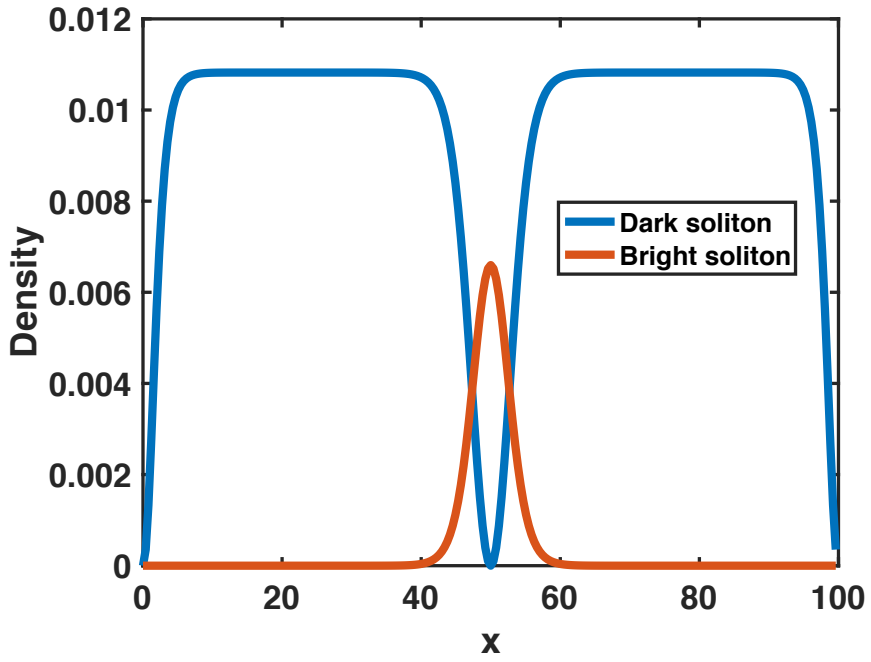

Figure 2.7 Dark-bright soliton obtained by ITP. The final result from Figure 2.6 and Figure 2.6.

popular options for the ansatz are the Gaussian function or the hyperbolic secant. The choice between these two functions depends on the problem we are dealing with. For example, in the case of one-component bright soliton, it is always preferable to select the hyperbolic secant. After all, this is the exact solution for the NLSE with attractive interaction coefficient (i.e., bright soliton) [6]. But with more complex situations like studying the propagation of two bright solitons, it is better to choose Gaussian functions for their relative ease in calculating integrals over the Lagrangian density. In addition, using Gaussian functions allow for the studying of the interaction between different bright solitons without restricting the widths to be identical. In the case of the dark soliton, the ansatz takes the form of hyperbolic tangent function. And since we are dealing in this thesis with two-component dark-bright soliton, we are using the hyperbolic tangent for the dark component and hyperbolic secant for the bright component in the dark-bright soliton. This choice imposes restrictions on the width of the two components such that they must be identical to solve the integrals for the Lagrangian density analytically. Also, a disadvantage of using Gaussian functions is that they are less accurate than using hyperbolic functions; in fact, it is precisely the non–Gaussianity of solitons that sets them apart from wave-packet solutions to the NLSE.

2.5 Numerical techniques

We numerically integrate Eq. (2.14) using the method of lines. The method of lines is a numerical method used to solve Schrodinger-like equations [41]. The general theme of the method is to solve partial differential equations by discretizing the spatial dimensions and leave the time dimension to be continuous. By doing so, we recast the problem in the following form,

$$i\hbar\frac{\partial}{\partial t}\psi\left(t\right)=H\left[\psi\left(t\right),t\right]\psi\left(t\right), \tag{2.20}$$

where $\psi\left(t\right)$ is an L-dimensional vector such that Eq. (2.20) form a coupled set of ordinary differential equations (ODEs). The result system of ODEs can be propagated forward in time using finite difference methods. In the following we discuss different methods used to

advance the system of ODEs in time.

2.5.1 Runge-Kutta

The Runge-Kutta method [41] is a numerical method used to integrate a system of ordinary differential equations by using a trial step at the midpoint of an interval to cancel out lower-order error terms. The general idea is to advance the wave function ψ to $\psi(t+\delta t)$. Therefore, the fourth-order formula of the method becomes,

$$\psi(t+\delta t) = \psi(t) + \delta t\left[\frac{1}{6}k_1(t) + \frac{1}{63}k_2(t) + \frac{1}{3}k_3(t) + \frac{1}{6}k_4(t)\right] + O\left(\delta t^5\right), \tag{2.21}$$

where,

$$\begin{aligned} k_1(t) &= \frac{1}{i}H\left[\psi(t), t\right]\psi(t), \\ k_2(t) &= \frac{1}{i}H\left[\psi(t), t\right]\{\psi(t) + \frac{\delta t}{2}k_1(t)\}, \\ k_3(t) &= \frac{1}{i}H\left[\psi(t), t\right]\{\psi(t) + \frac{\delta t}{2}k_2(t)\}, \\ k_4(t) &= \frac{1}{i}H\left[\psi(t), t\right]\{\psi(t) + \frac{\delta t}{2}k_3(t)\}. \end{aligned} \tag{2.22}$$

2.5.2 Pseudo-Spectral Methods

The pseudo-spectral method is a method used to also propagate a solution, $\psi(t)$, in time. To explain the procedure used in this method, we start from the Schrodinger equation,

$$i\hbar\frac{\partial}{\partial t}\psi(r,t) = H\left[\psi(r,t), t\right]\psi(r,t). \tag{2.23}$$

The general solution of this equation takes the form,

$$\psi(r,t) = e^{-iHt/\hbar}\psi(r,0), \tag{2.24}$$

where a power series define the exponential term. The next step is to separate the Hamiltonian into a kinetic term, $T = -\frac{\hbar^2}{2m}\frac{\partial^2}{\partial x^2}$, and potential term, $V = V(r)$. We focus now on the exponential term (i.e., $e^{-iHt/\hbar}$) in Eq. (2.24). If the potential is time independent then the exponential term in Eq. (2.24) becomes $e^{-i(T+V(r))t/\hbar}$. By choosing a small time step, we

can approximate the solution in Eq. (2.24) to the following form,

$$\psi\left(r,t\right)\approx e^{-iV(r)t/2\hbar}e^{-iTt/\hbar}e^{-iV(r)t/2\hbar}\psi\left(r,0\right). \tag{2.25}$$

The next step is to advance the solution, Eq. (2.25), in time such that we propagate $\psi\left(r,t\right)$ to $\psi\left(r,t+\Delta t\right)$. Therefore, Eq. (2.25) becomes,

$$\begin{aligned}\psi\left(r,t+\Delta t\right) &\approx e^{-iV(r)\Delta t/2\hbar}e^{-iT\Delta t/\hbar}e^{-iV(r)\Delta t/2\hbar}\psi\left(r,t\right)\\ &= e^{-iV(r)\Delta t/2\hbar}e^{-iT\Delta t/\hbar}\phi_1\left(r,t\right)\\ &= e^{-iV(r)\Delta t/2\hbar}\phi_2\left(r,t\right),\end{aligned} \tag{2.26}$$

where,

$$\begin{aligned}\phi_1\left(r,t\right) &= e^{-iV(r)\Delta t/2\hbar}\psi\left(r,t\right),\\ \phi_2\left(r,t\right) &= e^{-iT\Delta t/\hbar}\phi_1\left(r,t\right).\end{aligned} \tag{2.27}$$

The final step is to employ Fourier transform in Eq. (2.27) such that we convert the problem to a series of pointwise multiplication. Basically, we obtain $\Phi_1\left(k\right)=\mathcal{F}\left[\phi_1\left(r,t\right)\right]$ and $\Phi_2\left(k\right)=e^{-i\hbar k^2\Delta t/2m}\mathcal{F}\left[\phi_1\left(r,t\right)\right]$ where $\mathcal{F}$ represents a Fourier transform. Therefore, Eq. (2.26) becomes,

$$\psi\left(r,t+\Delta t\right)\approx e^{-iV(r)\Delta t/2\hbar}\mathcal{F}^{-1}\left[e^{-i\hbar k^2\Delta t/2m}\mathcal{F}\left[e^{-iV(r)\Delta t/2\hbar}\psi\left(r,t\right)\right]\right]. \tag{2.28}$$

We may calculate the pseudospectral derivatives using fast transform algorithms. We can approximate a function $f(x)$ by a truncated sine series.

$$f(x)\approx\sum_{k=1}^{N}\tilde{f}_k\sin\left(kx\right). \tag{2.29}$$

The coefficients $\tilde{f}_k$ can be computed by the discrete sine transform. The finite differences of the second derivative of the above equation is computed by the following equation,

$$\frac{f\left(x_{j+1}\right)-2f\left(x_j\right)+f\left(x_{j-1}\right)}{h^2}=\frac{2}{h^2}S_j\{\tilde{f}_k\left[\cos\left(\frac{\pi k}{N}\right)-1\right]\}, \tag{2.30}$$

where h is the grid spacing. For the kinetic energy term in Eq. (2.28) we see that the second derivative converted to multiplication by the coefficient, $\cos\left(\frac{\pi k}{N}\right)-1$ in Eq. (2.30).

Many numerical packages for fast Fourier transform can be used in order to utilize the propagation of the solution in Eq. (2.28). In this thesis, we are using the Pseudo-Spectral Method to simulate the GPE. In Figure 2.8 and Figure 2.9, we plot the propagation of the dark and bright components, respectively, in real time.

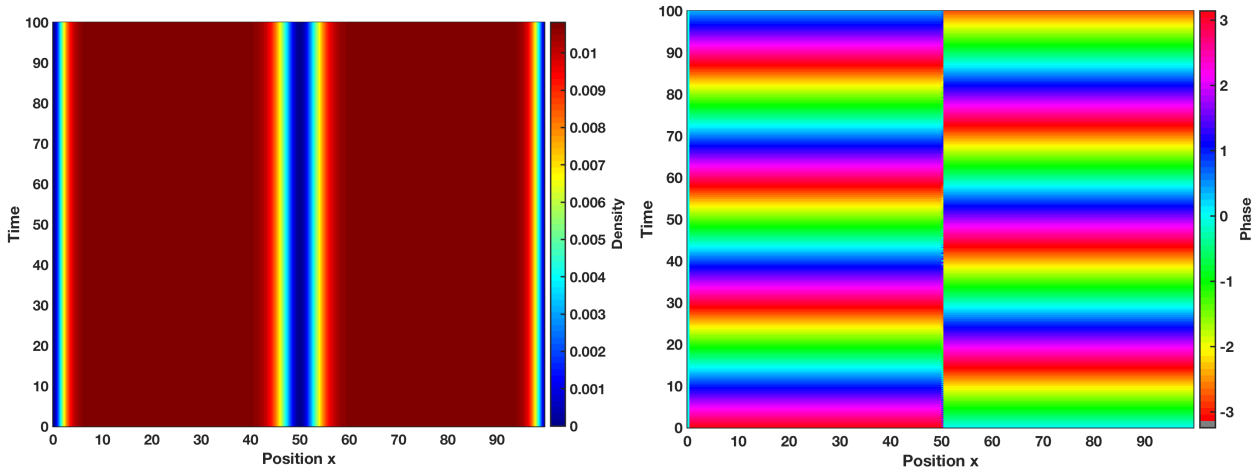

Figure 2.8 Dark soliton component in dark-bright soliton in real time. The left (right) panel shows the density (phase) of the propagation of dark soliton component in real time.

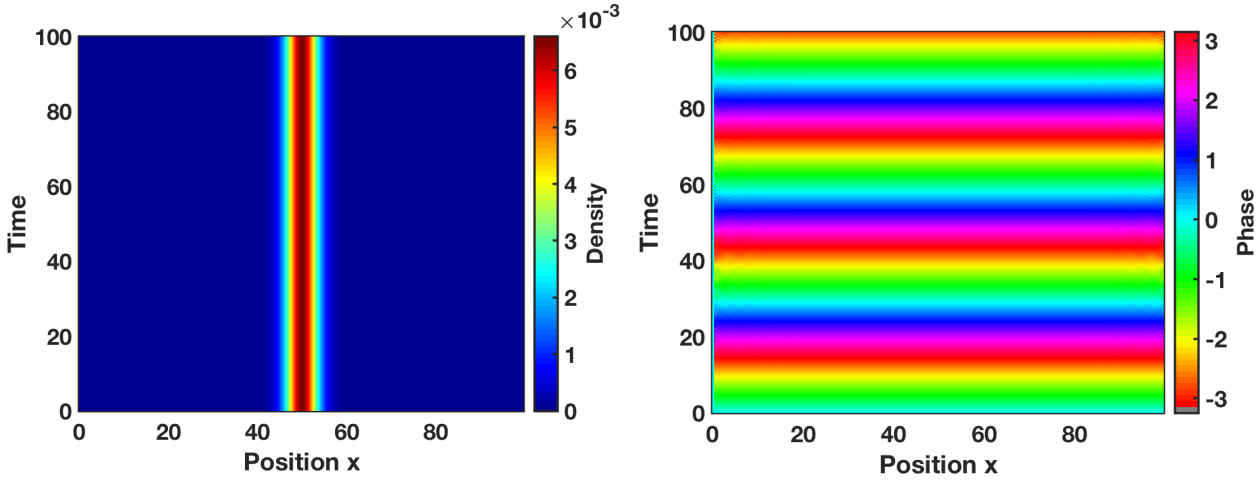

Figure 2.9 Bright soliton component in dark-bright soliton in real time. The left (right) panel shows the density (phase) of the propagation of bright soliton component in real time.

2.6 Feshbach Resonances

The Feshbach resonance is a valuable tool used to tune the interactions between atoms in ultracold atomic gases such as the BEC. By tuning the interaction, we can form a molecule also. The physics behind this technique can be understood by the two-channel model where we have an open channel and a closed one as can be seen in Figure 2.10. An interaction channel forbidden by energy conservation is referred to as a closed channel, whereas an energetically accessible interaction channel is referred to as an open channel.

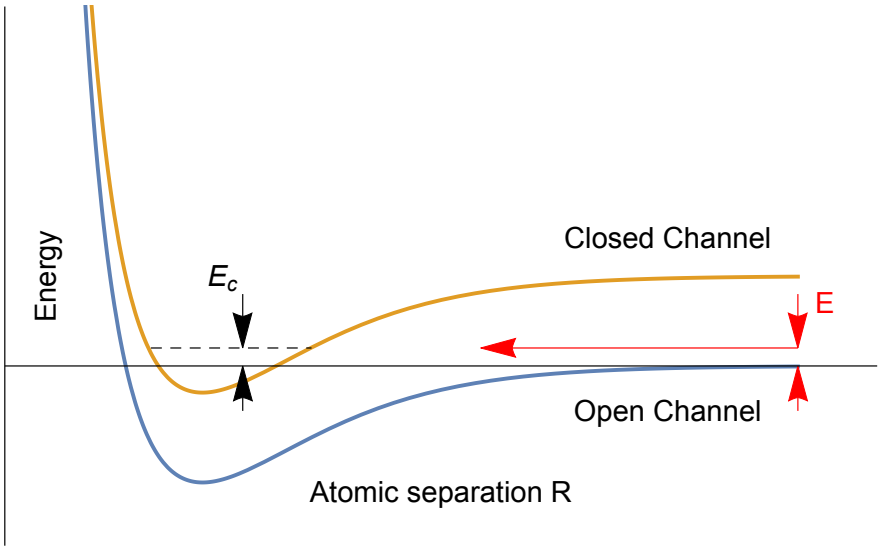

Figure 2.10 Two-channel model.

The event occurs when two atoms collide at energy E in the open channel. Then, the atoms resonantly coupled and a molecular bound state happen with E_c that is supported by the closed channel. Note that in the BEC condition mentioned above the collisions take place near zero energy. Then we realize the resonant coupling when we magnetically tuning E_c near zero.

2.7 Imaging techniques for two-component Bose-Einstein condensate systems

The imaging techniques for two-component BECs are divided into two categories: Destructive and nondestructive methods. In the former case, the procedure to obtain BEC

image heat up the condensate and causing damage to the sample. In this process, a near-resonant beam focused on the sample and produced a shadow that can be imaged on a camera where the atomic density distribution is captured. Since the condensates scattered the light that coming from the near-resonant beam, it will heat it up and destroyed it. In the case of multiple components, we can change the frequency of the laser beam such that we distinguish between the different species.

In the nondestructive methods, we are dealing with off-resonant beam this time. By shining a laser beam of this kind on the sample, we gain a phase-shift caused by the presence of the condensates. The information in the phase is then converted to intensity, and therefore we obtain information on the atomic density. In the case of two components BEC with different hyperfine states we can distinguish between the densities using this method by tuning the laser beam between the two hyperfine levels. It is also known that this method has significant advantages over the destructive techniques for the imaging of small and dense clouds. Experimentally, It is possible to take a hundred images of the same condensate and revealed important information of the dynamics of the condensates with the data that we can get from the phase-shift beam [42].

2.8 Dark-bright solitons in experiments

The first two-component BECs were realized in 1997 by Myatt [43]. In this experiment, a $|1,-1\rangle$ spin state of ^{87}Rb was cooled by the usual method (i.e., cooling the gas below the critical temperature followed by evaporation phase). To create the second component, in this case, a $|2,2\rangle$ spin state of ^{87}Rb, the authors thermally contact the $|2,2\rangle$ spin state with the $|1,-1\rangle$ spin state. This "sympathetic" cooling of one species by another is not a new technique. It has been used to cool trapped ions with strong interactions as mentioned in Myatt's paper. Other methods help to realize the creation of more sophisticated two component BECs. For example, ^{39}K–^{85}Rb, ^{85}Rb–^{87}Rb and ^{41}K–^{85}Rb.These mixtures are sometimes referred to as heteronuclear mixtures [6]. The two-component BECs with repulsive interactions allow for the creation of dark-bright soliton. In this case, the dark soliton, which

is an excited state with energy higher than the underlying BEC ground state, playing the role of an effective potential that supports the bright soliton.

A dark-bright soliton created in two hyperfine states of ^{87}Rb have a very close interaction coefficients, Eq. (2.19). Therefore, by tuning the Feshbach resonance to obtain a repulsive interaction in the two separated condensates, we still work with a Manakov system (i.e., a system where all the coefficients equal to unity) [44]. Working with different atom species in the two components allow for exploring systems other than the Manakov system.

CHAPTER 3

DYNAMICS OF DARK-BRIGHT VECTOR SOLITONS IN BOSE-EINSTEIN CONDENSATES

We analyze the dynamics of two-component vector solitons, namely dark-bright solitons, via the variational approximation in Bose-Einstein condensates. The system is described by a vector nonlinear Schrödinger equation appropriate to multi-component Bose-Einstein condensates. The variational approximation is based on a hyperbolic tangent (hyperbolic secant) for the dark (bright) component, which leads to a system of coupled ordinary differential equations for the evolution of the ansatz parameters. We obtain the oscillation dynamics of two-component dark-bright solitons. Analytical calculations are performed for same-width components in the vector soliton and numerical calculations extend the results to arbitrary widths. We calculate the binding energy of the system and find it proportional to the intercomponent coupling interaction, and numerically demonstrate the break up or unbinding of a dark-bright soliton. Our calculations explore observable eigenmodes, namely the internal oscillation eigenmode and the Goldstone eigenmode. We find analytically that the number of atoms in the bright component is required to be less than the number of atoms displaced by the dark soliton in the other component in order to find the internal oscillation eigenmode of the vector soliton and support the existence of the dark-bright soliton. This outcome is confirmed by numerical results. Numerically, we find that the oscillation frequency is amplitude independent. For dark-bright solitons in ^{87}Rb we find that the oscillation frequency range is 90 to 405 Hz, and therefore observable in multi-component Bose-Einstein condensate experiments.

3.1 Introduction

Nonlinear waves have been a fascinating subject since the discovery of the solitary wave in 1834 by John Scott Russell in the Union Canal in Scotland where he observed the "great

wave of translation," as he called it at the time [1]. Since then, solitary waves of all kinds have been observed in many systems. Solitons in Bose-Einstein condensates (BECs), which are the subject of this Article, have been the focus of research efforts since the creation of BECs [6, 9].

A special structure of a coupled dark-bright soliton may exist in two-component BECs with repulsive interatomic interactions, where a dark soliton in one component creates a potential well that traps a bright soliton in the second component [10, 12–15, 45, 46]. Although a bright soliton does not exist in a system with repulsive interactions [16], it can be supported in such a binary system due to the nonlinear interaction with the dark soliton component. These solitons can be referred to as symbiotic [17, 46]. A similar possibility for such a mechanism was proposed early in the literature in terms of a Bose-Fermi mixture where bosons and fermions attract each other but the interaction between the bosons themselves is repulsive [19]. Vector solitons also exist in fiber optics [20–22] including bright-bright solitons [23] and dark-bright solitons [24]. Different types of vector solitons in multiple component BECs, such as pseudo-spinor BECs or three- and higher-component spinor BECs [25, 26], can be created and transformed into each other by tuning the inter-component interaction via Feshbach resonances [14, 27, 28]. Examples of these vector solitons in two-component BECs include bright-bright solitons [29] and dark-dark solitons [15, 47], which exhibit rich dynamical far-from-equilibrium phenomena such as beating dark-dark solitons [30]. Among the techniques to create dark-bright solitons in a binary mixture of BECs are phase imprinting [10] and counter-flowing of two binary BEC mixtures [31].

Many studies have been conducted to investigate the oscillation of vector solitons to gain a better understanding of the dynamics of multicomponent nonlinear excitations. The oscillation of bright-bright solitons is one example of such studies. Another example is the oscillation of dark-dark solitons. In the case of dark-bright solitons, there have been investigations of the oscillation of multiple dark-bright solitons [31, 46, 48] and the oscillation of the internal modes for bright-bright solitons using a Gaussian ansatz [49] via variational

approximation methods. However, to the best of our knowledge no one has treated the internal oscillations of the dark-bright soliton case variationally using hyperbolic functions, which is the subject of this Article. A popular choice for the ansatz in the variational approximation method is Gaussian functions for their relative ease in calculating integrals over the Lagrangian density. In addition, Gaussian functions do not impose any restriction in the choice of the width of the two components in the vector soliton. A disadvantage of using Gaussian functions is that they are less accurate than using hyperbolic functions – in fact it is exactly the non-Gaussianity of solitons that sets them apart from wavepacket solutions to the linear Schrödinger equation. Thus in this Article we perform calculations with variational approximation methods using hyperbolic tangent (hyperbolic secant) for the dark (bright) component in the dark-bright soliton. This choice imposes restrictions on the width of the two components such that they must be identical in order to solve the integrals for the Lagrangian density analytically. We study the behavior of the dark-bright soliton when a phase is imprinted only on the bright component and find the oscillation modes of the system, in addition to the binding energy and the velocity of the dark-bright soliton, which is effected by the interaction coefficient between the two components. In this scenario the moving bright component pulls the dark component along with it, and oscillates in addition to moving the dark-bright soliton as a whole. One can think of this mode as a vibrational excitation of the dark-bright "soliton molecule," as two-component vector solitons are sometimes termed. We will use the term *dark-bright soliton* to describe these vector solitons. Our calculation shows that the system has a second oscillation mode in addition to the vibrational mode, namely a Goldstone mode [50], as expected since the whole dark-bright soliton is moving.

This Article is organized as follows. In Sec. 3.2 we study oscillation of the two components in the dark-bright soliton by imprinting a phase on the bright component and finding the normal modes of the system by means of a variational approximation method based on a hyperbolic tangent (hyperbolic secant) for the dark (bright) soliton component for the two-

component ansatz. In Sec. 3.5 we calculate the binding energy between the bright and dark component in the dark-bright soliton as a function of the distance between the center of each component. In Sec. 3.6 we investigate dark-bright soliton dynamics by numerically integrating the dimensionless nonlinear Schrödinger equation (NLSE) using an algorithm that is pseudo-spectral in time and adaptive Runge-Kutta in space. We focus on the inter-component dynamics for different interaction coefficients and discuss real experimental values for the internal oscillation frequency in ^{87}Rb. Finally, we present our conclusions in Sec. 5.4.

3.2 Analytical Calculations

The two-component dark-bright soliton is governed by coupled NLSEs [6], which describe the evolution of the macroscopic wave functions of Bose condensed atoms:

$$\begin{aligned} i\hbar\frac{\partial}{\partial\tilde{t}}\tilde{u}\left(\tilde{x},\tilde{t}\right) &= -\frac{\hbar^2}{2m}\frac{\partial^2\tilde{u}\left(\tilde{x},\tilde{t}\right)}{\partial\tilde{x}^2} + \Big[\tilde{g}_{11}|\tilde{u}\left(\tilde{x},\tilde{t}\right)|^2 \\ &\quad - \tilde{u}_0^2 + \tilde{g}_{12}|\tilde{v}\left(\tilde{x},\tilde{t}\right)|^2\Big]\tilde{u}\left(\tilde{x},\tilde{t}\right), \\ i\hbar\frac{\partial}{\partial\tilde{t}}\tilde{v}\left(\tilde{x},\tilde{t}\right) &= -\frac{\hbar^2}{2m}\frac{\partial^2\tilde{v}\left(\tilde{x},\tilde{t}\right)}{\partial\tilde{x}^2} + \Big[\tilde{g}_{22}|\tilde{v}\left(\tilde{x},\tilde{t}\right)|^2 \\ &\quad + \tilde{g}_{21}|\tilde{u}\left(\tilde{x},\tilde{t}\right)|^2\Big]\tilde{v}\left(\tilde{x},\tilde{t}\right), \end{aligned} \tag{3.1}$$

where tildes denote dimensional quantities. The wave function of the dark soliton is given by $\tilde{u}\left(\tilde{x},\tilde{t}\right)$ and of the bright soliton by $\tilde{v}\left(\tilde{x},\tilde{t}\right)$. The interaction strength, $\tilde{g}_{ij} = 2a_{ij}N\hbar\omega_\perp$ for $(i,j=1,2)$, is renormalized to 1D [51] where $\tilde{g}_{12}$ and $\tilde{g}_{21}$ are the inter-atomic interaction between the two components of the BEC and $\tilde{g}_{11}$ ($\tilde{g}_{22}$) represents the intra-atomic interaction for the dark (bright) component. The dark soliton wave function is rescaled to remove the background contribution, $\tilde{u}_0$, as is standard to avoid divergent normalization and energy [52]. The s-wave scattering length between components i and j is a_{ij}, N is the total number of atoms and $\omega_\perp$ is the oscillation frequency of the transverse trap. We assume the atomic masses for the two components m_1 and m_2 are equal to m, as appropriate for the case of multiple hyperfine components of e.g. ^{87}Rb. To nondimensionlize Eqs. (3.1) we multiply

them by $(\hbar\omega_\perp)^{-1}$ and scale all quantities according to the following units:

$$\begin{aligned} x &= \frac{\tilde{x}}{\ell_\perp}, \\ t &= \tilde{t}\omega_\perp, \\ g_{ij} &= \frac{\tilde{g}_{ij}}{\ell_\perp \hbar\omega_\perp}, \\ |u|^2 &= \ell_\perp |\tilde{u}|^2, \\ |v|^2 &= \ell_\perp |\tilde{v}|^2, \\ u_0^2 &= \frac{\tilde{u}_0^2}{\hbar\omega_\perp}, \end{aligned} \tag{3.2}$$

where $\ell_\perp = \sqrt{\hbar/(m\omega_\perp)}$ is the transverse harmonic oscillator length. In Sec. 3.10 we discuss specific choices that are consistent with experimental observations. For simplicity we take $g_{11} \equiv g_1, g_{22} \equiv g_2$, and $g_{12} = g_{21} \equiv g$. The dimensionless NLSE becomes

$$\begin{aligned} i\frac{\partial u}{\partial t} &= -\frac{1}{2}\frac{\partial^2 u}{\partial x^2} + \left[g_1 |u|^2 - u_0^2 + g |v|^2\right] u, \\ i\frac{\partial v}{\partial t} &= -\frac{1}{2}\frac{\partial^2 v}{\partial x^2} + \left[g_2 |v|^2 + g |u|^2\right] v. \end{aligned} \tag{3.3}$$

We work with the dimensionless 1D two-component coupled NLSE, Eq. (3.3), throughout the rest of this article. We use the normalization conditions

$$\int_{-\infty}^{\infty} dx \ \left(\frac{u_0^2}{g_1} - |u|^2\right) = \frac{N_1}{N}, \tag{3.4a}$$

$$\int_{-\infty}^{\infty} dx \ |v|^2 = \frac{N_2}{N}, \tag{3.4b}$$

for the dark and bright component, respectively. Noting the background subtraction in the first component of Eqs. (4.8), N_1 is the number of atoms displaced by the dark soliton, in other words, the number of atoms involved with creating the density notch or minimum. Thus we define the total number of atoms N involved in the dark and bright solitons as

$$N_1 + N_2 = N, \tag{3.5}$$

as appropriate for the two-component BEC and standard for the dark-bright soliton problem, thereby incorporating N into the definition of the nonlinear coefficient $\tilde{g}_{ij}$ [6]. To obtain

Eq. (3.3), we introduce the following Lagrangian density where we use Euler-Lagrangian equations to get the equations of motion, i.e., the coupled NLSE of Eq. (3.3):

$$\begin{aligned}\mathcal{L} =& \frac{i}{2}\left[u^{*}\frac{\partial u}{\partial t}-u\frac{\partial u^{*}}{\partial t}\right]\left[1-\frac{u_{0}^{2}}{g_{1}\left|u\right|^{2}}\right]-\frac{1}{2}\left|\frac{\partial u}{\partial x}\right|^{2}\\ &-\frac{1}{2}\left[\sqrt{g_{1}}\left|u\right|^{2}-\frac{u_{0}^{2}}{\sqrt{g_{1}}}\right]^{2}+\frac{i}{2}\left[v^{*}\frac{\partial v}{\partial t}-v\frac{\partial v^{*}}{\partial t}\right]\\ &-\frac{1}{2}\left|\frac{\partial v}{\partial x}\right|^{2}-\frac{g_{2}}{2}\left|v\right|^{4}-g\left|u\right|^{2}\left|v\right|^{2}\\ &+\frac{u_{0}^{2}}{2g_{1}}\left[2\theta_{2}\left(x+d\left(t\right)\right)+\theta_{1}\left(t\right)\right]^{2}.\end{aligned} \tag{3.6}$$

Note that the last term does not depend on the wave function of the dark or the bright component and was added to eliminate the infinity when using the ansatz, Eq. (3.7), with θ_1 and θ_2 to be defined in the following. We adopt the following trial functions as the dark-bright soliton solutions to Eq. (3.3):

$$\begin{aligned}u\left(x,t\right) &= \frac{u_{0}}{\sqrt{g_{1}}}\left\{iA+c\,\tanh\left[\frac{\left(d\left(t\right)+x\right)}{w}\right]\right\}\\ &\quad\times\exp\left\{i\left[\theta_{0}+\left(d\left(t\right)+x\right)\theta_{1}\left(t\right)+\left(d\left(t\right)+x\right)^{2}\theta_{2}\right]\right\},\\ v\left(x,t\right) &= \frac{u_{0}}{\sqrt{g_{2}}}F\,\mathrm{sech}\left[\frac{\left(b\left(t\right)+x\right)}{w}\right]\\ &\quad\times\exp\left\{i\left[\phi_{0}+\left(b\left(t\right)+x\right)\phi_{1}\left(t\right)+\left(b\left(t\right)+x\right)^{2}\phi_{2}\right]\right\}.\end{aligned} \tag{3.7}$$

The parameters A, c and F describe the amplitude of the two components, where $A^2+c^2=1$, as is standard in the formulation of an NLSE dark soliton [18]. In the exponential terms, ϕ_0 and θ_0 give rise to a complex amplitude. $\phi_1(t)$ and $\theta_1(t)$ are responsible for the dark and bright component velocities. Note that the velocity of a dark soliton also depends on the amplitude of the wave function as shown in Eq. (3.9d); ϕ_2 and θ_2 are essential to vary the width [53]; and $d(t)$ and $b(t)$ are the position of the dark and bright soliton, respectively. The two components are assumed to have the same width w. To study the oscillation of the two components in time, we chose the variational parameters to be the two component positions $d(t)$ and $b(t)$ and the phases $\theta_1(t)$ and $\phi_1(t)$. As mentioned in Sec. 3.1, the

analytical calculations use hyperbolic functions as an ansatz, which are more accurate than using Gaussian functions. This choice requires the two components to have identical width in order for the problem to remain analytically tractable, as opposed to using a Gaussian ansatz [49]. However, we will relax this constraint in Sec. 3.6. Using the ansatz, Eqs. (3.7), in the normalization, Eqs. (4.8), we find the relation between N_1, N_2 and the coefficients of the two components in the dark-bright soliton:

$$\begin{aligned} \frac{2c^2u_0^2w}{g_1} &= \frac{N_1}{N}, \\ \frac{2F^2u_0^2w}{g_2} &= \frac{N_2}{N}. \end{aligned} \tag{3.8}$$

3.3 Evolution Equations

Substituting Eq. (3.7) into the Lagrangian density Eq. (4.12) and integrating over space from $-\infty$ to ∞ results in the Lagrangian as a function of the variational parameters. Applying the Euler-Lagrange equations then yields a system of ordinary differential equations (ODEs) that describes the evolution in time of the position and phase for both components:

$$\begin{aligned} &\frac{d}{dt}\phi_1(t) = \alpha \operatorname{csch}\left(\frac{b\left(t\right)-d\left(t\right)}{w}\right)^4 && \text{(3.9a)} \\ &\times\left\{2\left(b\left(t\right)-d\left(t\right)\right)\left[2+\cosh\left(2\frac{b\left(t\right)-d\left(t\right)}{w}\right)\right]\right. \\ &\left.-3w\sinh\left(2\frac{b\left(t\right)-d\left(t\right)}{w}\right)\right\}, \\ &\frac{d}{dt}\theta_1(t) = \beta\frac{d}{dt}\phi_1\left(t\right), && \text{(3.9b)} \\ &\frac{d}{dt}b\left(t\right) = -\phi_1\left(t\right), && \text{(3.9c)} \\ &\frac{d}{dt}d\left(t\right) = -\gamma-\theta_1\left(t\right). && \text{(3.9d)} \end{aligned}$$

where

$$\alpha \equiv \frac{c^2gu_0^2}{g_1w^2},\ \beta \equiv \frac{F^2g_1}{c^2g_2},\ \gamma \equiv \frac{A}{cw}. \tag{3.10}$$

Equations. (4.13) can be reduced to one second order ODE:

$$\frac{d^2}{dt^2}l(t) = (\beta-1)\alpha \operatorname{csch}\left(\frac{l(t)}{w}\right)^4 \times \left\{2l(t)\left[2+\cosh\left(\frac{2l(t)}{w}\right)\right] - 3w\sinh\left(\frac{2l(t)}{w}\right)\right\}. \tag{3.11}$$

where $l(t) \equiv b(t) - d(t)$. Despite the attractive simplicity of this unified description, it is physically advantageous to address the problem with Eqs. (4.13) to illustrate the behavior of the evolution of the variational parameters in time and to clarify the physical meaning of the fixed point and linear stability analysis in the next section.

3.4 Normal Modes

Equations (4.13) possess one stable fixed point:

$$\phi_1 = 0,\ \theta_1 = -\gamma,\ l = 0. \tag{3.12}$$

Since $l = 0$, we can choose the original of the coordinate system such that $b = d = 0$. In Appendix 3.12 we prove that Eqs. (4.13) with the fixed point $l = 0$ do not possess a singularity. We proceed by linearizing Eqs. (4.13) around the fixed point Eq. (3.12), i.e., $a_i(t) = a_{\mathrm{fp}} + \delta a e^{\mathrm{i}\omega t}$, where a_i represents the variational parameters and a_{fp} is the fixed point mentioned above. This results in a matrix equation of form

$$\begin{bmatrix} i\omega & 0 & -A_1 & A_1 \\ 0 & i\omega & -A_2 & A_2 \\ 1 & 0 & i\omega & 0 \\ 0 & 1 & 0 & i\omega \end{bmatrix} \begin{bmatrix} \delta\phi_1 \\ \delta\theta 1 \\ \delta b \\ \delta d \end{bmatrix} = \begin{bmatrix} 0 \\ 0 \\ 0 \\ 0 \end{bmatrix} \tag{3.13}$$

where

$$A_1 = \big(8c^2 g u_0^2\big)/\big(15 g_1 w^2\big), \tag{3.14}$$

$$A_2 = \big(8F^2 g u_0^2\big)/\big(15 g_2 w^2\big). \tag{3.15}$$

Taking the determinant of the matrix and solving for eigenfrequencies ω and the associated eigenvectors yields

$$\nu_{\mp} = \begin{bmatrix} \mp\frac{2}{\sqrt{15}}\left(N_1/N_2\right) w^{-\frac{3}{2}} \sqrt{g}\sqrt{\frac{N_2-N1}{N}} \\ \mp\frac{2}{\sqrt{15}} w^{-\frac{3}{2}} \sqrt{g}\sqrt{\frac{N_2-N1}{N}} \\ N_1/N_2 \\ 1 \end{bmatrix}, \tag{3.16a}$$

$$\nu_{01} = \begin{bmatrix} 0 \\ 0 \\ 1 \\ 1 \end{bmatrix}, \nu_{00} = \begin{bmatrix} 0 \\ 0 \\ 0 \\ 0 \end{bmatrix}, \tag{3.16b}$$

and eigenfrequencies [1]

$$\omega_{\mp} = \mp 2i\sqrt{\frac{1}{15}}\sqrt{g} w^{-\frac{3}{2}} \sqrt{\left(N_2 - N_1\right)/N}, \tag{3.17a}$$

$$\omega_{01} = 0,\ \omega_{00} = 0, \tag{3.17b}$$

where the oscillation frequency ω_{01} in Eq. (3.17b) corresponds to the zero-energy mode, sometimes defined in the literature as a Goldstone mode [50, 54], and we have used the normalization Eqs. (4.8). This mode breaks translational symmetry with no energy cost. We can interpret it as a moving dark-bright soliton without internal oscillation of the two components. Also, the eigenvector of this mode, ν_{01}, shows no contribution from the phases that are responsible in the first place for the oscillation, and has b and d moving together with zero frequency, i.e., at constant velocity.

Turning to the nonzero frequency eigenmode, in Eq. (3.17a), stable oscillation requires the condition $N_1 > N_2$ be met, in other words, $g_2 > \frac{F^2}{c^2} g_1$. Thus for same amplitude components there is no oscillation. This result is supported by the numerical calculations in Sec. 3.7, where we find that the bright component in the dark-bright soliton does not exist when the total number of atoms in the bright component is equal to or greater than the total number of atoms displaced by dark soliton in the other component (Figure 3.3). Using $N_2 = N - N_1$ we can rewrite the oscillation frequency as

[1] We note that the simplification of Eq. (3.11) produces the same eigenfrequencies, as we verified in an independent calculation.

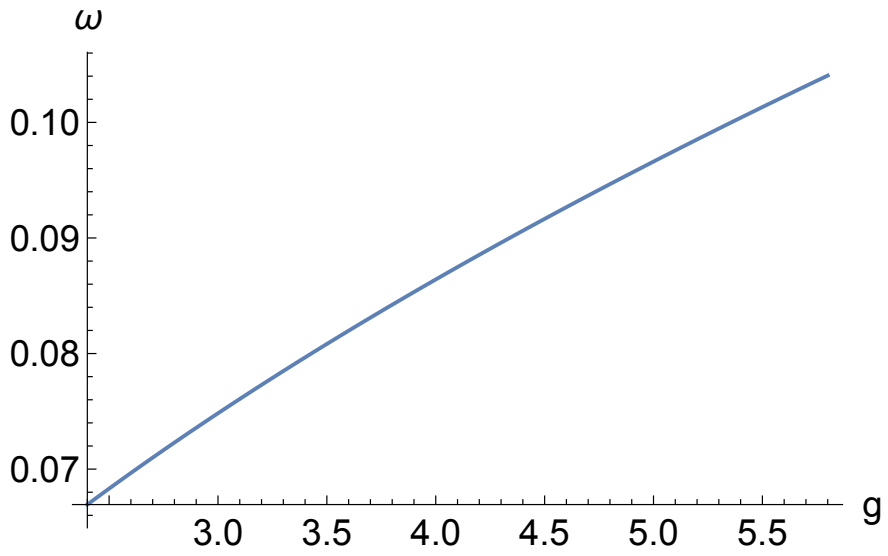

Figure 3.1 Oscillation frequency of the two components in the dark-bright soliton versus the interaction coefficients, g. We set $N_1 \approx 0.503 * 10^5$ atoms and width w=1 where ω and g are unitless. The range of the values in g is from 2.4 to 5.8, matching the range of g in the numerical calculations.

$$\omega_{\mp} = \mp 2\sqrt{\frac{1}{15}} w^{-\frac{3}{2}} \sqrt{g} \sqrt{(2N_1/N) - 1}. \tag{3.18}$$

Note that for a real oscillation the normalization constant $2N_1/N$ should be greater than one, which in turn makes $N_1 > N_2$. Considering the typical number of atoms in ^{87}Rb experiment, we set $N = 10^5$ and $N_1 \approx 0.503 \times 10^5$. Setting w = 1 in Eq. (3.18) we plot the relative frequency versus the interaction coefficient g in Figure 3.1.

3.5 Binding Energy of Vector Soliton

In the Lagrangian density, Eq. (4.12), the term $g\left|u\right|^2\left|v\right|^2$ represents the coupling interaction per unit space between the two components of the dark-bright soliton. Using the ansatz Eq. (3.7), we can integrate this term over x to find the coupling interaction of the system. The binding energy can be found when we subtract the coupling interaction energy at $l = 0$ from $l = \infty$ where l is the separation between the bright and dark solitons. The energies associated with all other terms in the Lagrangian density turn out to be independent of l. The coupling interaction energy of the system is

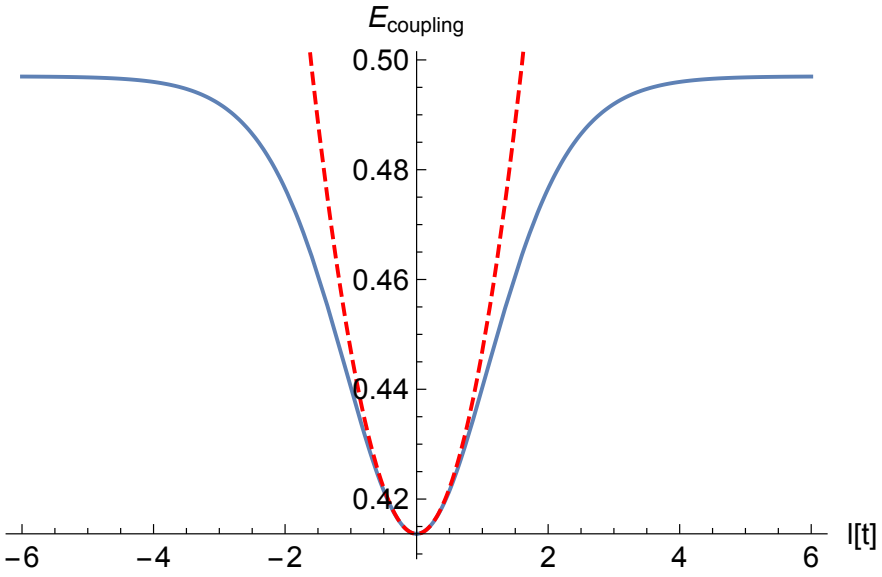

Figure 3.2 Coupling energy versus the distance between the two components, $l\,(t)$, when t=0. Here we normalize the interaction coefficients to unity and set $N_1 \approx 0.503 * 10^5$ atoms. The solid blue line represent Eq. (3.19) and the dashed red line represent Eq. (3.20).

$$\mathrm{E_{coupling}} = \frac{F^2 g u_0^4}{g_1 g_2} \mathrm{csch}\left[\frac{l\,(t)}{w}\right]^2 \times \left[4c^2\left(w - l\coth\left[\frac{l\,(t)}{w}\right]\right) + 2w\sinh\left[\frac{l\,(t)}{w}\right]^2\right]. \tag{3.19}$$

In Figure 3.2 we plot Eq. (3.19). As expected for a binding energy, the coupling interaction energy is minimum at the center where the location of the bright soliton maximum and dark soliton minimum coincide. Applying a phase to the bright component, i.e., giving it a "kick", causes it to experience a force due to the coupling interaction energy that brings it back to the energy minimum, which creates an oscillation between the two components. If the imprinted phase is large enough to separate the two solitons beyond their relative widths, the system reaches a point where the bright soliton escapes and is then destroyed, as we will show in Sec. 3.6.

To analytically explore the behavior of the oscillation around the fixed point when $l \ll 1$ we expand Eq. (3.19) to quadratic order in l:

$$\mathrm{E}_{\mathrm{coupling}} = \frac{2(3-2c^2)F^2 g u_0^4 w}{3g_1 g_2} + \frac{8c^2F^2 g u_0^4}{15 g_1 g_2 w} l^2 \tag{3.20}$$

As a result, we see that the coupling energy when $l << 1$ behaves as a parabolic potential energy near the fixed point. Therefore, we should expect the oscillation frequency to be amplitude independent for small amplitude excitations, and this is indeed the result we obtain in Sec. 3.6 (see Figure 3.7).

We can treat the coupling energy as a potential energy and derive the equation of motion for $l(t)$.

$$\begin{aligned} m\frac{d^2}{dt^2}l(t) &= -\frac{d}{dl}\mathrm{E}_{\mathrm{coupling}} \\ &= \frac{2c^2F^2 g u_0^4}{g_1 g_2 w}\ \mathrm{csch}(\frac{l(t)}{w})^4 \left\{2l(t)\left[2\right.\right. \\ &\quad \left.\left.+\cosh(\frac{2l(t)}{w})\right] - 3w\sinh(\frac{2l(t)}{w})\right\}, \end{aligned} \tag{3.21}$$

where $m = 1$ in our units. Comparing Eq. (3.21) to Eq. (3.11) we find that the two equations are different only by the coefficients and therefore yield different frequencies. This can be understood by examining the Lagrangian density, Eq. (4.12), where we subtract the background contributions from the dark soliton momentum term and the intra-component mean field energy term. The calculations leading to Eq. (3.11) account for this subtraction whereas the calculations leading to Eq. (3.21) do not. Consequently, the coefficients are different.

By taking the difference between Eq. (3.19) at $l = 0$ and $l = \infty$ we find the binding energy:

$$\begin{aligned} \mathrm{E}_{\mathrm{binding}} &= \mathrm{E}_{\mathrm{coupling}(l\to 0)} - \mathrm{E}_{\mathrm{coupling}(l\to\infty)} \\ &= -\frac{4c^2F^2 g u_0^4 w}{3g_1 g_2}. \end{aligned} \tag{3.22}$$

We note that the binding energy is thus proportional to the intercomponent coupling g and inversely proportional to the intracomponent couplings g_1, g_2. The latter inverse proportionality is due to normalization. In addition, we calculate the kinetic energy (KE) and the intra-component mean-field energy (MFE) of the dark and bright component, separately, and compare them to the binding energy above.

For the dark component in the dark-bright soliton,

$$\mathrm{KE} = \frac{N_1[-2+\pi^2 w^4\theta_2^2]}{6Nw^2} + \frac{1}{2}\theta_1\left(\frac{4Acu_0^2}{g_1} + \frac{N_1\theta_1}{N}\right), \tag{3.23}$$

$$\mathrm{MFE} = -\frac{g_1 N_1^2}{6wN^2}. \tag{3.24}$$

For the bright component in the dark-bright soliton,

$$\mathrm{KE} = -\frac{N_2[1+\pi^2 w^4\phi_2^2]}{6Nw^2} - \frac{N_2\phi_1^2}{2N}, \tag{3.25}$$

$$\mathrm{MFE} = -\frac{g_2 N_2^2}{6wN^2}. \tag{3.26}$$

We found the KE and the MFE of the dark (bright) soliton component is inversely proportional to the intracomponent coupling g_1 (g_2). Note that both the KE and the MFE of the two components does not depend on the intercomponent coupling g as expected. This result can be understood when we examine the Lagrangian density, Eq. (4.12), where the intercomponent coupling g only appears in the coupling term and therefore only contributes to the binding energy.

Finally, we compare the binding energy to the kinetic energies (i.e., Eqs. (3.23), (3.25)) and the mean field energies (i.e., Eqs. (3.24), (3.26)) of the dark-bright soliton. We find that in order to break or unbind the dark-bright soliton the imprinted phase on the bright component should be greater than the following quantity:

$$\phi_1 > \frac{1}{\sqrt{3N_2}}[-\frac{2N_1+N_2-2N_1w}{w^2}-\frac{N_1^2(2+g_1)+g_2N_2^2}{Nw} + \pi^2w^2(N_1\theta_2^2-N_2\phi_2^2)+3N_1\theta_1^2 + \frac{6\,\theta_1\sqrt{N_1}\sqrt{2Nu_0^2w-g_1N_1}}{w\sqrt{g_1}}]^{-1}\,. \tag{3.27}$$

In Sec. 3.8, we compare Eq. (3.27) to Figure 3.9.

3.6 Numerical Calculations

In this section we numerically investigate the interaction between the two components. First, we explore the approach to the integrable Manakov case of equal interaction coefficients $g = g_1 = g_2$ and find the ground state density of a dark-bright soliton. The Manakov case formally precludes a dark-bright soliton, since the number of atoms in the bright soliton component must be less than the number of atoms displaced by the dark component soliton. In Sec. 3.4 we derived this condition as a requirement to find a real oscillation of the two component dark-bright soliton. Second, we investigate the interaction between the two components with unequal interaction coefficients by finding the ground state of the system when the interatomic interaction goes from the miscible to the immiscible domain, representing a quantum phase transition for the dark-bright soliton. Third, we investigate dark-bright soliton dynamics, studying the velocity of the dark-bright soliton, the oscillation frequency mode as a function of the interaction coefficients, and unbinding or break-up process when the dark-bright soliton is too strongly perturbed. Fourth, we end this section with a discussion of the experimental case for ^{87}Rb where we can use these units to convert between the dimensionless variables in the study conducted and physically measurable quantities such as the oscillation time. Note that throughout this section, we performed the simulations with grid size $n_x = 256$ and in a box with hard wall boundaries. The box length was set to L=50 unless otherwise noted.

3.7 Dark-Bright Soliton with Equal Interaction Coefficients

We obtain our initial state numerically by using the imaginary-time-propagation method to find the ground state energy of the coupled NLSEs. Starting with constant initial wave-functions for both components, where we imprinted a phase on the constant dark component only, we perform two sets of simulations. We allow the particle number to fluctuate between the two components during imaginary time propagation. Fixing $g_1 = g_2 = 1$ and allowing g to increase toward the Manakov case of $g = g_1 = g_2$, we find the result shown in Figure 3.3, where in the last two panels the dark-bright soliton ceases to exist and all atoms pile up in the "bright" component.

3.8 Dark-Bright Soliton with Unequal Interaction Coefficients

We explore the miscible-immiscible quantum phase transition at $g^2 = g_1 g_2$ in a non-Manakov system for which $g_1 \neq g_2$, as shown in Figure 3.4, where we again tune g through the transition. For $g < 2.3$ we do not find a true bright soliton but rather a bump on a non-zero background, in fact a finite-size effect. For $g > 2.3$ in the last two panels the dark-bright soliton appears, since the number of atoms in the bright component is less than that displaced by the dark component. In the miscible domain in Figure 3.4(a)-(f), the strength of the repulsive interaction between the two components is less than the repulsive interaction between the particles in the bright component which allows the bright soliton to expand and reach the boundaries. In the immiscible domain in Figure 3.4(g)-(h), the coupling interaction is strong to the point that it forces the bright component to live within the dark soliton only.

To highlight the effect of the miscibility transition, in Figure 3.5, as we increase the inter-component coupling, g, the amplitude of the bright component decreases and the amplitude of the dark component increases. With increasing intercomponent coupling g, the ground state of the dark-bright soliton shows that the density of the bright component decreases and therefore the amplitude too. This can be understood by examining Figure 3.4. We see

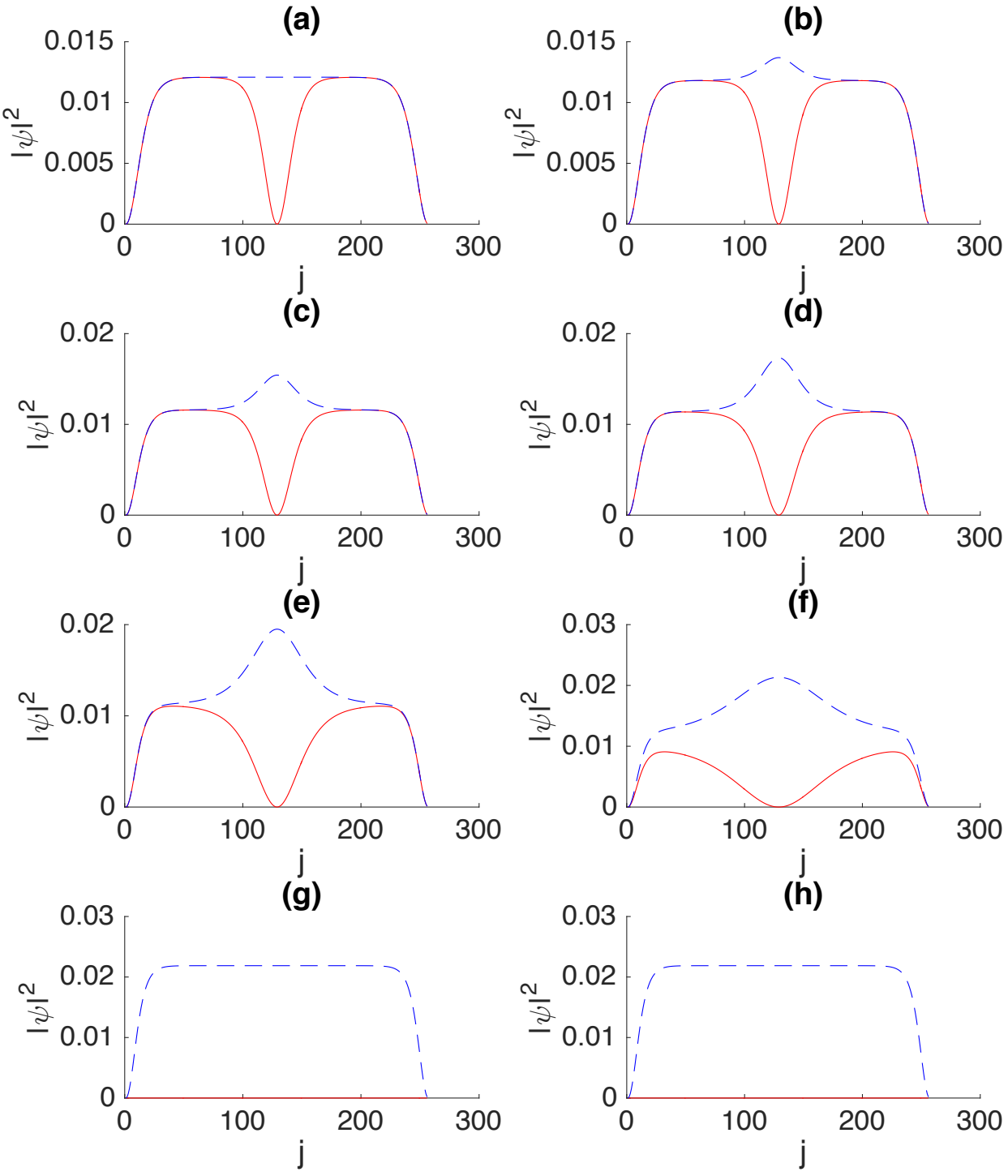

Figure 3.3 Approach to the Manakov case. Ground state density of a two-component BEC when the interaction coefficients g_1, g_2 are equal to unity, versus the coupling interaction coefficient g. The bright (dark) component is the dashed blue (solid red) line. In (a)-(h) $g = 0.0, 0.2, 0.4, 0.6, 0.8, 0.95, 1.0, 1.2$, respectively. We allow the relative particle number between the two components to fluctuate, and past the Manakov point at $g = 1$ the lowest energy solution places all atoms in one component.

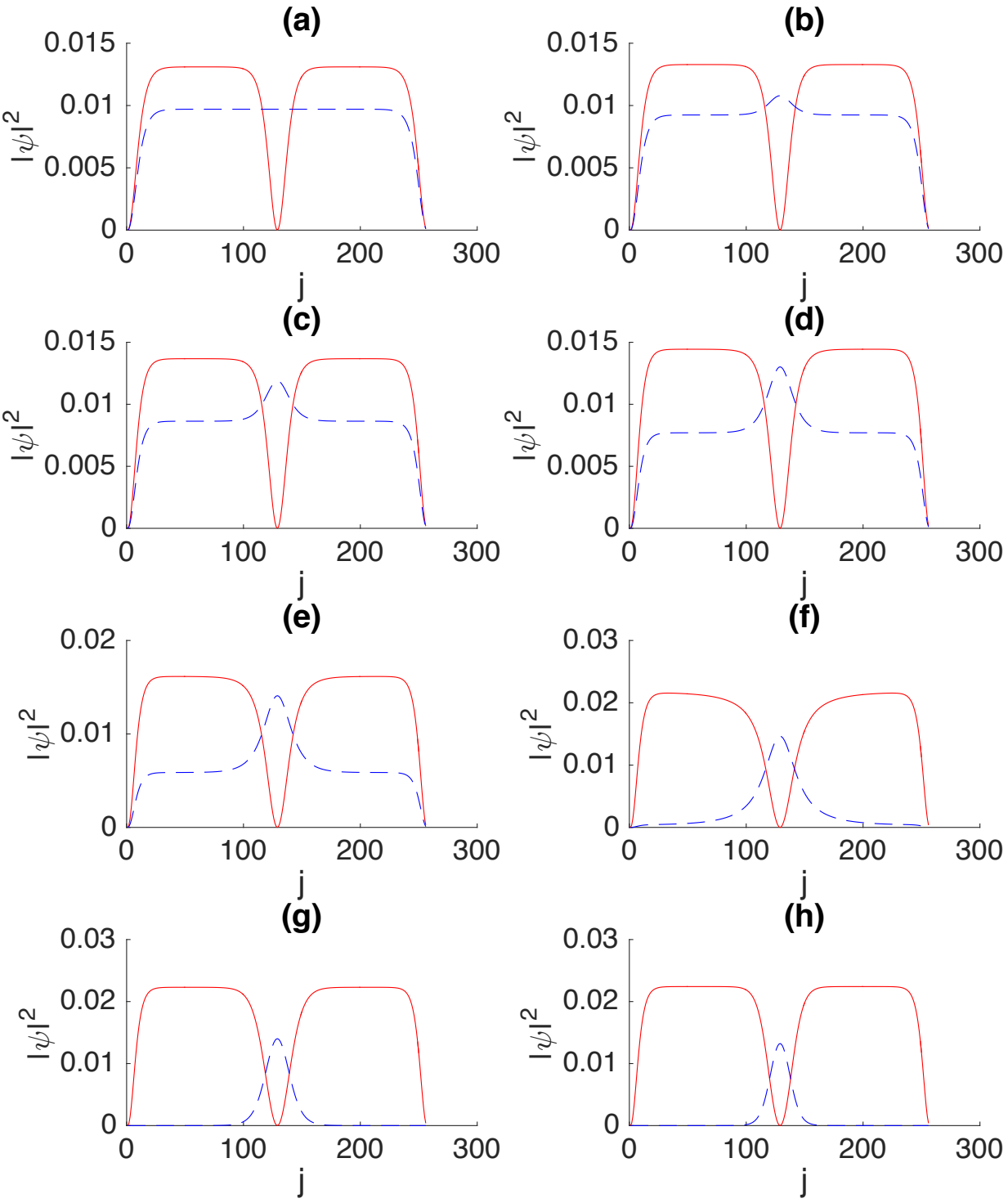

Figure 3.4 Dark-bright solitons through the miscible/immiscible phase transition. We take $g_1 = 2.0$ and $g_2 = 2.7$. in (a)-(h) $g = 0.0, 0.4, 0.8, 1.2, 1.6, 2.0, 2.4, 2.8$, respectively. The phase transition occurs at $g = 2.3$, leading to well-localized bright solitons in the immiscible domain in the last two panels.

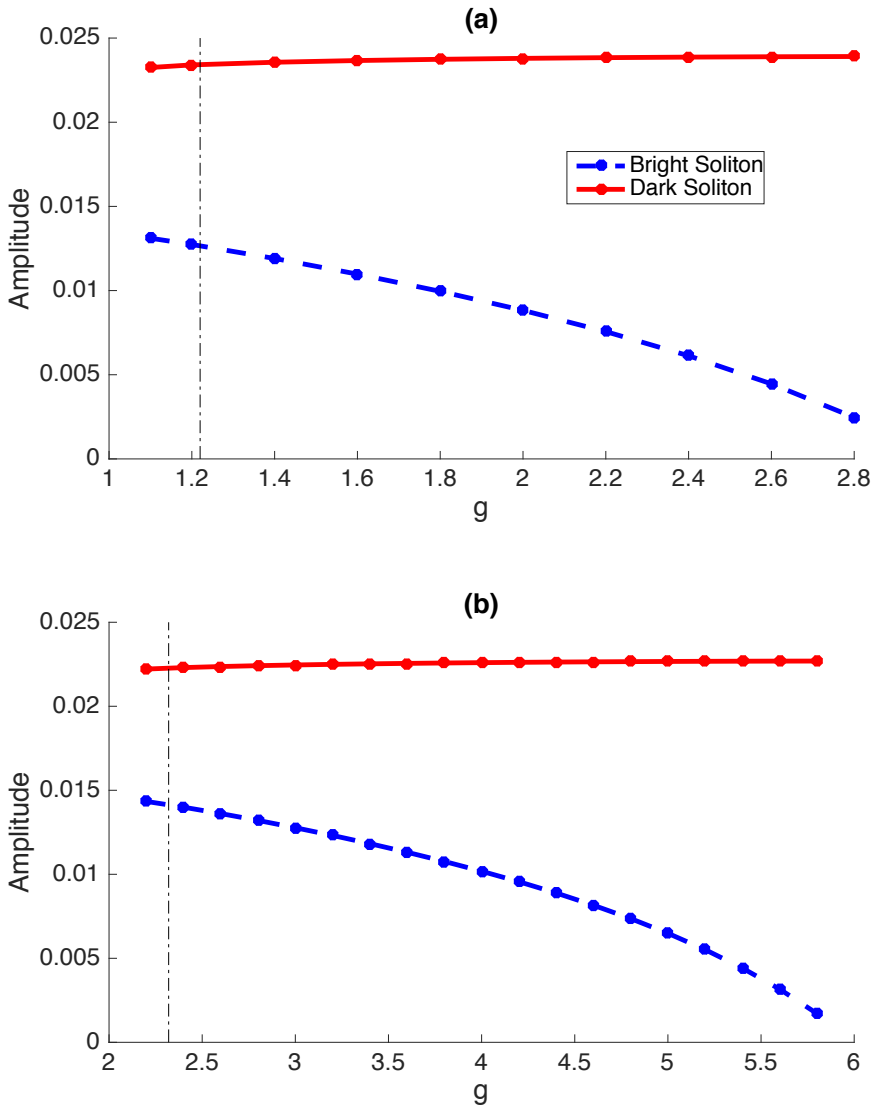

Figure 3.5 Amplitude of the bright and dark component versus the coupling interaction g. We measure the amplitudes of the two components at the ground state with different values of g_1, g_2 and g. (a) $g_1 = 1.0, g_2 = 1.5$ (b) $g_1 = 2.0, g_2 = 2.7$.

that when the intercomponent coupling is zero the size of the two densities of the dark and bright component is governed by the intra-component couplings, g_1 and g_2, respectively. As we increase g, the dark component density exerts a repulsive force on the bright component density and forces it to localize in the center. As we pass the phase transition point when $g > 2.3$, the density of the bright soliton component continues to decrease, thus its amplitude decreases too, and the density of the dark soliton component increases at a slow rate compared to the change in the bright component density. The difference between the rate of change with g in the density between the two components depends on their sizes. The dark soliton component is larger than the bright soliton component, as shown in Figure 3.4, and therefore increasing the density of the dark soliton component will have a small effect on increasing its amplitude. Finite size effects allow the soliton to exist slightly beyond the miscibility boundary indicated by the dot-dashed line in Figure 3.4.

3.9 Dark-Bright Soliton Dynamics

We now turn to internal excitations of the dark-bright soliton. Our procedure is to imprint a phase solely on the bright component, via state-selective manipulation of BECs. The ensuing dynamics involves not only internal oscillations but also an overall velocity of both dark and bright components, i.e., the Goldstone mode. The results for our two case studies from Figure 3.5 are shown in Figure 3.6. We find the velocity of the dark-bright soliton drops quickly at the beginning then it slowly decreases as the coupling interaction increases. This behavior can be understood if we examine the density of the bright component. We find the form depicted in Figure 3.5, i.e., that the amplitude (and therefore the density) of the bright component decreases as the coupling interaction increases. In this case, the imprinted phase on the "small" bright component will not pull the dark soliton quickly and therefore the velocity of the dark-bright soliton changes at a small rate as the bright component amplitude decreases. In addition, the initial velocity of the dark-bright soliton when g_1=2.0 and g_2=2.7 is higher than the case when g_1=1.0 and g_2=1.5 because the difference between the amplitudes of the two components in the former case is less than in the latter. In

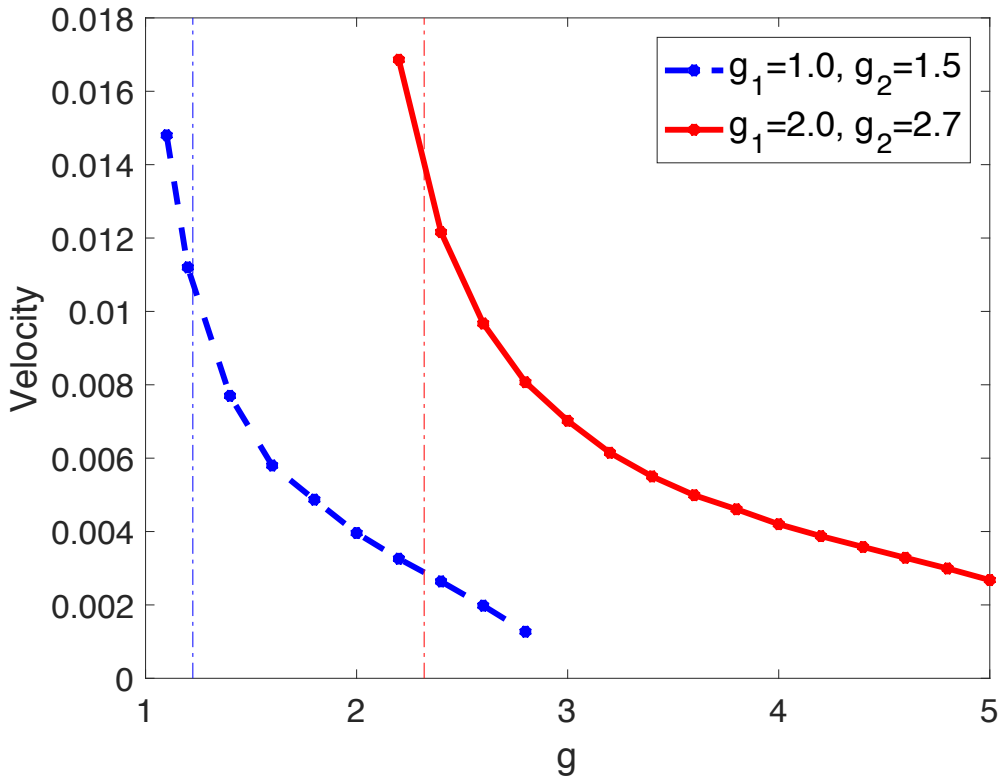

Figure 3.6 Collective velocity of dark-bright soliton after phase imprint. We take a phase imprint of ϕ=0.5 and two different cases for g_1 and g_2, in the immiscible domain when $g > \sqrt{g_1 g_2}$. See Sec. 3.10 for converted units. Note that a dark-bright soliton can be created as we get very close to this line from the miscible domain. The amplitude of the bright soliton controls the rate of the velocity of the dark-bright soliton. As we increase the intercomponent coupling interaction, g, the amplitude of the bright soliton decreases as shown in Figure 3.5 and therefore the density of the bright soliton decreases too. Imprinting a phase on the small density bright soliton will have a small effect on dragging the dark soliton and therefore will result in a small velocity of the dark-bright soliton.

other words, a phase imprinted on the bright component will have a bigger impact in the former case. The dashed lines distinguish the miscible and immiscible domains. Note that a dark-bright soliton can be created as we approach this line from the miscible domain.

Having explicated the trends in the overall velocity or Goldstone mode, we examine our second mode of interest, namely the frequency of internal excitations. In Figure 3.7, we first discuss the numerical results then we will discuss the comparison between these outcomes and the analytical results. Numerically, different values of imprinted phases on the bright component are shown in the figure ($\phi = 0.7$ and $\phi = 1.0$). The oscillation frequency of the two components versus the coupling interaction g is almost identical, indicating that the frequency is amplitude independent. Imprinting a large phase on the bright component can decouple the two components in the dark-bright soliton. In the case with $\phi = 1.0$ the imprinted phase is large enough to cause a disturbance when the coupling coefficient is close to the miscible domain and therefore it shows a different oscillation frequency for g just above the critical value for the phase transition. In the same figure we plot also the analytical results obtained from Eq. (3.18). We did not include the oscillation of the width, i.e., the breather mode, in the analytical calculations because we can only perform the calculations for in-phase width oscillation analytically. In contrast, in the numerical calculations the motion also includes arbitrary-phase width oscillation. The range of the values of g is bounded between two limits. In the lower limit, when $g < \sqrt{g_1 g_2}$, i.e., in the miscible domain, the bright component in the dark-bright soliton exists on a top of a finite background caused by finite size effects (for example see Figure 3.4). Therefore, imprinting phase on the bright soliton component to start the oscillation motion will also move the finite background density, causing a larger scale disturbance and affecting the frequency results. The upper limit of the values of g come from the fact that for large g the ground state energy of the system does not support a dark-bright soliton because of the strong intercomponent interactions between the dark component and the bright component.

We see also in Figure 3.7 that the comparison between the numerical and the analytical results becomes better as we increase the intercomponent interactions g. When g is close to the miscible domain the oscillation of the width of the two components is stronger due to the fact that g is small and therefore the width oscillation contributes to the oscillation of the two components. When g is large, the oscillation of the width of the two components becomes smaller due to the fact that the repulsive interaction between the two component is stronger and therefore it will force the two components to be confined in their region. Thus as we increase g we will have a smaller contribution of the width oscillation mode in the oscillation of the two components which will improve the comparison between the numerical and the analytical results.

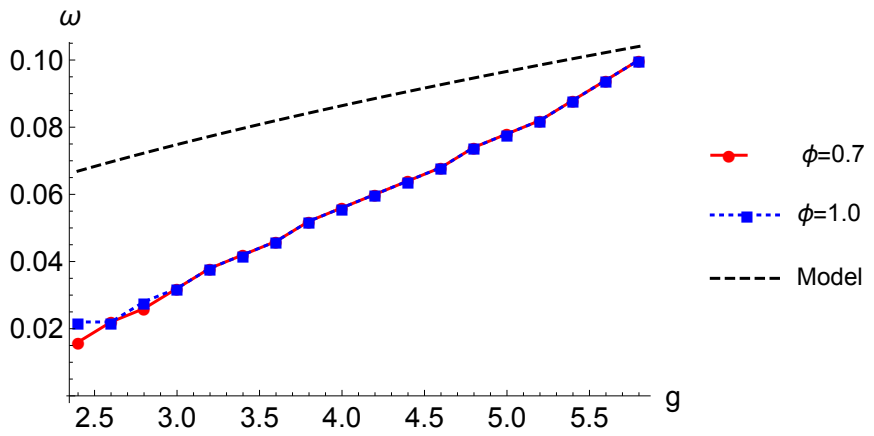

Figure 3.7 Trends in internal dynamics. Oscillation frequency of the two components in the dark-bright soliton, with $g_1 = 2.0$, $g_2 = 2.7$ and $\phi = 0.7$ and 1.0, obtained from numerical integration of Eq. (3.3) verses the oscillation frequency obtained from the analytical calculations, Eq. (3.18). Numerically, the oscillation frequency of the two components versus the coupling coefficient g for different values of ϕ shows that the oscillation frequency is amplitude independent in the case explored. We also plot the result from Eq. (3.18) to compare the two outcomes from the analytical and numerical calculations. The discrepancy between numerics and the model are due to the restricted ansatz (equal soliton widths) in the variational calculation.

To explain the data underlying Figs. Figure 3.6 and Figure 3.7, we show an example of the complete numerical integration and the resulting density and phase of the two-component wavefunction in Figure 3.8. To obtain this data, we numerically integrate Eq. (3.3) using a pseudo-spectral method as mentioned in Sec. 3.1. Figure Figure 3.8 clarifies many

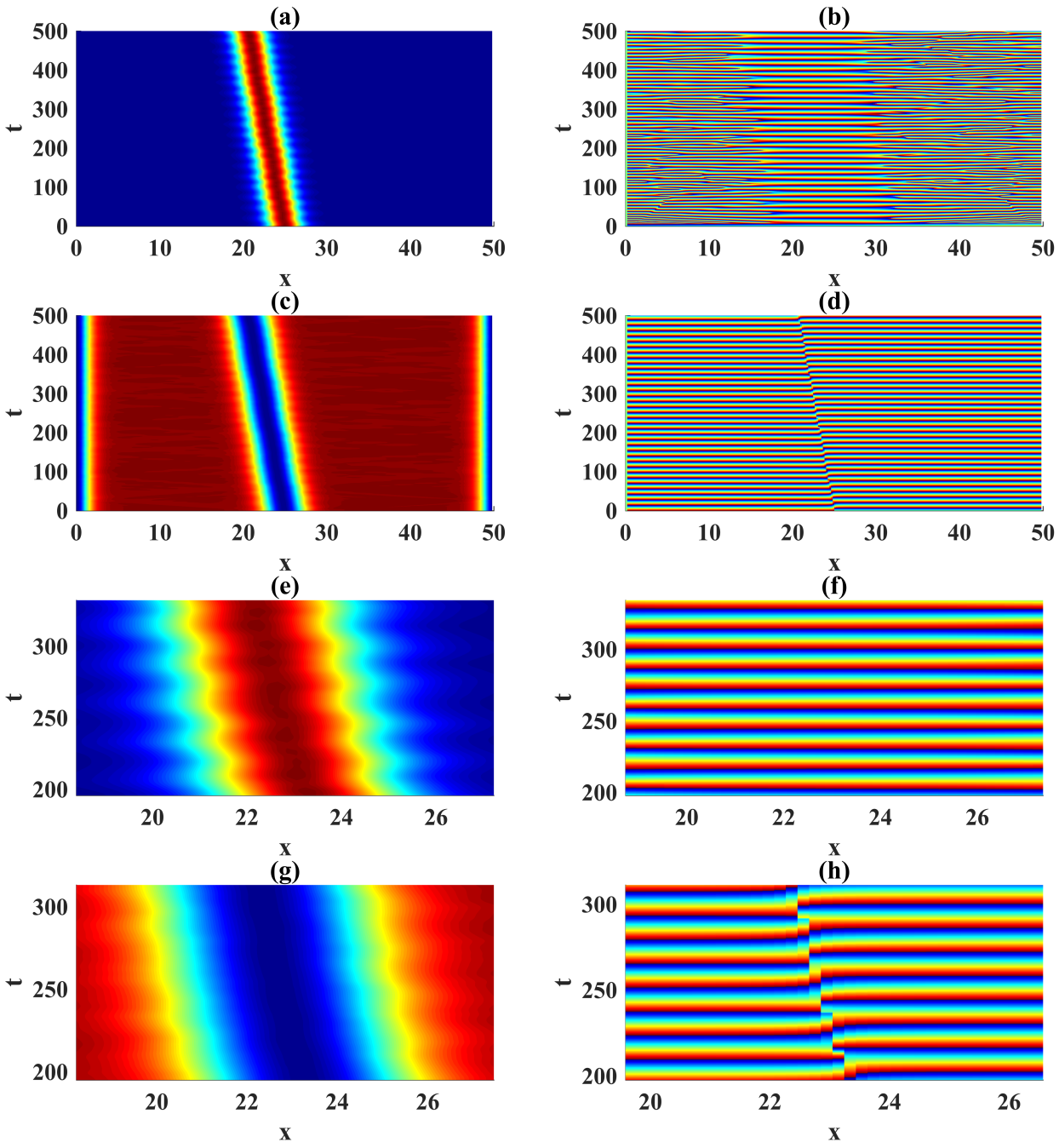

Figure 3.8 Oscillation of the two-component wave function $|u(x,t)|^2$ and $|v(x,t)|^2$ in the immiscible domain with $g_1 = 2.0$, $g_2 = 2.7$, $g = 3.2$ and ϕ=0.7. In (a), (b), (c) and (d) represent the density and the phase of the bright and dark components, respectively. In figures (e), (f), (g) and (h) we plot the previous figures with a small time and space intervals to show the oscillations.

features of the interactions between the two components in dark-bright soliton. Figures Figure 3.8(a)-(b) show the density and the phase of the oscillating bright component, while Figures Figure 3.8(c)-(d) show the corresponding dark component oscillations. Figures Figure 3.8(e)-(h) present a zoom window on a small interval to display the oscillation more clearly. The interaction coefficients are g_1=2.0, g_2=2.7, g=3.2 and ϕ=0.7. The oscillation frequency amplitude of the dark component decreases as we increase the interaction coefficient which in turn makes the observation of the oscillation in the dark component not obvious compared to the oscillation of the bright component. For the above interaction coefficient values the amplitude of the bright component is almost half the amplitude of the dark component, as shown in Figure 3.8 and Figure 3.5 both.

Finally, we examine the break-up of a dark-bright soliton. In Figure 3.9, we again plot the dark-bright soliton density and phase in both components, but this time we imprint a relatively large phase on the bright soliton component in order to unbind the dark-bright soliton. We emphasize that the bright component of a dark-bright soliton can only exist at long times in bound form. When the imprinting phase is large (i.e. $\phi = 6$ and 10) a significant portion of the bright soliton density escapes from the effective potential created by the dark soliton component (see Figure 3.10) and therefore breaks up the dark-bright soliton. Using the interaction coefficients mentioned in Figure 3.9 in Eq. (3.27) in addition to setting $N_1 \approx 0.503 * 10^5$, $N = 1 * 10^5$, $\theta_1 = 1$, $\phi_2 = 1$, $\theta_2 = 2$ and the width = 1 we find that the system oscillates as long as $\phi < 3.4$. Above this value the dark-bright soliton start to unbind or break up. We find this value in good agreement with the numerical results obtained in Figure 3.9 where we see that a significant fraction of the bright soliton component breaks away from the effective potential created by the dark soliton component around $\phi = 6$ and above.

To quantify the breakup, in Figure 3.10 we plot the percentage of density loss of the bright component in the dark-bright soliton as a function of time for different phase imprinting values. Below the critical value of ϕ, the bright component density is almost intact. Above

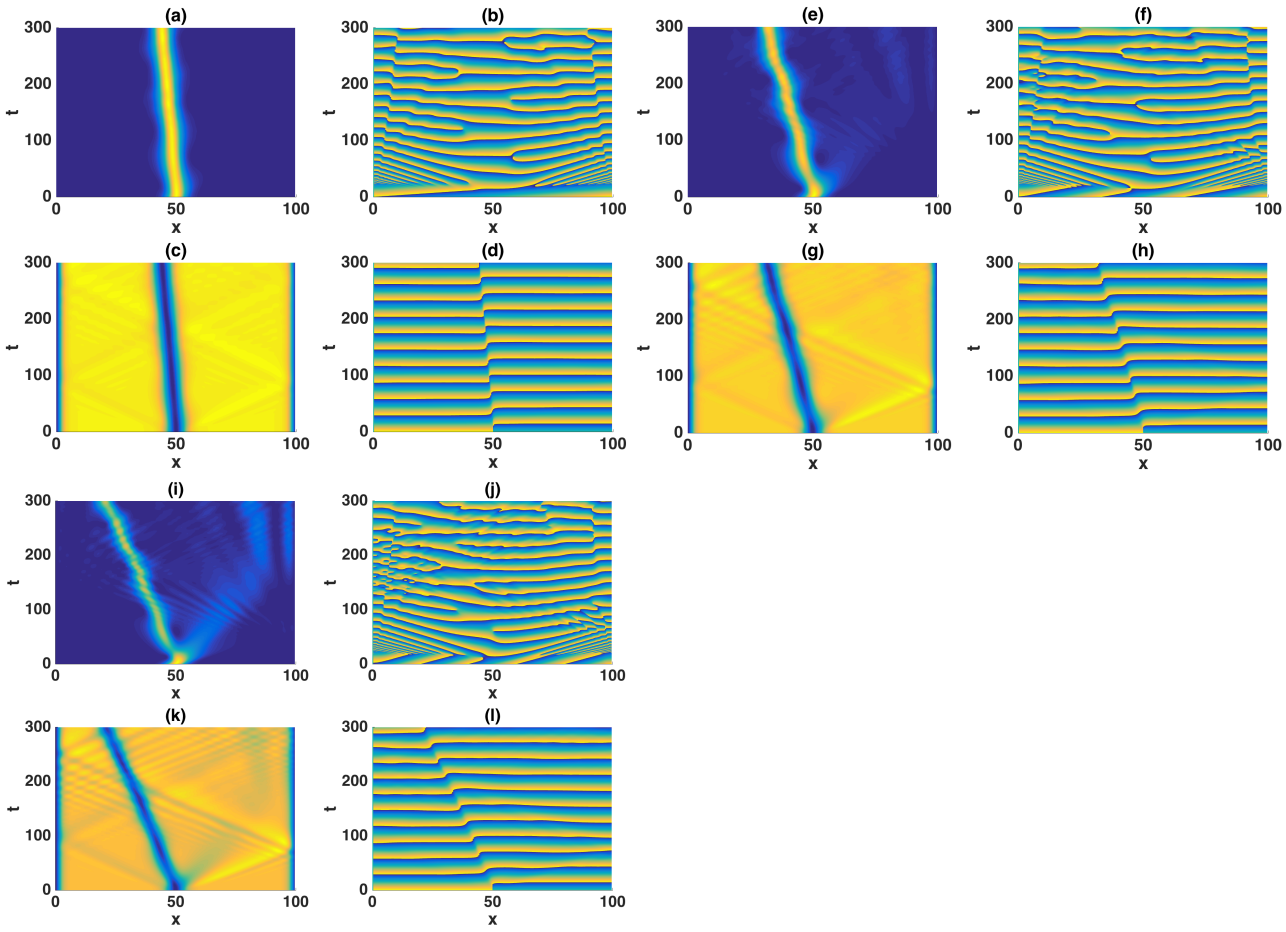

Figure 3.9 Unbinding of a dark-bright soliton. We demonstrate break-up of the dark-bright soliton by imprinting different values of the phase, ϕ, on the bright component with interaction coefficients $g_1 = 2.0$, $g_2 = 2.7$, $g = 2.6$. Panels (a)-(d), (e)-(h) and (i)-(l) use phase imprintings of $\phi = 2$, 6 and 10, respectively. In the left (right) panel, is the density (phase) of the bright and the dark component. The box dimension is $L = 100$.

the critical value the bright component start to lose a significant portion of the density, characteristic of the breaking up of the dark-bright soliton. The integration region for the bright component density is taken to be the line extending a distance, r, on either side of the dark component center, r_0. Therefore, the local bright component density is given by

$$E_{BS} = \int_{r_0-r}^{r_0+r} dx \ |v|^2 \tag{3.28}$$

We interpret the dark soliton component center as the point of minimum density. We define numerically the distance $r = c_1(L/n_x)$ where L and n_x represents box dimension and grid size, respectively. The factor $c_1 = 50$ defines the cut-off region which is wide enough to capture the dark component area, as can be seen in Figure 3.9.

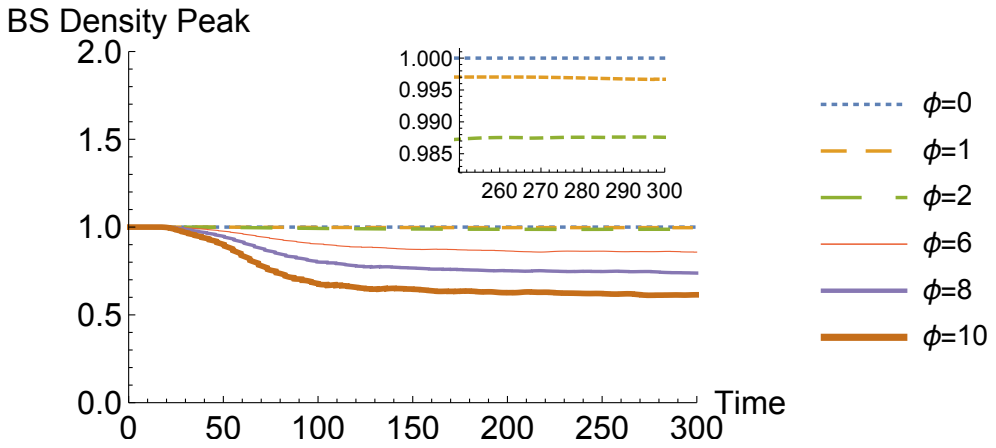

Figure 3.10 Percentage density loss of the bright component in the dark-bright soliton for different phase imprinting values. Below the critical value mentioned above (i.e. $\phi = 0$, 1 and 2) the dark-bright soliton maintains its internal structure and the bright soliton component density is almost intact, see the inset. Above the critical value (i.e. $\phi = 6$, 8 and 10) we see that the bright soliton losses density due to the relative strong kick that allows for a significant portion of the density to escape. The inset also highlights the stability of the dark-bright soliton at long times for small enough phase imprinting.

3.10 Units

Typical experimental values for a ^{87}Rb BEC are $\omega_\perp \approx 2\pi \times 720$ Hz, $a_s \approx 5.1 * 10^{-9}$m and $N \approx 10^5$. For these parameters, the length scale is $\ell_\perp \approx 0.4\ \mu m$ and the time scale is $t_\perp \approx 0.22\ ms$. An example of using the units in the table to calculate the frequency of the

Table 3.1 Converted Units.

SI Units	Factor per Unit	Unitless	Unit
$\tilde{x}$	$0.4 * 10^{-6}$	x	meter
$\tilde{t}$	$0.22 * 10^{-3}$	t	second
$\tilde{g_{ij}}$	13.7	g_{ij}	k_B·nK· μm
$\tilde{\omega}$	$4.5 * 10^3$	ω	Hz
$\tilde{u_0}^2$	33.9	u_0^2	k_B·nK
$\tilde{u}\left(\tilde{x},\tilde{t}\right)$	$1.57 * 10^3$	$u\left(x,t\right)$	$\frac{1}{\sqrt{\text{meter}}}$
$\tilde{v}\left(\tilde{x},\tilde{t}\right)$	$1.57 * 10^3$	$v\left(x,t\right)$	$\frac{1}{\sqrt{\text{meter}}}$

oscillation mode in ^{87}Rb is obtained by examining Figure 3.7. For $g = 4$ we find that the oscillation frequency ω is 0.056. Using the units in Table 3.1, the equivalent SI units are ω=252 Hz with g=54.8 $k_B \cdot \text{nK} \cdot \mu\text{m}$, which are reasonable numbers for an experiment in ^{87}Rb.

3.11 Conclusions

We calculated the normal modes of the system using hyperbolic tangent for the dark component and hyperbolic secant for the bright component. We found the velocity of each component depends on the imprinted phase, following the known expression for the velocity of the condensate in which the phase depends on x in order to cause the dark-bright soliton components to move. In the dark component, the velocity also depends on the amplitude. There are two modes of the oscillation of the dark-bright soliton, the Goldstone mode, which we interpreted as a moving dark-bright soliton without internal oscillation of the two components, and the oscillation mode of the two components relative to each other. In addition, we found numerically that in order to find a bright component in a dark-bright soliton the density of the bright component is required to be less than the density of the dark component. This result was supported by analytical calculations in Sec. 3.4 where we found that in order to make the dark and bright components oscillate we must meet this criterion. In Sec. 3.6, we calculated different aspects of the interaction between the two components. Of particular interest is the two-component oscillation in the dark-bright soliton, where we

found that the oscillation frequency is nearly independent of the imprinted phase up to a critical value, meaning that the frequency is amplitude independent. We illustrated the oscillation of the density and the phase of the two-component dark-bright soliton. Also, we calculated the binding energy of the dark-bright soliton. We compared the binding energy to the kinetic energy and the mean field energy of the dark-bright soliton in order to find the critical value of the imprinted phase on the bright component that breaks or unbinds the dark-bright soliton. Future work may extend our study to three-component solitons in different hyperfine states of the same condensate or for different species of atoms. In the multi-component case, the phase between the different components is coherent and the norm is not separately conserved.

3.12 Fixed point singularity

Here we wish to prove that the system of Equations (4.13) does not posses a singularity. In particular, Eq. (3.9a) with $l \equiv b(t) - d(t)$ becomes

$$\begin{aligned}\frac{d}{dt}\phi_1(t) =& \alpha \operatorname{csch}\left(\frac{l}{w}\right)^4 \left\{ 2l\left[2+\cosh\left(2\frac{l}{w}\right)\right] \right. \\ & \left. -3w\sinh\left(2\frac{l}{w}\right)\right\} \\ =& 4l\alpha\operatorname{csch}\left(\frac{l}{w}\right)^4 + 2l\alpha\cosh\left(2\frac{l}{w}\right)\operatorname{csch}\left(\frac{l}{w}\right)^4 \\ & - 3w\alpha\operatorname{csch}\left(\frac{l}{w}\right)^4 \sinh\left(2\frac{l}{w}\right) .\end{aligned}$$

When we expand the r.h.s of the above equation around the fixed point the terms l^{-3} and l^{-1} cancel out, and we are left with terms proportional to l. That is, the fixed point of the system (i.e. $l = 0$) is valid. Note that we will not be able to address this fact if we work with Eq. (3.11) instead of Eqs. (4.13).

CHAPTER 4

SCATTERING OF A DARK-BRIGHT SOLITON BY AN IMPURITY

We study the dynamics of a dark-bright soliton interacting with a fixed impurity using a mean-field approach. The system is described by a vector nonlinear Schrodinger equation (NLSE) appropriate to multicomponent Bose-Einstein condensates. We use the variational approximation, based on hyperbolic functions, where we have the center of mass of the two components to describe the propagation of the dark and bright components independently. Therefore, it allows the dark-bright soliton to oscillate. The fixed local impurity is modeled by a delta function. Also, we use perturbation methods to derive the equations of motion for the center of mass of the two components. The interaction of the dark-bright soliton with a delta function potential excites different modes in the system. The analytical model capture two of these modes: the relative oscillation between the two components and the oscillation in the widths. The numerical simulations show additional internal modes play an important role in the interaction problem. The excitation of internal modes corresponds to inelastic scattering. In addition, we calculate the maximum velocity for a dark-bright soliton and find it is limited to a value below the sound speed, depending on the relative number of atoms present in the bright soliton component and excavated by the dark soliton component, respectively. Above a critical value of the maximum velocity, the two components are no longer described by one center of mass variable and develop internal oscillations, eventually breaking apart when pushed to higher velocities. This effect limits the incident kinetic energy in scattering studies and presents a smoking gun experimental signal.

4.1 Introduction

Scattering is a fundamental physical process and essential tool to investigate objects in quantum theory [55]. We determine the low-energy interactions of subatomic particles by

the well-known quantity, scattering length. Within this process, we acquire information regarding the nature of the interaction. Additionally, the interaction of solitons with localized impurities is a general and fundamental problem [6]. Utilizing the NLSE, many studies investigate the scattering of a bright or dark soliton with a localized impurity [56–62]. An impurity can be represented by a delta function as long as the size of the impurity is small enough compared to the soliton size. In BECs, one can create a delta function by a sharply focused far-detuned laser beam [6]. Of particular interest in soliton interactions with impurities is the interaction of two-component solitons with a delta function potential due to the rich dynamics that can be seen in these systems. The interaction of dark-bright solitons with an impurity has been the focus of other studies [63, 64]. But, to the best of our knowledge, the problem of the interaction of dark-bright solitons, with two independent centers of mass for the dark and bright components, with localized impurities and using the Lagrangian approach method has not been addressed so far. As we will show, the interplay between internal modes and the impurity is key to understanding the scattering process correctly.

In this work, we study the problem using coupled NLSEs, sometimes called the vector NLSE, that is appropriate to describe matter-wave dark-bright soliton in BEC [65]. The existence of the delta function potential modifies the background of the dark soliton component, and therefore one should account for this effect. We do so by considering a perturbation method [46, 66] where we adjust the coupled NLSEs to account for the delta function as a small perturbation term. We proceed by adopting a modified Euler-Lagrange equation, called the variational Lagrangian approach, to calculate the equations of motion for the two propagating centers of mass (i.e., the locations of the dark component and the bright component) [52, 67, 68]. The second part of this work is dedicated to investigating the dark soliton maximum velocity when interacting with a bright soliton in a dark-bright soliton. It is a well-known fact that the maximum velocity of a one-component dark soliton is the speed of sound [9]. We show that this qualitative characteristic of the dark soliton velocity is changing when we add a bright soliton to the picture. We adopt a known ansatz to describe

the propagation of the dark-bright soliton. This ansatz is the exact solution for a dark-bright soliton with equally interacting coefficients (i.e., Manakov case [69]). We then extend our results numerically in the more general case. We show that the incident velocity and therefore kinetic energy of the dark-bright soliton on the impurity is limited by the number of atoms in the bright soliton relative to the "hole" or density notch made by the dark soliton. Above a critical velocity, the dark-bright soliton develops oscillations, and when pushed further breaks up. This sets definite limits on scattering studies.

This article is organized as follows. In Sec. 4.2, we study the scattering of the dark-bright soliton by a delta function potential using a variational approximation method based on a hyperbolic tangent (hyperbolic secant) for the dark (bright) soliton component for the two-component ansatz and utilizing a perturbation method to account for the effect of the delta function on the background. In Sec. 4.2.3, we examine the velocity of the dark-bright soliton and obtain an analytical expression describing the effect of the bright component amplitude on the velocity of the dark-bright soliton. In Sec. 4.3.1, we investigate the scattering of the dark-bright soliton by a delta function potential by numerically integrating the dimensionless NLSE using an algorithm employing a pseudospectral method. We study the velocity of the dark-bright soliton numerically in Sec. 4.3.2. Finally, we present our conclusions in Sec. 5.4.

4.2 Analytical Calculations

4.2.1 Lagrangian density and ansatz

We start by introducing the coupled NLSEs:

$$\begin{aligned} i\frac{\partial}{\partial t}u + \frac{1}{2}\frac{\partial^2}{\partial x^2}u - \left[g_1|u|^2 + g|v|^2 - u_0^2\right]u &= V(x)u, \\ i\frac{\partial}{\partial t}v + \frac{1}{2}\frac{\partial^2}{\partial x^2}v - \left[g_2|v|^2 + g|u|^2\right]v &= V(x)v, \end{aligned} \tag{4.1}$$

where $u \equiv u(x,t)$ and $v \equiv v(x,t)$ are the wave functions for the dark and bright soliton components, respectively. The dark soliton wave function is rescaled to remove the background contribution, u_0, which is a standard procedure to avoid divergent normalization and

energy [52]. The potential in the above equations takes the form,

$$V(x) = \alpha\ \delta\left(x\right), \tag{4.2}$$

for both components. We assume $\alpha \ll u_0$, and therefore we consider the potential to behave like a small perturbation effect which allows us to use the perturbation method. The same length-based units as we have described previously [65] are used here: [x]=[L], [t]=[L^2], $[g_1, g_2, g]=[u_0]=[L^{-1}]$, $[\alpha]=[\delta(x)]=[L^{-1}]$, $|u, v|^2 = [L^{-1}]$, where the square brackets mean "the units of." The existence of a delta function affects the background of the dark-bright soliton, as seen in Figure 4.1, and we need to modify the background also to account for this effect. We assume the dark soliton component lives on a modified Thomas–Fermi cloud, $|u_{\rm TF}|^2$, which accounts for the effect of the delta function on the background [63],

$$|u_{\rm TF}|^2 \approx \frac{1}{g_1}(u_0^2 - \alpha u_0 \exp(-2|x|)), \tag{4.3}$$

and by using the following transformations,

$$|u|^2 \to |u_{\rm TF}|^2|u|^2,\ |v|^2 \to \frac{|v|^2}{u_0^2},\ t \to u_0^2 t,\ x \to u_0 x, \tag{4.4}$$

we recase Eqs. (4.1) into the following:

$$\begin{aligned} i\frac{\partial}{\partial t}u + \frac{1}{2}\frac{\partial^2}{\partial x^2}u - \left[g_1\left|u\right|^2 + g\left|v\right|^2 - 1\right]u &= R_u \\ i\frac{\partial}{\partial t}v + \frac{1}{2}\frac{\partial^2}{\partial x^2}v - \left[g_2\left|v\right|^2 + g\left|u\right|^2\right]v &= R_v, \end{aligned} \tag{4.5}$$

where the RHS of Eqs. (4.5) represent the perturbation effects,

$$\begin{aligned} R_u &= \frac{\alpha}{u_0}\left[(1 - g_1|u|^2)u - \frac{x}{|x|}\frac{d}{dx}u\right]e^{-2|x|} \\ R_v &= \frac{\alpha}{u_0}\left[\delta\left(x\right) - g|u|^2 e^{-2|x|}\right]v, \end{aligned} \tag{4.6}$$

where $\alpha \ll 1$ in these units. We work with the following ansatz,

$$u(x,t) = \frac{1}{\sqrt{g_1}}\{c(t)\tanh\left[\frac{(x+d(t))}{\mathrm{w}(t)}\right] + iA(t)\} \tag{4.7}$$
$$v(x,t) = \frac{1}{\sqrt{g_2}}F(t)\mathrm{sech}\left[\frac{(x+b(t))}{\mathrm{w}(t)}\right] e^{i[\phi_0(t)+x\phi_1(t)]}.$$

Here $c(t)$ and $A(t)$ are the amplitude and velocity for the dark soliton component, respectively. The amplitude for the bright soliton component is $F(t)$. The velocity of the bright soliton is given by $\phi_1(t)$, and $d(t)$ and $b(t)$ are the position of the dark and bright soliton, respectively. The width for the two components is $\mathrm{w}(t)$ and $\phi_0(t)$ is a phase that gives rise to a complex amplitude of the bright component. We have a total of eight variational parameters that describe the propagation of the dark-bright soliton. The perturbation terms account for the effect of the potential (i.e., delta function). In the absence of the perturbation terms, the problem reduced to a propagation of the two–component dark-bright soliton [65]. We use the normalization conditions,

$$\int_{-\infty}^{\infty} dx\ \left(\frac{1}{g_1} - |u|^2\right) = \frac{N_1}{N}, \tag{4.8a}$$
$$\int_{-\infty}^{\infty} dx\ |v|^2 = \frac{N_2}{N}, \tag{4.8b}$$

for the dark and bright component, respectively. We subtract the background in the first component of Eqs. (4.8), therefore, N_1 is the number of atoms displaced by the dark soliton. We define the total number of atoms N involved in the dark and bright solitons as

$$N_1 + N_2 = N, \tag{4.9}$$

Using the ansatz, Eqs. (4.7), in the normalization, Eqs. (4.8), we find the relation between N_1, N_2 and the coefficients of the two components in the dark-bright soliton:

$$\frac{2c^2 w}{g_1} = \frac{N_1}{N}, \tag{4.10}$$
$$\frac{2F^2 w}{g_2} = \frac{N_2}{N}.$$

The modified Euler-Lagrange equation [52],

$$\frac{\partial L}{\partial a_j} - \frac{d}{dt}\left(\frac{\partial L}{\partial a_j'}\right) = 2\ \mathrm{Re}\left\{\int_{-\infty}^{\infty} R_u^* \frac{\partial u}{\partial a_j} + R_v^* \frac{\partial v}{\partial a_j}\, dx\right\}, \tag{4.11}$$

here a_j represent the variational parameters in the ansatz. The Lagrangian density for the system of coupled equations, Eqs. (4.5) when $R_u = R_v = 0$ is:

$$\begin{aligned}\mathcal{L} =& \frac{i}{2}\left[u^*\frac{\partial u}{\partial t} - u\frac{\partial u^*}{\partial t}\right]\left[1 - \frac{1}{g_1\left|u\right|^2}\right] - \frac{1}{2}\left|\frac{\partial u}{\partial x}\right|^2 \\ & - \frac{1}{2}\left[\sqrt{g_1}\left|u\right|^2 - \frac{1}{\sqrt{g_1}}\right]^2 + \frac{i}{2}\left[v^*\frac{\partial v}{\partial t} - v\frac{\partial v^*}{\partial t}\right] \\ & - \frac{1}{2}\left|\frac{\partial v}{\partial x}\right|^2 - \frac{g_2}{2}\left|v\right|^4 - g\left|u\right|^2\left|v\right|^2.\end{aligned} \tag{4.12}$$

We utilize the modified Euler-Lagrange equation, Eq. (4.11), to account for the effect of the delta function on the background. By inserting the ansatz, Eq. (4.7), into the Lagrangian density, Eq. (4.12), we obtain the Lagrangian as a function of the variational parameters. Then, we use Eq. (4.11) with the perturbation terms, Eq. (4.6) to find the equations of motion (EOMs) of the system.

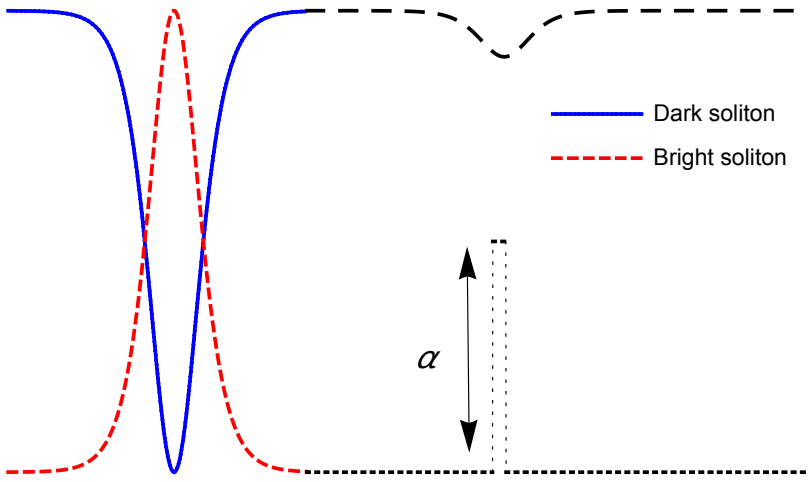

Figure 4.1 The effect of a delta function potential on the background of a dark-bright soliton. The delta function potential is modeled by Thomas-Fermi cloud as described by Eq. (4.3).

4.2.2 Evolution equations

The outcome of the calculations in Sec. 4.2.1 is a system of ordinary differential equations (ODEs) that describe the propagation of dark-bright solitons toward a delta function. Below, we write down only the equations that we are going to use to form a system of second order coupled ODEs,

$$\frac{d}{dt}\phi_1(t) = \frac{gc^2(t)}{g_1 \mathrm{w}^2(t)} \operatorname{csch}\left(\frac{b\,(t)-d\,(t)}{\mathrm{w}(t)}\right)^4 \tag{4.13a}$$
$$\times\left\{2\left(b\,(t)-d\,(t)\right)\left[2+\cosh\left(2\frac{b\,(t)-d\,(t)}{\mathrm{w}(t)}\right)\right]\right.$$
$$\left.-3\mathrm{w}(t)\sinh\left(2\frac{b\,(t)-d\,(t)}{\mathrm{w}(t)}\right)\right\}+\frac{g_2}{2F^2(t)\mathrm{w}(t)}\Gamma_1,$$
$$\frac{d}{dt}A(t) = \frac{gc(t)F^2(t)}{2g_2 \mathrm{w}(t)} \operatorname{csch}\left(\frac{b\,(t)-d\,(t)}{\mathrm{w}(t)}\right)^4 \tag{4.13b}$$
$$\times\left\{2\left(b\,(t)-d\,(t)\right)\left[2+\cosh\left(2\frac{b\,(t)-d\,(t)}{\mathrm{w}(t)}\right)\right]\right.$$
$$\left.-3\mathrm{w}(t)\sinh\left(2\frac{b\,(t)-d\,(t)}{\mathrm{w}(t)}\right)\right\}-\frac{g_1}{4c(t)}\Gamma_2,$$
$$\frac{d}{dt}b\,(t) = -\phi_1\,(t)\,, \tag{4.13c}$$
$$\frac{d}{dt}d\,(t) = -\frac{g_1 N_1 A(t)}{2N\sqrt{1-A^2(t)}}. \tag{4.13d}$$

Here, Eq. (4.13d) is obtained by inserting the ansatz, Eq. (4.7), in the coupled NLSEs, Eqs. (4.5), and separate the imaginary and real parts. In our calculations we take the delta function as located at the origin $x = 0$ without loss of generality. We assume that the oscillations between the two component is very small (i.e. $b(t) - d(t) << 1$). The perturbation component Γ_1 in Eq. (4.13a) is obtained by solving the RHS of Eq. (4.11) with $a_j = b$ and the perturbation component Γ_2 in Eq. (4.13b) is obtained by solving the RHS of Eq. (4.11) with $a_j = d$. As a result, we obtain the following terms,

$$\Gamma_1 = \frac{8g\alpha b(t)F^2(t)\exp(\frac{2b(t)}{\mathrm{w}(t)})}{g_1 g_2 u_0 \mathrm{w}^2(t)} + \frac{4g\alpha c^2(t)F^2(t)}{15 g_1 g_2 u_0 \mathrm{w}^2(t)} \tag{4.14a}$$
$$\times (b(t)-d(t))\,\mathrm{sech}^4\left(\frac{b(t)}{\mathrm{w}(t)}\right)\left\{-1+2\cosh\left(\frac{2b(t)}{\mathrm{w}(t)}\right)\right\}$$
$$-\frac{8g\alpha F^2(t)}{g_1 g_2 u_0 \mathrm{w}(t)}\sinh\left(\frac{2b(t)}{\mathrm{w}(t)}\right)\log\left[1+\exp(\frac{2b(t)}{\mathrm{w}(t)})\right]$$
$$+\frac{2g\alpha F^2(t)}{g_1 g_2 u_0 \mathrm{w}(t)}\cosh\left(\frac{2b(t)}{\mathrm{w}(t)}\right)\mathrm{sech}^2\left(\frac{b(t)}{\mathrm{w}(t)}\right)\tanh\left(\frac{b(t)}{\mathrm{w}(t)}\right)$$
$$-\frac{2\alpha F^2(t)\left(-3g+3g_1+gc^2(t)\right)}{3g_1 g_2 u_0 \mathrm{w}(t)}\mathrm{sech}^2\left(\frac{b(t)}{\mathrm{w}(t)}\right)\tanh\left(\frac{b(t)}{\mathrm{w}(t)}\right)$$

and for Γ_2 we get,

$$\Gamma_2 = \frac{\alpha c(t)\left[2+c^2(t)\mathrm{w}(t)\right]}{6u_0\mathrm{w}^2(t)}\mathrm{sech}^2\left(\frac{d(t)}{\mathrm{w}(t)}\right)\tanh\left(\frac{d(t)}{\mathrm{w}(t)}\right). \tag{4.14b}$$

As a quick consistency check, note that when we set $\alpha = 0$ (i.e. no potential), Γ_1 and Γ_2 are equal to zero too and therefore the perturbation terms are eliminated. By taking the second derivative of Eq. (4.13c) and Eq. (4.13d) we can further simplify the system of equations, Eqs. (4.13), and obtain the following second order differential equations:

$$\frac{d^2}{dt^2}d(t) = -\frac{gN_2}{4N\mathrm{w}(t)}\,\mathrm{csch}\left(\frac{b(t)-d(t)}{\mathrm{w}(t)}\right)^4 \tag{4.15a}$$
$$\times\left\{2\left(b(t)-d(t)\right)\left[2+\cosh\left(2\frac{b(t)-d(t)}{\mathrm{w}(t)}\right)\right]\right.$$
$$\left.-3\mathrm{w}(t)\,\sinh\left(2\frac{b(t)-d(t)}{\mathrm{w}(t)}\right)\right\}+\frac{N\mathrm{w}^2(t)\,\Gamma_2}{2N_1},$$
$$\frac{d^2}{dt^2}b(t) = -\frac{gN_1}{2N\mathrm{w}^3(t))}\,\mathrm{csch}\left(\frac{b(t)-d(t)}{\mathrm{w}(t)}\right)^4 \tag{4.15b}$$
$$\times\left\{2\left(b(t)-d(t)\right)\left[2+\cosh\left(2\frac{b(t)-d(t)}{\mathrm{w}(t)}\right)\right]\right.$$
$$\left.-3\mathrm{w}(t)\,\sinh\left(2\frac{b(t)-d(t)}{\mathrm{w}(t)}\right)\right\}+\frac{N\Gamma_1}{N_2},$$

where we used the normalization, Eq. (4.10). Equations (4.15) describe the propagation of the two component dark-bright soliton in the vicinity of delta function potential located at

$x = 0$.

By fixing the initial velocity of the dark-bright soliton, $V_{\mathrm{CM}} = 0.06$ and depending on the strength of the potential, α, we obtain three distinctive behavior of the dark-bright soliton as seen in Figure 4.2, Figure 4.3 and Figure 4.4. These scenarios comprise reflection, reflection with resonance and a subsequent delay, and transmission, respectively. In all figures, we find that the internal oscillation of the two components did not change for the incident and reflected dark-bright soliton. This means that there is ultimately no energy exchange between the internal modes and the kinetic energy of the dark-bright soliton. In Figure 4.2, Figure 4.3 and Figure 4.4 we set $g_1 = 2, g_2 = 2.7$, $g = 2.6$, w $= 1$ and $N_1 = 0.521 \times 10^5$. In Sec. 4.3.1, we compare these analytical predictions to the numerical calculations.

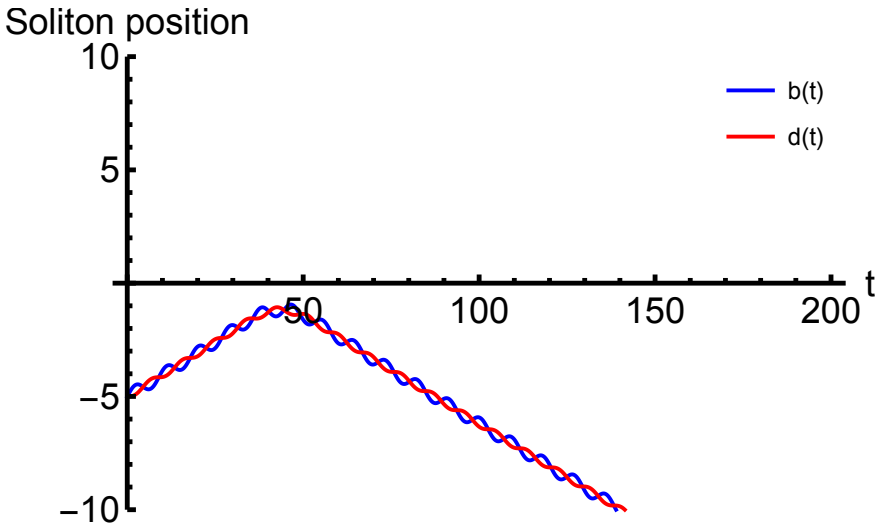

Figure 4.2 Reflection of dark-bright soliton. We found the dark-bright soliton reflected by the potential when $\alpha = 0.15$. We set the center of mass velocity $V_{\mathrm{CM}} = 0.06$.

4.2.3 Dark-bright soliton velocity

In this section, we work with the velocity of the dark-bright soliton. Here we are working with different units [70]. The dimentionless coupled NLSEs,

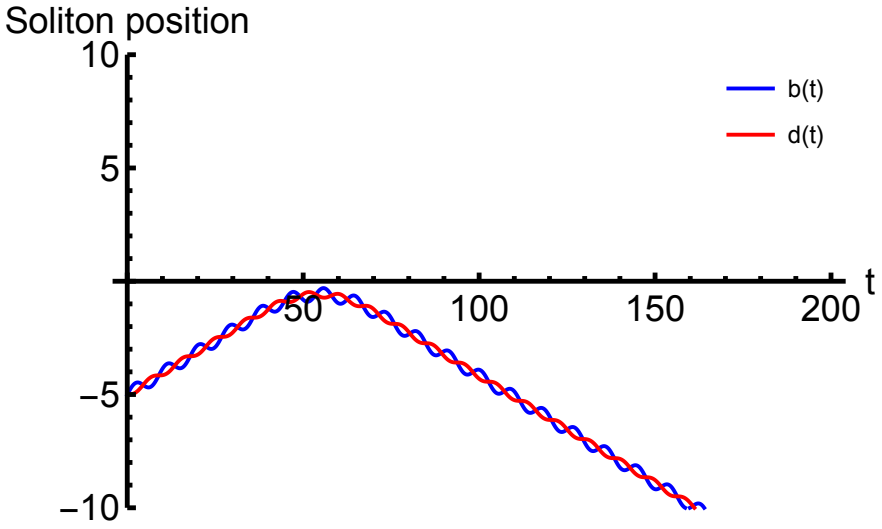

Figure 4.3 Reflection of dark-bright soliton with resonance. Here we set $\alpha = 0.04$ and we see that the dark-bright soliton oscillates at the location of the potential for a finite time before it reflects back for the same value of V_{CM} used in Figure 4.2. Thus our model appears to capture a quasibound state or resonance.

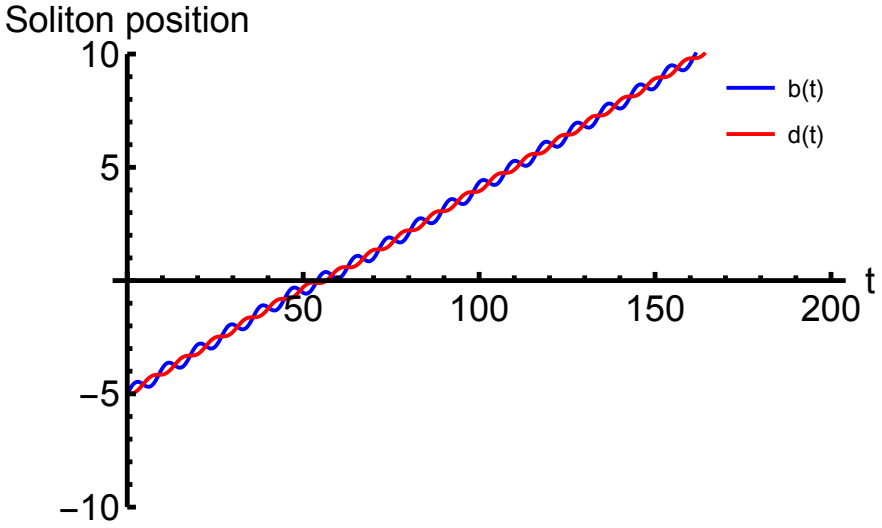

Figure 4.4 Transmission of dark-bright soliton. Here we set $\alpha = 0.01$. The dark and bright soliton locations oscillate around their center of mass position. We found the dark-bright soliton passes over the potential for the same value of V_{CM} used in Figure 4.2.

$$
\begin{aligned}
i\frac{\partial\psi_1}{\partial t} &= -\frac{1}{2}\frac{\partial^2\psi_1}{\partial x^2} + \left[|\psi_1|^2 + |\psi_2|^2 - u_0^2\right]\psi_1, \\
i\frac{\partial\psi_2}{\partial t} &= -\frac{1}{2}\frac{\partial^2\psi_2}{\partial x^2} + \left[|\psi_2|^2 + |\psi_1|^2\right]\psi_2.
\end{aligned} \tag{4.16}
$$

are integrable (i.e., Manakov case) and possess an exact analytical dark-bright soliton solution of the following form [71]:

$$
\begin{aligned}
\psi_1(x,t) &= \cos\Delta\phi\,\tanh\xi + i\,\sin\Delta\phi, \\
\psi_2(x,t) &= \eta\,\mathrm{sech}\xi\,\exp\{i\left[\phi_0 + x\phi_1\right]\}.
\end{aligned} \tag{4.17}
$$

Here $\psi_1(x,t)$ and $\psi_2(x,t)$ are the wave functions for the dark and bright soliton components, respectively. The argument of the hyperbolic functions is $\xi = D\left(x - x_0(t)\right)$, $\cos\Delta\phi$ and η are the dimensionless amplitudes of the dark and bright components, respectively, and D and $x_0(t)$ are the inverse width and the centre position of the dark-bright soliton. The phase jump over the dark soliton is $\Delta\phi$. By using the variational method, we obtain the EOMs,

$$\dot{x}_0 = D\,\tan\Delta\phi \tag{4.18}$$

$$D^2 = \cos^2\Delta\phi - \eta^2 \tag{4.19}$$

Plugging Eq. (4.19) into Eq. (4.18), we get:

$$\dot{x}_0 = \sqrt{\cos^2\Delta\phi - \eta^2}\,\tan\Delta\phi. \tag{4.20}$$

For $\eta = 0$ (i.e. $v(x,t) = 0$), we have $\dot{x_0} = \sin\Delta\phi$ which is the velocity of dark soliton in one-component BECs, a Josephson-type relation based on the phase jump phi over the soliton [72]. The two extreme limits of the phase jump over the dark soliton are $\Delta\phi = 0$ and $\Delta\phi = \frac{\pi}{2}$. In the former the depth of the dark soliton is maximum, and the velocity is zero. In the latter case, the depth of the dark soliton is zero whereas the velocity is maximum (i.e., the speed of sound, c). By examining Eq. (4.20), we find that the existence of a bright component affects the velocity of the dark-bright soliton and sets an upper limit

for the maximum velocity depending on the amplitude of the bright component. Also, the term $\cos^2\Delta\phi - \eta^2$ in Eq. (4.20) restricts the range of the real values of the velocity of the dark-bright soliton. By equating this term to zero, we find that $\Delta\phi$ gives a real value only for $\Delta\phi : 0 \to \cos^{-1}(\eta)$. This implies that there is a finite range of the velocity of the dark-bright soliton as well as a finite range of the depth of the dark component in the dark-bright soliton. Since the depth of the dark component is governed by $\cos\Delta\phi$, the range of the dark soliton amplitude goes from u_0 when $\Delta\phi = 0$ to η when $\Delta\phi = \cos^{-1}(\eta)$. That is, the minimum depth of the dark soliton component in the dark-bright soliton is not zero as it is the case for one-component dark soliton. It depends on the amplitude of the bright soliton component. In the range $\Delta\phi : 0 \to \cos^{-1}(\eta)$ the dark-bright soliton velocity is zero on both ends as seen form Eq. (4.20). So, in this interval, the velocity increases to a finite value and decreases, see Figure 4.5. To find the maximum velocity of the dark-bright soliton we differentiate Eq. (4.20) and solve it for $\Delta\phi$. As a result, we obtain the following equation,

$$\dot{x}_0^{\max} = 1 - \eta = 1 - \sqrt{\frac{N_2 D}{2(N_1 + N_2)}}. \tag{4.21}$$

Above this maximum value, $\dot{x}_0^{\max}$, an internal oscillation develops between the two components which means the two component are no longer described by one center of mass variable for the dark-bright soliton. Therefore, the above ansatz, Eq. (4.17), is not valid beyond this maximum velocity. Note that for $\eta \to 1$, $\dot{x}_0^{\max} \to 0$, $N_2 \to N_1$ from below, and the dark-bright soliton ceases to exist, as shown in [65]. In Figure 4.5 we plot the velocity of the dark-bright soliton for $\eta = 0.5$ (i.e., the bright component is half the amplitude of the dark component). Since the amplitude squared of both components is proportional to the number of atoms in each component, the case where $\eta = 0.5$ is equivalent to $N_1 = 2N_2$, where N_1 is the number of atoms displaced by the dark soliton and N_2 is the number of atoms in the bright soliton, as described in Sec. 4.2.1.

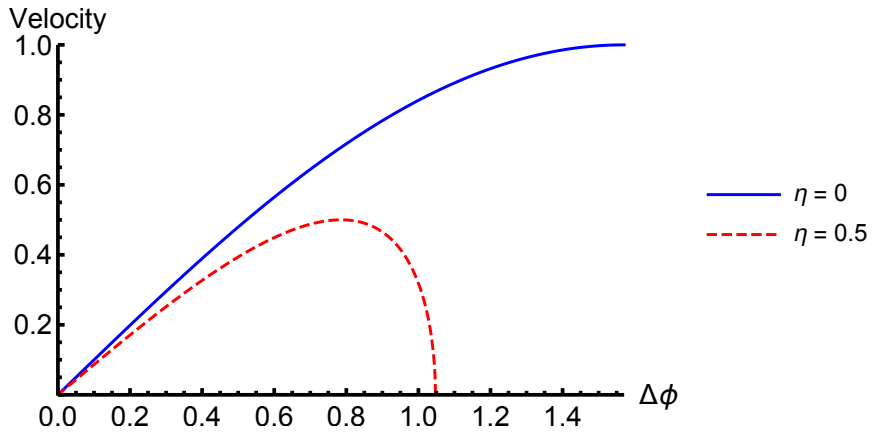

Figure 4.5 Dark-bright soliton velocity. The bright soliton amplitude is η. We set $\eta = 0.5$ in Eq. (4.20) such that the amplitude of the bright component is half the amplitude of the dark component. Notice that the speed of sound, c, is 1 and the maximum velocity of the dark-bright soliton in this case is $c/2$ where we can calculate it from Eq. (4.21). Above $c/2$ the two components in the dark-bright soliton start to oscillate, as can be seen in the numerical simulation in Figure 4.10, therefore an ansatz with one variable to describe the location of the two components is not valid. We plot the case for one-component dark soliton, $\eta = 0$, for comparison.

4.3 Numerical Calculations

We numerically study the interaction between the two components in the dark-bright soliton and the potential barrier in Sec. 4.3.1 where we use a delta function as described by Eq. (4.2). The strength of the delta function potential can be modified by varying the amplitude α. In addition, we study the effect on a one-component dark soliton velocity when interacting with another component, in this case a one-component bright soliton. The velocity of the dark soliton component is fundamentally different than the velocity of the bright soliton. As we increase the speed of the dark soliton, its width goes to infinity, and the depth goes to zero. As a result, the dark soliton disappears and we left with a plane wave. Also, the maximum velocity of a one-component dark soliton is the speed of sound in BEC. In contrast, the one-component bright soliton velocity is unbounded and its width is not a function of its velocity at all. These known facts raise questions when we are dealing with the dark-bright soliton, as we explored under certain simplifying assumptions amenable to analytical treatment in Sec. 4.2.3, where we found a maximum velocity dependent on

the difference between the amplitudes of the two components. Therefore, the presence of the bright soliton component will qualitatively change the behavior of the well-known dark soliton velocity. We now relax those assumptions to treat the general case numerically. Throughout this section, we performed the simulations with grid size $n_x = 256$ in a box with hard-wall boundaries. The box length was set to $L = 100$ unless otherwise noted.

4.3.1 Scattering of dark-bright soliton by potential barrier

We now explore the scattering problem numerically by creating a moving dark-bright soliton incident on a delta-function potential. We make no other assumptions, allowing for internal excitations of the dark-bright soliton around its center of mass. There are two ways to to impart a velocity to the dark-bright soliton. The first is to imprint a linear phase ramp on the bright soliton component. As a result the bright soliton will drag the dark soliton, and therefore we will have a moving dark-bright soliton.

The second is to imprint a phase to one side of a dark soliton, creating a phase jump $\Delta\phi$, therefore, we obtain the same moving dark-bright soliton. There is however a significant difference in the outcome in terms of excitation of internal modes. In the first case, imprinting a phase on the bright soliton will produce an internal oscillation of the two components of the dark-bright soliton. We use this method here to move the dark-bright soliton. The second method is used in the second part of the numerical section where we are interested in having the two components move without any internal oscillation.

We thus first imprint a phase on the bright component and therefore the dark-bright soliton moves toward the delta function which is for convenience located at $x = 60$ in our simulation, with the grid of 256 points running from $x = 0$ to $x = 100$. Depending on the strength of the delta function (i.e., α), where we fixed the incident velocity for all cases, we have three distinctive sets of dark-bright soliton dynamics ensue. In Figure 4.6, where we have both the analytical and numerical results plotted on the same graph, we set $\alpha = 0.01$ and find that the dark-bright soliton is passing over the potential. When the dark-bright soliton interacts with the delta function, we found that numerically the dark-bright soliton

moves slightly faster than the analytical prediction. At the end of this section, we discuss the physical reasons for the discrepancy between the analytical and numerical results.

In Figure 4.7, we set $\alpha = 0.04$, and the outcome of this comparison between the analytical and numerical calculations is that the dark-bright soliton hovers around the location of the potential for a finite time, appearing to be briefly quasibound or resonant, and then is reflected. The analytical predictions and the numerical calculations show that the dark-bright soliton reflects with different velocities. We consider this case as an inelastic scattering of the dark-bright soliton by a delta function as can be seen in Figure 4.9. Numerically, when the dark-bright soliton interacts with the potential barrier an internal state is excited (i.e., the internal oscillation of the two components) and therefore the dark-bright soliton come out of the interaction with a different velocity than the initial one.

In contrast, in Figure 4.8 we found that the dark-bright soliton reflects rapidly from the potential for $\alpha = 0.15$. The delta function potential, in this case, does not allow for the creation of a quasibound state as in Figure 4.8.

In Figure 4.9, we compare the analytical predictions to the numerical calculations for a wide range of delta function strength (i.e., α) and the center of mass velocity of the dark-bright soliton. We identify three regions. The transmission of the dark-bright soliton over the barrier, the reflection, and the inelastic scattering region. These three case studies outline the basic kinds of dynamical outcomes. The dark-bright soliton has an additional characteristic that during the scattering process, for a small range of delta function strength, energy can be absorbed into the internal mode. In this case, the oscillation mode. We defined this region as an inelastic scattering region. It is noteworthy to mention that the inelastic scattering and the excitation of the internal modes occur only when we allow for an additional degree of freedom, as we do in this article, namely, the internal oscillation of the two components.

The basic idea is the scattering process interaction with the impurity transfers kinetic center of mass energy into internal modes, resulting in inelastic scattering. Two of these modes are captured by the analytical model: the dominant feature of relative oscillation

between the two components, as well as the oscillation in the widths. However, the analytical model requires these widths oscillate in sync. The numerical simulations allow further internal modes to enter the problem, starting with out-of-sync oscillations of the soliton widths, and including even shape deformations of various kinds. In general, the scattering of a dark-bright soliton is a complex inelastic process which will require experiments to properly understand, especially since quantum fluctuations are well known to concentrate at mean field minima, in this case the interstices where the bright soliton meets the dark soliton. A proper treatment of such quantum fluctuations is an excellent subject for future study and involves at a minimum solution of the dynamical Bogoliubov equations.

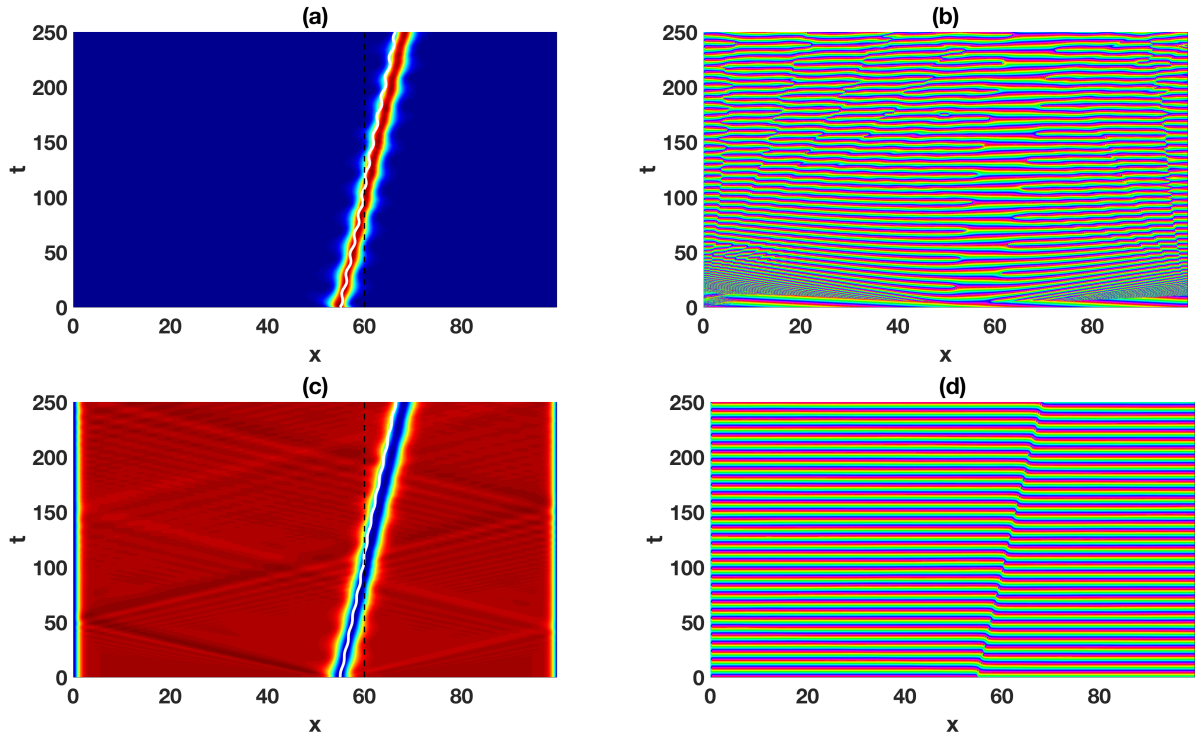

Figure 4.6 Transmission of a dark-bright soliton. (a) Density and (b) phase of the bright soliton; (c) density and (d) phase of the dark soliton. The kinetic energy of the two-component dark-bright soliton is greater than the potential energy of the barrier and therefore the dark-bright soliton passes over it. The phonons appear as bright yellow bands moving at a much higher velocity, primarily associated with the initial velocity kick applied at $t = 0$. We set $\alpha = 0.01$ and $V_{\mathrm{CM}} = 0.06$. The delta function located at $x = 60$. The white thick line represents the analytical results.

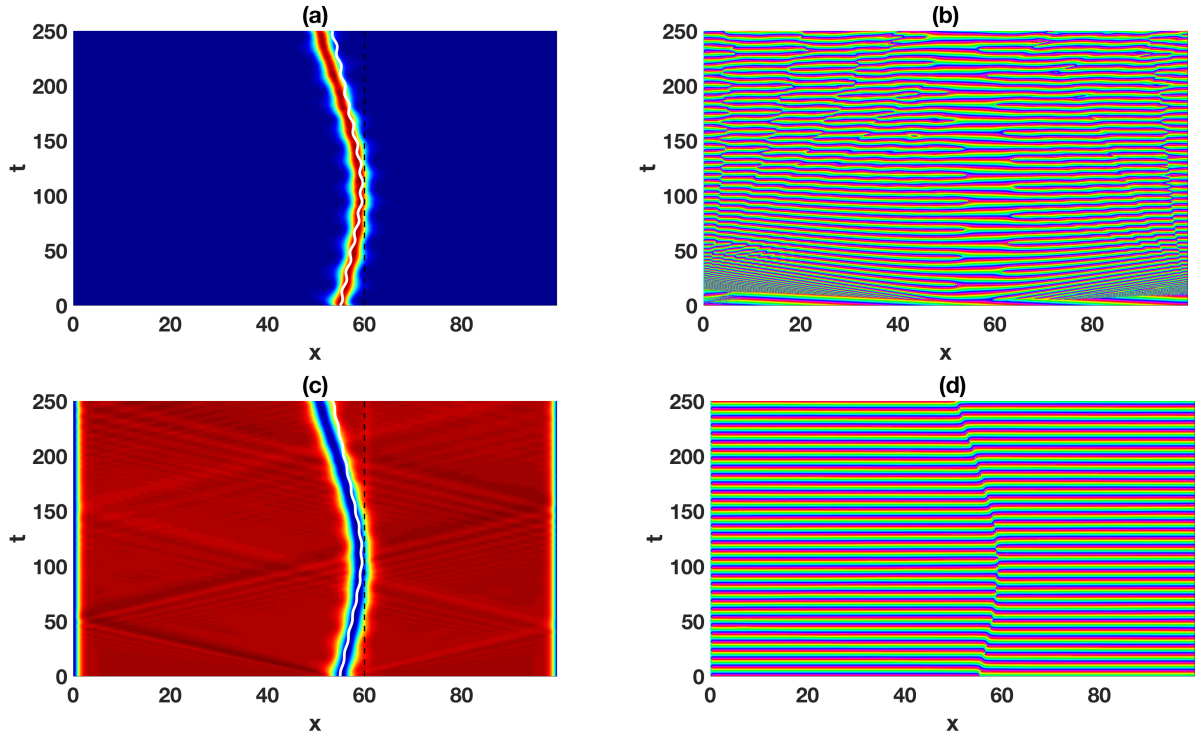

Figure 4.7 Resonant reflection of a dark-bright soliton. (a) Density and (b) phase of the bright soliton; (c) density and (d) phase of the dark soliton. The kinetic energy of the two components dark-bright soliton is almost equal to the potential energy of the barrier and therefore the dark-bright soliton hovers over the barrier for a finite time where energy goes into internal modes, not phonons. We set $\alpha = 0.04$ and $V_{\mathrm{CM}} = 0.06$. The delta function located at $x = 60$. The white thick line represents the analytical results.

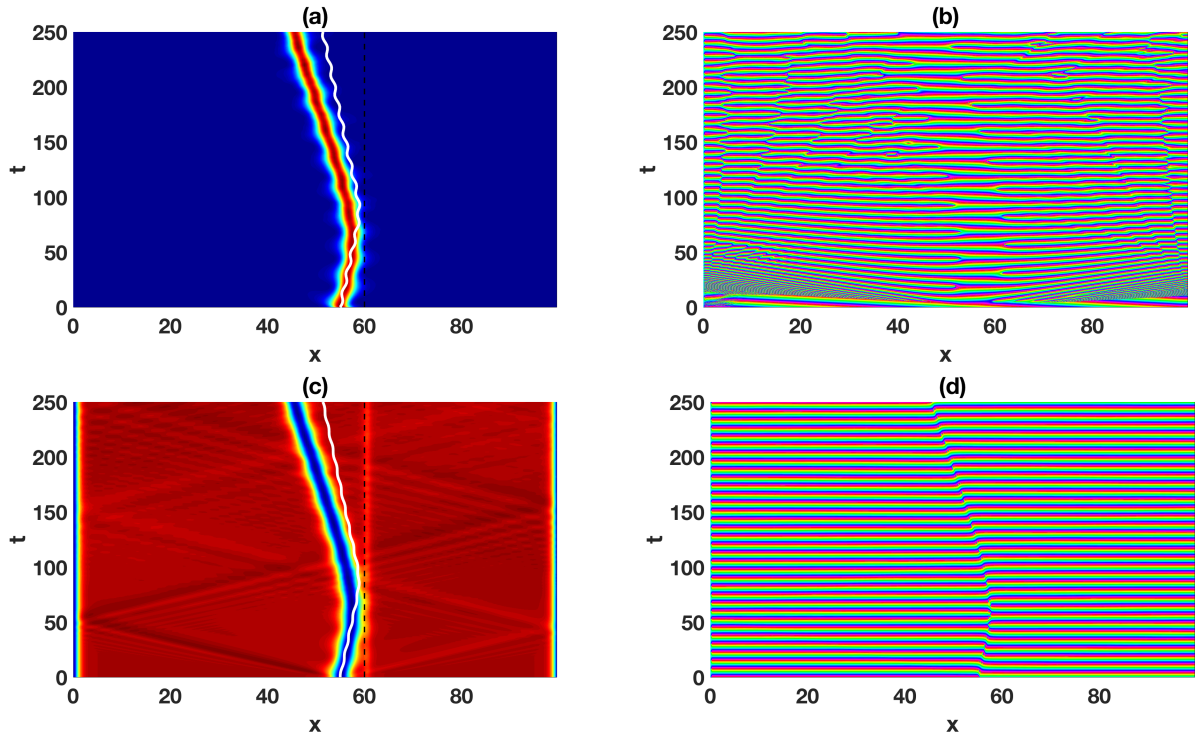

Figure 4.8 Simple reflection of a dark-bright soliton. (a) Density and (b) phase of the bright soliton; (c) density and (d) phase of the dark soliton. The kinetic energy of the two components dark-bright soliton is less than the potential energy of the barrier and therefore the dark-bright soliton reflects from the barrier. We set $\alpha = 0.15$ and $V_{\mathrm{CM}} = 0.06$. The delta function located at $x = 60$. The white thick line represents the analytical results.

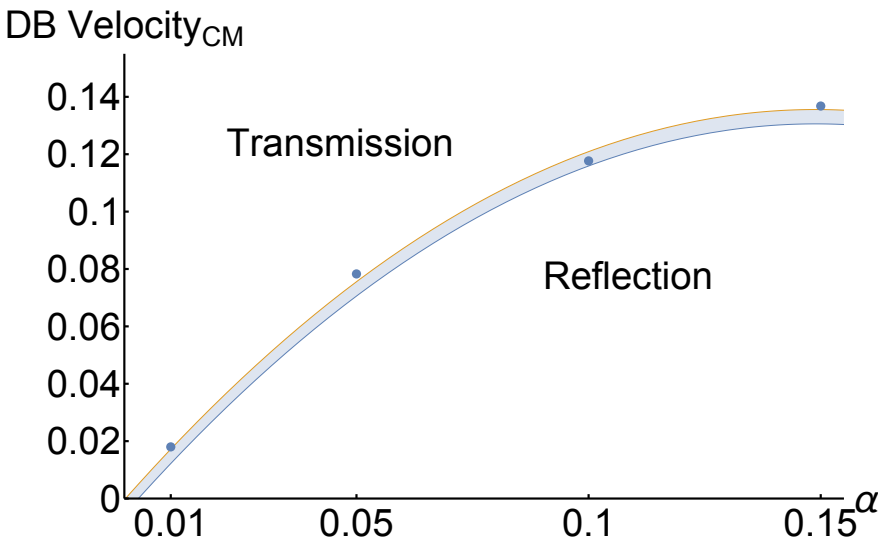

Figure 4.9 Transmission and reflection of dark-bright soliton for different values of the potential strength and center of mass velocity. We compare the analytical predictions to numerical results for a wide range of the delta function amplitude, α, and the dark-bright center of mass velocity, V_{CM}. We identify the regions for the transmission and reflection of the dark-bright soliton by the potential barrier based on the parameter domain, α and V_{CM}. The gray area represents inelastic scattering (i.e., internal excitation), showing that excitation of inelastic modes generally occur when close to the border between transmission and reflection. Note for $V_{\mathrm{CM}} = 0.06$ we have a transmission of the dark-bright soliton for $\alpha = 0.01$ and reflection when $\alpha = 0.04$ and 0.15 as described in Figure 4.6, Figure 4.7 and Figure 4.8

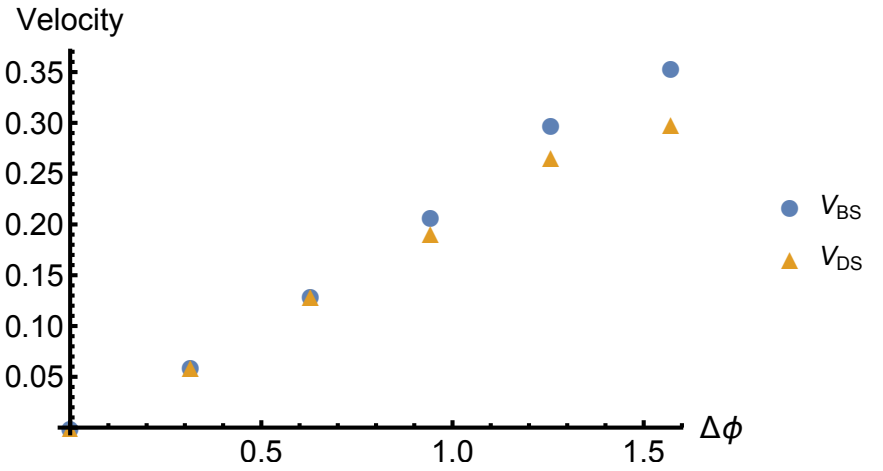

Figure 4.10 Dark-bright soliton component velocities. We plot the velocities of the two components vs the phase difference imprinted on the dark component only, $\Delta\phi$. For a bright soliton component with half the amplitude of the dark soliton component the maximum velocity of the dark-bright soliton before it oscillates is half the speed of sound, $c/2$, as predicted from Figure 4.5. In the simulation units, $c/2 = 0.15$. Above this value, the two components start to oscillate.

4.3.2 Dark-bright soliton velocity

The behavior of the dark soliton velocity changes when interacting with another component, in this case, a bright soliton component in a dark-bright soliton. To study this behavior numerically, we imprint a phase jump, $\Delta\phi$, on the dark soliton component only. In this way, we adiabatically move the two components such that we do not cause an oscillation between them, to explore our analytical predictions for the Manakov case from Sec. 4.2.3. It is important to mention that the interaction coefficients (i.e., g_1 and g_2) are all positive in this case. This means that the bright soliton component can only live in such repulsive media by interacting with the dark soliton component. As mentioned in Sec. 4.2.3, Eq. (4.16) possesses an exact analytical dark-bright soliton solution, Eq. (4.17). By examining this solution, we find that both component locations of the dark-bright soliton are expressed by one single spatial variable, $x_0(t)$. This is a criterion for an exact solution of Eq. (4.16).

In Figure 4.5, we see that the existence of the bright soliton component with half the amplitude of the dark soliton component prevents the dark soliton component from reaching its maximum velocity, μ_1 and puts an upper limit on it. This is the upper limit for the velocity of the dark-bright soliton before the two components oscillate. By adopting the method mentioned above to move the dark-bright soliton we are in a position to compare the analytical results obtained in Sec. 4.2.3 with the numerical results we have in this section.

In Figure 4.10, we imprint a phase difference on the dark soliton component only with interaction parameters $g_1 = 2$, $g_2 = 3$ and $g = 2.6$. We find that the two components in the dark-bright soliton have the same velocity below a critical value of the phase imprinted. Therefore, no internal oscillation happens and the one variable,$x_0(t)$, represents the two-component locations. Above the critical value, we find the two components start to acquire different velocities. Consequently, an internal oscillation between the two components occurs and the positions of the dark component and the bright component no longer coincide. Therefore, the two-component cannot be expressed by one variable as described in Eq. (4.17).

4.4 Conclusions

We obtained a system of equation of motions for a dark-bright soliton scattering off a fixed localized impurity, modeled by a delta function potential. We used a variational method with a hyperbolic tangent for the dark component and a hyperbolic secant for the bright component. The existence of the delta function altered the background of the dark soliton component, and therefore a perturbation method was needed to incorporate the effect of the delta function. The interaction of the dark-bright soliton with the potential excites different modes in the system. As a result, the dark-bright soliton emerges with a different velocity. Our analytical model capture two of these modes: the dominant feature of relative oscillation between the two components, as well as the oscillation in the widths. However, the analytical model requires these widths oscillate in sync. The numerical simulations allow further internal modes to enter the problem, starting with out-of-sync oscillations of the soliton widths, and including even shape deformations of various kinds.

We identify regions for the transmission, reflection and inelastic scattering of the dark-bright soliton by the potential barrier. We present three case studies outlining the basic kinds of dynamical outcomes. The many internal modes excited in this problem show the complexity of the nonlinear dynamical multicomponent problem. Our study rather points to different physical regimes, and one can follow up by applying our model to any particular experiment intending to pursue the scattering question. Nevertheless, we have provided at least one case study of transmission/reflection in Figure 4.9, to give the reader a general idea of the sorts of regimes that may occur. The scattering of a dark-bright soliton could also cause quantum fluctuations, as one might model, e.g., in dynamical Bogoliubov theory. In this case, the kinetic energy would go not only into internal mean-field modes but also into enhanced quantum fluctuations localized in and near the dark-bright soliton. If that is the case, then a reduced velocity of a scattered dark-bright soliton beyond mean-field predictions will be a sign of quantum fluctuations. This is another strong reason to get the mean-field inelastic scattering correct, carefully understanding all internal modes created by interaction

with the impurity.

In scattering theory, we usually put no limit on the incident kinetic energy. However, dark solitons are well known to be limited to the speed of sound c in the medium. The dark soliton grows shallower as the velocity is increased and eventually disappears. The dark-bright soliton is also limited in velocity and therefore incident kinetic energy. However, the limit is much more stringent. We showed in the Manakov or equal-interaction case where it scales with the relative number of atoms in the bright and dark components. That is, as the dark soliton goes faster and is therefore shallower, it can no longer support the bright soliton. For example, when the bright soliton has half of the number of atoms as the dark one excavates or pushes aside, the maximum velocity is half the sound speed. Above this critical velocity the soliton components begin to oscillate, and eventually break apart. This limits the kind of scattering experiments that can be performed in multicomponent BEC experiments and presents a smoking gun signal.

Future work may extend the investigation of the interaction of vector soliton with an impurity to three-component. We might rip apart the dark-bright soliton with the proper resonance condition, as found for exciton transport. In this sense, the barrier can be used to reflect, transmit, excite, or even destroy the dark-bright soliton [73, 74]. In addition, by solving this single impurity problem, we may extend the work for solving the disordered problem. It is noteworthy to mention that the excitation of the internal modes occur only when we allow for an additional degree of freedom, as we do in this article, namely, the internal oscillation of the two components which reflect the importance of using ansatz with two independent positions for the dark and bright soliton components.

CHAPTER 5
INTERNAL OSCILLATIONS OF A DARK-BRIGHT SOLITON IN A HARMONIC POTENTIAL

We investigate the dynamics of a dark-bright soliton in a harmonic potential using a mean-field approach via coupled nonlinear Schrödinger equations appropriate to multicomponent Bose-Einstein condensates. We use a modified perturbed dynamical variational Lagrangian approximation, where the perturbation is due to the trap, taken as a Thomas-Fermi profile. The wavefunction ansatz is taken as the correct hyperbolic tangent and secant solutions in the scalar case for the dark and bright components of the soliton, respectively. We also solve the problem numerically with psuedo-spectral Runge-Kutta methods. We find, analytically and numerically, for weak trapping the internal modes are nearly independent of center of mass motion of the dark-bright soliton. In contrast, in tighter traps the internal modes couple strongly to the center of mass motion, showing that for dark-bright solitons in a harmonic potential the center of mass and relative degrees of freedom are not independent. This result is robust against noise in the initial condition and should, therefore, be experimentally observable.

5.1 Introduction

Solitons are emergent excitations of atomic matter waves in Bose-Einstein condensates (BECs). In their simplest form they appear in highly visible form as density peaks (bright soliton) or notches (dark solitons) in scalar BECs [1, 6, 9, 75]. The experimental realization of multiple-component BECs, where different atom species or internal states of the same atom type can be populated, has aroused considerable interest in vector solitons. The two-component vector soliton of different forms (i.e., dark-dark solitons [15, 30, 47], bright-bright solitons [29] or dark-bright solitons [10–14, 46]) give rise to much richer phenomena than the single-component BECs, where one already finds, for example, soliton trains [76], domain

walls [77], collective excitations and complex dynamics. In this Article we focus on the case of the dark-bright soliton. Although in scalar BECs the bright soliton can only exist for attractive interatomic interactions [78], it can also be induced in purely repulsive multi-component BECs when a second component is occupies the density notch formed by a dark soliton in the first component. In this way, a dark soliton in one component forms an effective potential that traps the bright soliton component and therefore allows the creation of a nonlinear excited state. These solitons are sometimes referred to as symbiotic. We use the term *dark-bright soliton* for clarity [17, 46].

The nonlinear Schrödinger equation (NLSE) without the potential term is an integrable equation and possess solitonic solutions. By adding a potential term, in our case a harmonic potential, we work with the celebrated Gross-Pitaevskii equation (GPE). The oscillation of nonlinear excitations in a harmonic potential is a common problem that has been the focus of many studies, as such large scale motions are easily observable in BEC experiments. Of particular interest is the oscillation of two-component excitation like a bright-bright soliton, dark-dark soliton or dark-bright soliton [70]. In these studies, usually, the ansatz used to describe the dark-bright soliton contains one variable to describe the position of the dark and bright components. A more realistic situation is to relax this restriction and allow the two components to move freely by adding one more degree of freedom to the problem, namely, the internal oscillation between the two components. We study the coupling between the internal oscillation of the two components in the dark-bright soliton and the oscillation of the whole system in a harmonic potential. The harmonic potential modifies the background of the dark component in a dark-bright soliton. Therefore a Thomas-Fermi background approximation is needed where the new dark component wave function is represented by subtracting the old dark component density from the harmonic potential function. The result is a dark soliton on a top of parabola-shaped background, Figure 5.1.

It is well-known in the classical two-body problem that relative and center of mass degrees of freedom are independent in a harmonic potential. A dark-bright soliton represents an

emergent two-body semiclassical object in the context of the mean-field approximation on the many-body wavefunction underlying the BEC. To what extent does this emergent structure have the same properties as a classical two-body problem? An elementary consideration is separation of relative and center of mass degrees of freedom. Previous treatments have avoided this question by pinning the dark and bright solitons to the same position. By relaxing this constraint, in this Article, via both variational Lagrangian analytical methods and numerical solution of the GPE, we show that in general relative and center-of-mass degrees of freedom are not independent for the dark-bright soliton. In contrast, these degrees of freedom are independent in the uniform case, where the center-of-mass motion is associated with a Goldstone mode [65]. For a weak enough trap, the separation of variables from the uniform case is only very weakly affected by the trap. However, as the trap strength grows this separation of variables is lost.

This Article is structured as follows. In Sec. 5.2 we present the two-component GPE, the variational Lagrangian model, use perturbation theory, and derive the equations of motion for the bright and dark soliton components. In Sec. 5.3 we numerically integrate the dimensionless GPE using a psuedo-spectral Runge-Kutta method and study the dynamics of the oscillation of the dark-bright soliton in a harmonic potential. Finally, in Sec. 5.4 we summarize our conclusions.

5.2 Analytical Calculations

5.2.1 Lagrangian density and ansatz

The two-component dark-bright soliton is governed by coupled GPEs [6], which describe the evolution of the macroscopic wave functions of Bose condensed atoms:

$$\begin{aligned} i\hbar\frac{\partial}{\partial\tilde{t}}\tilde{u} &= -\frac{\hbar^2}{2m}\frac{\partial^2\tilde{u}}{\partial\tilde{x}^2} + \left[\tilde{g}_1|\tilde{u}|^2 - \tilde{u}_0^2 + \tilde{g}|\tilde{v}|^2 + \tilde{V}(\tilde{x})\right]\tilde{u}, \\ i\hbar\frac{\partial}{\partial\tilde{t}}\tilde{v} &= -\frac{\hbar^2}{2m}\frac{\partial^2\tilde{v}}{\partial\tilde{x}^2} + \left[\tilde{g}_2|\tilde{v}|^2 + \tilde{g}|\tilde{u}|^2 + \tilde{V}(\tilde{x})\right]\tilde{v}, \end{aligned} \tag{5.1}$$

where tildes denote dimensional quantities. The wave function of the dark soliton is given by $\tilde{u} \equiv \tilde{u}\left(\tilde{x},\tilde{t}\right)$ and of the bright soliton by $\tilde{v} \equiv \tilde{v}\left(\tilde{x},\tilde{t}\right)$. The dark soliton wave function is rescaled to remove the background contribution, $\tilde{u_0}$ [52]. Although this is not necessary for the harmonic trap since there is no divergence in the total number of atoms, in order to match smoothly onto the untrapped limit and connect well with previous results from a uniform system [65], we include this subtraction. The interaction strength, $\tilde{g}_j = 2a_j N\hbar\omega_\perp$ for $(j = 1, 2)$, is renormalized to 1D [51] where $\tilde{g}_1$ ($\tilde{g}_2$) represents the intra-atomic interaction for the dark (bright) component and g is the inter-atomic interaction between the two components of the BEC. The total number of atoms is N, the scattering length is a_j and $\omega_\perp$ is the oscillation frequency of the transverse trap. To nondimensionlize Eqs. (5.1) we multiply them by $(\hbar\omega_\perp)^{-1}$ and scale all quantities according to the following units:

$$\begin{aligned} x &= \frac{\tilde{x}}{\ell_\perp}, \\ t &= \tilde{t}\omega_\perp, \\ g_{ij} &= \frac{\tilde{g}_{ij}}{\ell_\perp\hbar\omega_\perp}, \\ |u|^2 &= \ell_\perp|\tilde{u}|^2, \\ |v|^2 &= \ell_\perp|\tilde{v}|^2, \\ V(x) &= \frac{\tilde{V}(\tilde{x})}{\hbar\omega_\perp}, \\ u_0^2 &= \frac{\tilde{u}_0^2}{\hbar\omega_\perp}, \end{aligned} \tag{5.2}$$

where $\ell_\perp = \sqrt{\hbar/\left(m\omega_\perp\right)}$ is the transverse harmonic oscillator length.

The dimensionless version of the coupled GPEs is,

$$\begin{aligned} i\frac{\partial}{\partial t}u &= -\frac{1}{2}\frac{\partial^2}{\partial x^2}u + V(x)u + \left[g_1|u|^2 + g|v|^2 - u_0^2\right]u, \\ i\frac{\partial}{\partial t}v &= -\frac{1}{2}\frac{\partial^2}{\partial x^2}v + V(x)v + \left[g_2|v|^2 + g|u|^2\right]v, \end{aligned} \tag{5.3}$$

The potential in Equations 5.3 takes the form,

$$V(x) = \frac{1}{2}\Omega^2 x^2, \tag{5.4}$$

for both components. We assume $\Omega \ll 1$ and therefore we treat the harmonic potential as a small perturbation effect. Despite the fact that $x^2 \to \infty$ in Eq. (5.4), because $V(x)$ always multiplies a background Thomas-Fermi wavefunction, the total perturbation is always small. Even outside the Thomas-Fermi approximation, Gaussian tails in realistic BEC profiles in a harmonic trap will fall away much faster than x^2 diverges, making this perturbative picture a physically reasonable one beyond our approximations. The existence of the harmonic potential affects the background density of the dark-bright soliton, Figure 5.1. Consequently, we have to modify the usual assumption for a dark soliton of a uniform background and assume the dark soliton is supported by a Thomas-Fermi background condensate of form

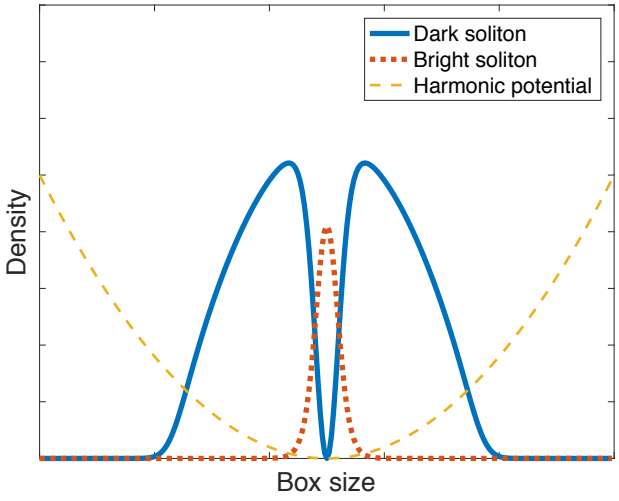

Figure 5.1 Dark-bright soliton in harmonic potential well. The background is affected by the harmonic trap, and therefore we work with the modified Thomas-Fermi cloud as described by Eq. (5.5).

$$|u_{\mathrm{TF}}|^2 = u_0^2 - V(x). \tag{5.5}$$

We recast Eqs. (5.3) to the following:

$$\begin{aligned} i\frac{\partial}{\partial t}u + \frac{1}{2}\frac{\partial^2}{\partial x^2}u - \left[g_1 |u|^2 + g |v|^2 - u_0^2\right] u = R_u \\ i\frac{\partial}{\partial t}v + \frac{1}{2}\frac{\partial^2}{\partial x^2}v - \left[g_2 |v|^2 + g |u|^2\right] v = R_v, \end{aligned} \tag{5.6}$$

where the RHS of Eqs. (5.6) represent the perturbation effects,

$$\begin{aligned} R_u &= \frac{1}{2u_0^2}\left[2u(u_0^2 - g_1|u|^2)V(x) + V'(x)\partial_x u\right] \\ R_v &= \frac{V(x)}{u_0^2}\left[(u_0^2 - g|u|^2)v\right]. \end{aligned} \tag{5.7}$$

Here $V'(x) \equiv \frac{dV(x)}{dx}$. The Lagrangian density for the system of coupled equations, Eqs. (5.6) is:

$$\begin{aligned} \mathcal{L} =& \frac{i}{2}\left[u^*\frac{\partial u}{\partial t} - u\frac{\partial u^*}{\partial t}\right]\left[1 - \frac{u_0^2}{g_1\left|u\right|^2}\right] - \frac{1}{2}\left|\frac{\partial u}{\partial x}\right|^2 \\ &- \frac{1}{2}\left[\sqrt{g_1}\left|u\right|^2 - \frac{u_0^2}{\sqrt{g_1}}\right]^2 + \frac{i}{2}\left[v^*\frac{\partial v}{\partial t} - v\frac{\partial v^*}{\partial t}\right] \\ &- \frac{1}{2}\left|\frac{\partial v}{\partial x}\right|^2 - \frac{g_2}{2}\left|v\right|^4 - g\left|u\right|^2\left|v\right|^2. \end{aligned} \tag{5.8}$$

We adopt the following trial functions as the dark-bright soliton solutions to Eqs. (5.6):

$$\begin{aligned} u\left(x,t\right) &= \frac{u_0}{\sqrt{g_1}}\left\{iA\left(t\right) + c\left(t\right)\ \tanh\left[\frac{\left(d\left(t\right)+x\right)}{\mathrm{w}\left(\mathrm{t}\right)}\right]\right\}, \\ v\left(x,t\right) &= \frac{u_0}{\sqrt{g_2}}F\left(t\right)\ \mathrm{sech}\left[\frac{\left(b\left(t\right)+x\right)}{\mathrm{w}\left(\mathrm{t}\right)}\right] \\ &\quad \times \exp\{i\left[\phi_0\left(t\right) + x\phi_1\left(t\right)\right]\}. \end{aligned} \tag{5.9}$$

The parameters A, c, F describe the amplitude of the two components where,

$$A^2 + c^2 = 1, \tag{5.10}$$

and A determines the velocity of the dark soliton component. In the exponential term in Eqs. 5.9, ϕ_0 gives rise to a complex amplitude to the bright soliton component. The velocity of the bright soliton is given by ϕ_1, and d and b are the position of the dark and bright soliton, respectively. Since we are using hyperbolic functions as an ansatz, we assume the two components have the same width, w, for the problem to remain analytically tractable [49]. There are 8 variational parameters subject to 1 constraint. The 8 variational parameters

as shown in Eq. (5.9) are A, c, d, w, F, b, ϕ_0 and ϕ_1 where we note Eq. (5.10) effectively reduces the number to 7.

In this ansatz, we have assumed a fixed background, i.e., there is no motion of the Thomas-Fermi background with respect to the harmonic trap. The ansatz also neglects phonon effects. Both of these restrictions will be relaxed in our numerical treatment in Sec. 5.3. We utilize the following normalization conditions,

$$\int_{-\infty}^{\infty} dx \ \left(\frac{u_0^2}{g_1} - |u|^2\right) = \frac{N_1}{N}, \tag{5.11a}$$

$$\int_{-\infty}^{\infty} dx \ |v|^2 = \frac{N_2}{N}. \tag{5.11b}$$

Here N_1 is the number of atoms displaced by the dark soliton and N_2 is the number of atoms in the bright soliton, and N the total number of holes and atoms involved in the emergent feature of the dark-bright soliton only. In contrast, the total number of atoms in the condensate is $N_{\rm total} = \int dx|v|^2 + \int dx|u_{\rm TF}|^2|u|^2$. In general, $N_2 \ll N_{\rm total}$ as many more atoms are in the Thomas-Fermi background supporting the dark soliton, see the sketch in Figure 5.1. Likewise the number of holes, i.e. the atoms displaced by the dark soliton, is typically much less than the total number of atoms even after subtracting out N_2, i.e., $N_1 \ll N_{\rm total} - N_2$. This choice corresponds to the same normalization choice as used in unbounded systems without traps, and therefore allows us to check all results in the limit that trap frequency $\Omega \to 0$. By inserting the ansatz, Eqs. (5.9), in the normalization, Eqs. (5.11), we find the relation between N_1, N_2 and the coefficients of the two components in the dark-bright soliton:

$$\frac{2u_0^2c^2w}{g_1} = \frac{N_1}{N}, \tag{5.12a}$$

$$\frac{2u_0^2F^2w}{g_2} = \frac{N_2}{N}, \tag{5.12b}$$

$$N = N_1 + N_2 \tag{5.12c}$$

Out of the 8 experimental parameters $g, N, g_1, N_1, g_2, N_2, u_0$ and Ω, only 5 remain after taking into account the 3 constraints of Eqs. (5.12) after the variational procedure. We choose $g, N_1/N_2, g_1, g_2$ and Ω as the "free parameters".

5.2.2 Evolution equations

Using a perturbation technique in the variational method also modifies the standard Euler-Lagrange. To find the equations of motion that govern the behavior of the variational parameters we utilize the following modified Euler-Lagrange equation as defined in [52]:

$$\frac{\partial L}{\partial a_j} - \frac{d}{dt}\left(\frac{\partial L}{\partial \dot{a}_j}\right) = 2\ \mathrm{Re}\{\int_{-\infty}^{\infty}(R_u^*\frac{\partial u}{\partial a_j} + R_v^*\frac{\partial v}{\partial a_j})\ dx\}. \tag{5.13}$$

Here $L = \int_{-\infty}^{\infty} dx\mathcal{L}$, $\mathcal{L}$ is the Lagrangian density in Eq. (5.8) and a_j represents the variational parameters where $\dot{a}_j \equiv da/dt$. We obtain R_u^* and R_v^* by inserting Eq. (5.9) into Eq. (5.7) and take the conjugate of the outcome. Also, inserting Eqs. (5.9) into Eq. (5.8) and integrating, we obtain the Lagrangian as a function of the variational parameters,

$$\begin{aligned}
L = &-\frac{2u_0^2c^2}{3g_1\mathrm{w}} - \frac{u_0^2F^2}{3g_2\mathrm{w}} - \frac{2u_0^4c^4\mathrm{w}}{3g_1} + \frac{2gu_0^4(-1+c^2)F^2\mathrm{w}}{g_1g_2} \\
&- \frac{2u_0^4F^4\mathrm{w}}{3g_2} + \frac{gu_0^4c^2F^2}{g_1g_2}\mathrm{csch}\left(\frac{b-d}{\mathrm{w}}\right)^2 \\
&\times\left\{4\coth\left(\frac{b-d}{\mathrm{w}}\right)(b-d) - \left[3+\cosh\left(2\frac{b-d}{\mathrm{w}}\right)\mathrm{w}\right]\right\} \\
&- \frac{u_0^2F^2\mathrm{w}\phi_1^2}{g_2} - \frac{2u_0^2}{g_1}\left[\tan^{-1}\left(\frac{c}{A}\right) - Ac\right]\frac{d}{dt}d \\
&- \frac{2u_0^2F^2\mathrm{w}}{g_2}\frac{d}{dt}\phi_0 + \frac{2u_0^2bF^2\mathrm{w}}{g_2}\frac{d}{dt}\phi_1.
\end{aligned} \tag{5.14}$$

Applying the modified Euler-Lagrange equations, Eq. (5.13), yields a system of coupled nonlinear ordinary differential equations (ODEs) that describe the evolution in time of the variational parameters under the influence of the harmonic potential,

$$\dot{\phi}_1 = \frac{g u_0^2 c^2}{g_1 \mathrm{w}} \Gamma_1 + \frac{\Omega^2}{45 g_1} \{ b [45(g_1 - g) \tag{5.15a}$$
$$-g(\pi^2 - 15)c^2 + g\pi^2 c^2 d] \}$$
$$\dot{A} = \frac{g u_0^2 c F^2}{2 g_2 \mathrm{w}} \Gamma_1 + \frac{c(2 + u_0^2 c^2 \mathrm{w}^2) d}{6 u_0^2 \mathrm{w}} \Omega^2 \tag{5.15b}$$
$$\frac{2u_0^2 c}{g_1} \dot{d} + \frac{2u_0^2 c}{g_1 A^2 \left(1 + \frac{c^2}{A^2}\right)} \dot{d} = \frac{\pi^2 u_0^2 A c^2 \mathrm{w}^3}{6 g_1} \Omega^2 \tag{5.15c}$$
$$\frac{2u_0^2 A}{g_1} \dot{d} - \frac{2u_0^2}{g_1 A \left(1 + \frac{c^2}{A^2}\right)} \dot{d} = \tag{5.15d}$$
$$\frac{c\mathrm{w} \left[18 + (12 + \pi^2) u_0^2 c^2 \mathrm{w}^2\right]}{18 g_1} \Omega^2 - \frac{2 g u_0^4 c F^2 \Gamma_2}{g_1 g_2}$$
$$- \frac{4u_0^2 c}{3 g_1 g_2 \mathrm{w}} \left[-g_2 + u_0^2 \left(-2 g_2 c^2 + 3 g F^2\right) \mathrm{w}^2\right]$$
$$2\mathrm{w}\dot{F} + F\dot{\mathrm{w}} = 0 \tag{5.15e}$$
$$F\mathrm{w} \left(\phi_1 + \dot{b}\right) + b \left(2\mathrm{w}\dot{F} + F\dot{\mathrm{w}}\right) = 0 \tag{5.15f}$$
$$\frac{4u_0^4 \mathrm{w}^2}{3 g_1 g_2 F \mathrm{w}} \left(g_2 c^4 - g_1 F^4\right) - \frac{4u_0^2}{3 g_1 g_2 F \mathrm{w}} \left(g_2 c^2 - g_1 F^2\right)$$
$$+ \frac{4 g u_0^4 c^2 F \, \Gamma_1}{g_1 g_2 \mathrm{w}} (d - b) = \Omega^2 \left\{ \frac{2(\pi^2 - 6) c^2 \mathrm{w}}{9 g_1 F} \right.$$
$$+ \frac{2 g \pi^2 u_0^2 c^2 d F w}{45 g_1 g_2} + \frac{u_0^2 \mathrm{w}^3}{18 g_1 g_2 F} \left[(\pi^2 - 6) c^2 \right.$$
$$\left. \left. (3 g_2 c^2 - g F^2) + 6(g - g_1) \pi^2 F^2 \right] \right\} \tag{5.15g}$$
$$- \frac{2u_0^2 F}{3 g_2 \mathrm{w}} - \frac{4u_0^4 \mathrm{w} F}{3 g_1 g_2} \left(3g + 2 g_1 F^2\right) + \frac{2 g u_0^4 c^2 F}{g_1 g_2} \left(\Gamma_2 + 2\mathrm{w}\right)$$
$$- \frac{2u_0^2 F \mathrm{w}}{g_2} \left(\phi_1^2 + 2\dot{\phi}_0 - 2b\dot{\phi}_1\right) = \frac{u_0^2 F \mathrm{w}}{90 g_1 g_2} \Omega^2$$
$$\times \left[8 g \pi^2 b c^2 d + 5 \left(3 \left(g_1 - g\right) \pi^2 + 2g \left(\pi^2 - 6\right) c^2\right) \mathrm{w}^2\right], \tag{5.15h}$$

where Γ_1 and Γ_2 in Eq. (5.15a), Eq. (5.15b) and Eq. (5.15d) are represented as follows,

$$\Gamma_1 = \operatorname{csch}\left(\frac{b-d}{\mathrm{w}}\right)^4 \left\{2\left[2+\cosh\left(2\frac{b-d}{\mathrm{w}}\right)\right](b-d)\right. \tag{5.16a}$$
$$\left. -3\sinh\left(2\frac{b-d}{\mathrm{w}}\right)\mathrm{w}\right\},$$
$$\Gamma_2 = \operatorname{csch}\left(\frac{b-d}{\mathrm{w}}\right)^2 \left\{4\cosh\left(\frac{b-d}{\mathrm{w}}\right)(b-d)\right. \tag{5.16b}$$
$$\left. -\left[3+\cosh\left(2\frac{b-d}{\mathrm{w}}\right)\right]\mathrm{w}\right\}.$$

In Eqs. (5.15) we have an algebraic equation, Eq. (5.15g), where we do not have any derivatives of the variational parameters. In addition we use the the constraint, Eq. (5.10). In this case, we expect to find only 6 frequencies out of the total 8 equations of the system in Eqs. (5.15).

5.2.3 Normal modes

The system of equations, Eqs. (5.15) has a fixed point,

$$\begin{aligned} &b_{\mathrm{fp}} = 0,\ d_{\mathrm{fp}} = 0,\ A_{\mathrm{fp}} = 0,\ c_{\mathrm{fp}} = 1,\ F_{\mathrm{fp}} = 1, \\ &w_{\mathrm{fp}} = w_{\mathrm{fp}},\ \phi_{1fp} = 0,\ \phi_{0fp} = 0, \end{aligned} \tag{5.17}$$

where w_{fp} is determined by the constraints of Eqs. (5.12). We continue by linearizing Eqs. (5.15) around the fixed point Eq. (5.17). Here we set,

$$a_j(t) = a_{j\mathrm{fp}} + \delta a_j\, e^{i\omega t}, \tag{5.18}$$

where ω is the oscillation frequency between the two components and the a_j are the 8 variational parameters. Keeping δa_j to linear order results in a matrix equation of the form,

$$\begin{bmatrix} A_{11} & A_{12} & A_{13} & 0 & 0 & 0 & 0 & 0 \\ 0 & A_{22} & A_{23} & A_{24} & 0 & 0 & 0 & 0 \\ 0 & A_{32} & 0 & A_{34} & 0 & 0 & 0 & 0 \\ 0 & 0 & 0 & 0 & A_{45} & A_{46} & A_{47} & 0 \\ 0 & 0 & 0 & 0 & A_{55} & A_{56} & 0 & 0 \\ A_{61} & 0 & A_{63} & 0 & A_{65} & A_{66} & 0 & 0 \\ 0 & 0 & 0 & 0 & A_{75} & A_{76} & A_{77} & 0 \\ 0 & 0 & 0 & 0 & A_{85} & A_{86} & A_{87} & A_{88} \end{bmatrix} \begin{bmatrix} \delta\phi_1 \\ \delta d \\ \delta b \\ \delta A \\ \delta F \\ \delta \mathrm{w} \\ \delta c \\ \delta\phi_0 \end{bmatrix} = \begin{bmatrix} 0 \end{bmatrix} \tag{5.19}$$

where [0] refers to a column vector with eight entries of value zero. The nonzero terms are written in Appendix 5.5. Taking the determinant of the matrix and solving for the eigenfrequencies, ω, we obtain,

$$\alpha_1\omega^6 + \alpha_2\omega^4 + \alpha_3\omega^2 = 0\,, \tag{5.20}$$

where as mentioned already only six eigenfrequencies are expected due to constraints and the form of the coupled nonlinear ODEs in Eqs. 5.15. Solving the determinant we obtain,

$$\begin{aligned} \omega_\pm = 0,\ 0,\ \frac{1}{\sqrt{2}}\sqrt{-\frac{\alpha_2}{\alpha_1} \pm \frac{1}{\alpha_1}\sqrt{\alpha_2^2 - 4\alpha_1\alpha_3}}, \\ -\frac{1}{\sqrt{2}}\sqrt{-\frac{\alpha_2}{\alpha_1} \pm \frac{1}{\alpha_1}\sqrt{\alpha_2^2 - 4\alpha_1\alpha_3}}. \end{aligned} \tag{5.21}$$

where we write out the long expressions for α_1, α_2 and α_3 in Appendix 5.5. Since we are considering a small oscillation frequency, $\Omega \ll 1$, we expand the coefficients (i.e., α_1, α_2 and α_3) around $\Omega \to 0$ and find that $\alpha_3 \to 0$. Therefore, we end up with one internal oscillation frequency of interest,

$$\omega_{\mathrm{internal}} = \sqrt{\frac{\alpha_2}{-\alpha_1}}. \tag{5.22}$$

The dark-bright soliton we consider exists in repulsive media, therefore, g, g_1 and g_2 all take positive values. In this case, $\alpha_1 < 0$, $\alpha_2 > 0$ for any values of the free parameters mentioned in Sec. 5.2.1. In Figure 5.2 we plot a typical case for in the internal oscillation frequency, Eq. 5.22, using the same parameters as our previous treatment of the uniform case

for comparison [65]. The result is nearly independent of trapping frequency until a sudden strong coupling for larger Ω, beyond which the result turns imaginary. However, this is also beyond the assumptions of the model, namely $\Omega \ll 1$. Therefore we examine the questions of the real trend in a more thorough numerical treatment in Sec. 5.3.

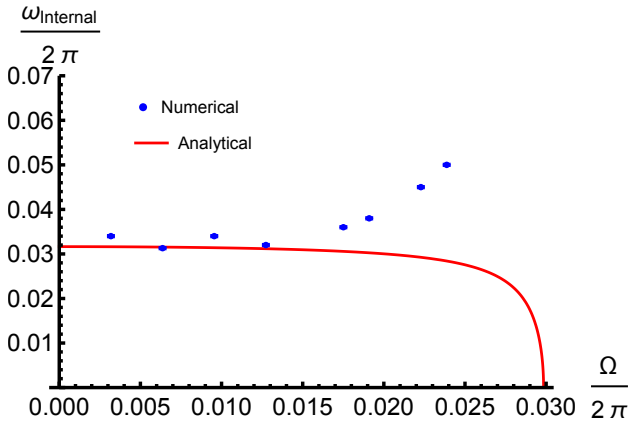

Figure 5.2 Internal oscillation frequency of the dark-bright soliton verses the trap frequency. The relative degree of freedom of a dark-bright soliton is nearly independent of the center of mass degree of freedom up to a trapping frequency of about 0.0159, in units of the transverse trap frequency, at which point the internal and external motion becomes strongly coupled. This corresponds to a trapping length ratio of $\omega^2 = 0.32$, or an approximately 3:1 prolate trap. Here we take $g_1 = 2$, $g_2 = 2.6$, $g = 2.6$, $N_1/N_2 = 0.503$. The error bars for the numerical calculations are smaller than the point size, e.g. ± 0.00017 for $\Omega/2\pi = 0.0222$.

5.2.4 Nonlinear dark-bright soliton motion

The system of Eqs. (5.15) also can be simplified to a smaller set of second order nonlinear coupled ODEs. From Eq. (5.15e) and Eq. (5.15f), we obtain the following,

$$\dot{b} = -\phi_1, \tag{5.23}$$

with the help of Eq. (5.15a), we get our first second order differential equation (ODE),

$$\begin{aligned} \ddot{b} = &-\frac{g u_0^2 c^2}{g_{1\mathrm{W}}}\Gamma_1 - \frac{\Omega^2}{45 g_1} \\ &\times \left\{45(g_1 - g) - g(\pi^2 - 15)c^2 + g\pi^2 c^2 d\right\} b. \end{aligned} \tag{5.24}$$

Note that when we set $c = 0$ (i.e., eliminating the dark soliton) Eqs. (5.24) recovers the well-known oscillation frequency of the one-component bright soliton in a harmonic potential,

$$\ddot{b} + \Omega^2 b = 0. \tag{5.25}$$

In the limiting case, $g = 0$ because there is no interaction between the bright soliton and the dark soliton. The second ODE is obtain by inserting Eq. (5.15c) into Eq. (5.15d) and use the normalization conditions, Eqs. (5.12), we obtain,

$$\begin{aligned}\dot{d} = \frac{1}{576A(1-A)^{5/2}} \Bigg[& \frac{3g_1^3 N_1^3 \pi^2 \Omega^2}{N^3 u_0^6} \\ & + \frac{4g_1^3 N_1^3 (3+\pi^2)\Omega^2(-1+A^2)}{N^3 u_0^6} \\ & - \frac{72 g_1 N_1 \Omega^2 (-1+A^2)^2}{N u_0^4} \\ & + \frac{96(2g_1 N_1 - 3gN_2)(-1+A^2)^3}{N} \\ & - \frac{96 u_0^2 (4N - 3gN_2\Gamma_2)(-1+A^2)^4}{g_1 N_1}. \Bigg]\end{aligned} \tag{5.26}$$

Equation (5.26) take the form $\dot{d} = f(A(t), \Gamma_2(t))$. Taking the total time derivative of Eq. (5.26) yields,

$$\ddot{d} = \alpha \dot{A}, \tag{5.27}$$

where α is obtained from Eq. (5.26) and Eq. (5.15b),

$$\begin{aligned}\alpha = & -\frac{gN_2\Gamma_1}{6g_1^3 N_1^3}\left(-4 - 4g_1^2 N_1^2 + 6g g_1 N_1 N_2 + 3gN_2\Gamma_2\right) \\ & + \frac{\Gamma_1}{6g_1^3 N_1^3 A^2}\left(-4gN_2 - 2g g_1^2 N_1^2 N_2 + 3g^2 g_1 N_1 N_2^2\right. \\ & \left. + 3g^2 N_2^2 \Gamma_2\right) + \Omega^2 \Bigg\{ \frac{gN_2\Gamma_1}{576 g_1 N_1 A^2}\left[-72 - 12g_1^2 N_1^2\right. \\ & \left. - g_1^2 N_1^2 \pi^2 + 216A^2 + 48 g_1^2 N_1^2 A^2 + 7 g_1^2 N_1^2 \pi^2 A^2\right] \\ & - \frac{1}{72 g_1^2 N_1^2 A^2}\left[32 + 20 g_1^2 N_1^2 + 2 g_1^4 N_1^4\right. \\ & - 3g g_1^3 N_1^3 N2 - 24 g N_2 \Gamma_2 - 12 g_1^2 N_1^2 A^2 \\ & \left. + 24 g g_1 N_1 N_2\left(-1 + A^2\right) - 3g g_1^2 N_1^2 N_2 \Gamma_2\left(1 + A^2\right)\right] d. \Bigg\}\end{aligned} \tag{5.28}$$

By plotting Eq. (5.24) and Eq. (5.27) we obtain Figure 5.3, where the interplay between external and internal degrees of freedom of the dark-bright soliton is clearly evident, showing that the assumption of the two components moving together, as found in previous treatments before this Article, does not capture the richness of the dynamics.

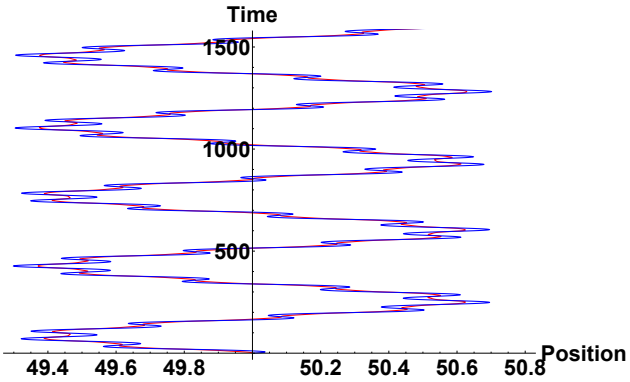

Figure 5.3 Oscillation of dark-bright soliton in a harmonic potential well. The nonlinear ODE evolution of the dark and bright soliton positions resulting from our variational Lagrangian treatment shows a rich structure to the internal dynamics, even for a small trapping frequency of $\Omega/2\pi = 0.0064$. The free parameters are the same as in Figure 5.2.

5.3 Full numerical evolution of the coupled GPEs

We now numerically study the oscillation of the dark-bright and the internal oscillation between the two components in a harmonic potential described by Eq. (5.4), making no other assumptions beyond coupled GPEs. Throughout this section, we present the simulations with grid size $n_x = 256$ in a box with hard-wall boundaries, noting that this is sufficient to converge our simulations. For example, the error bars are smaller than the point size for internal frequencies (see Figure 5.2) even when we cut the grid in half to 128 points. The box length is set to $L = 100$ unless otherwise noted.

5.3.1 Dark-bright soliton in harmonic potential

To move a dark-bright soliton in a harmonic potential, we may imprint a phase on the bright component or the dark component but with a fundamental difference between these two methods. If we imprint a phase difference on the dark component only, it will

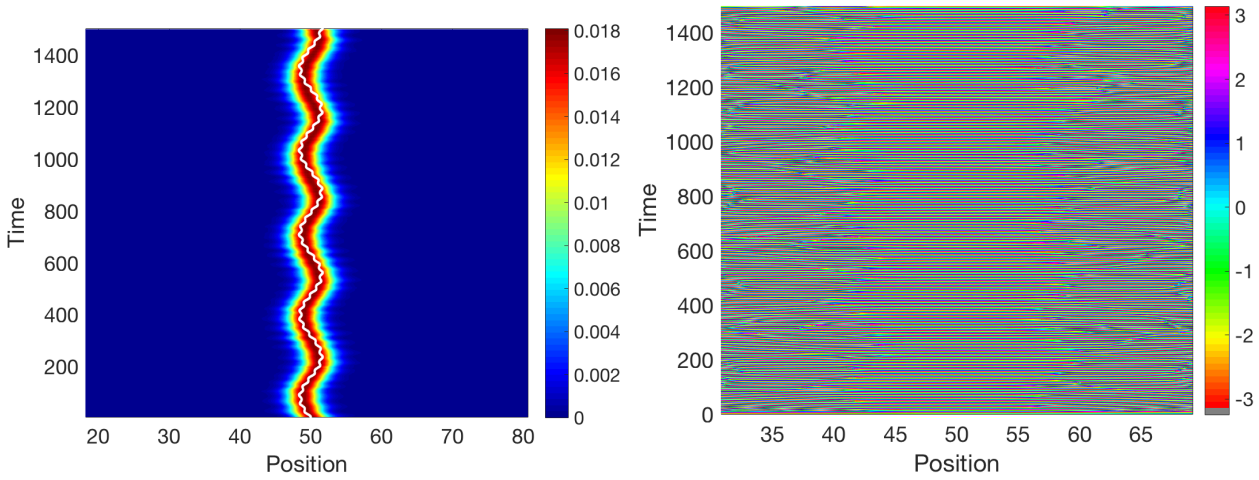

Figure 5.4 Bright component in dark-bright soliton. The oscillation of the bright soliton component in dark-bright soliton. The white line represents the analytical result for the bright soliton position, Eq. (5.24). We set the trap frequency $\Omega/2\pi = 0.0064$. We find the dark-bright soliton oscillates with $\omega_{\rm DB}/2\pi = 0.0039$. In the lower panel, we plot the phase.

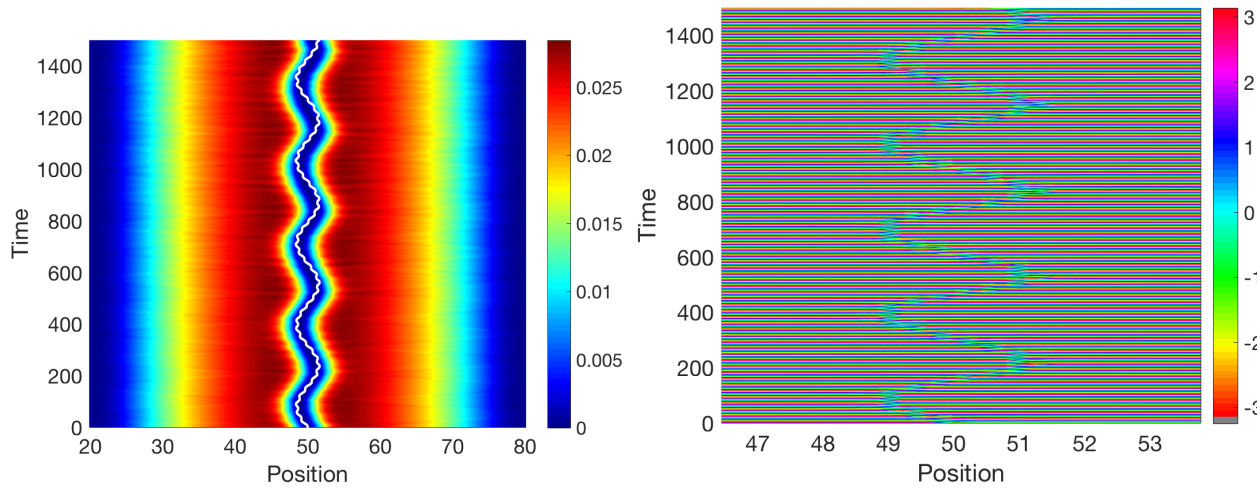

Figure 5.5 Dark component in dark-bright soliton. The oscillation of the dark soliton component in dark-bright soliton. In the upper panel, the white line represents the analytical plot from Eq. (5.24). We set the trap frequency $\Omega/2\pi = 0.0064$. We find the dark-bright soliton oscillates with $\omega_{\rm DB}/2\pi = 0.0039$. In the lower panel, we plot the phase.

move slowly such that it will pull the bright component with it but without any oscillation between the two components. For this method, it is noteworthy to mention that an ansatz with only one variable to represent the location of the dark and bright components is a valid choice to describe the moving dark-bright in a harmonic potential as this is the case for other studies [70]. But since we are interested in the oscillation of dark-bright soliton in a harmonic potential with an additional degree of freedom, namely, the internal oscillation of the two components, we work with the second method (i.e., imprinting a phase on the bright component only). In this method, the relatively small density of the bright component moves faster when imprinting a phase on it and as a result, it will drag the dark soliton with it and form an oscillation between the two components. Therefore, the dark-bright soliton will move, and we study the center-of-mass trajectory to calculate the oscillation of the dark-bright soliton as a whole.

In Figure 5.4 and Figure 5.5, we plot the outcomes from the numerical simulations and the analytical calculations of the bright and dark components, respectively. In each plot, the upper panel shows the density, and the lower panel the phase. The analytical results, the white line in the center of the bright and dark components, oscillate with nearly the same frequency as the numerical results, showing a small deviation after many trap periods. This deviation is a result of the interaction between the dark-bright soliton with the reflected phonons, not captured in the analytical model where we assumed an inert Thomas-Fermi background. When the dark-bright soliton moves in a harmonic potential, phonons are created and propagate away with the speed of sound. They then reach the low density regions of the BEC at the harmonic trap edges and turn back around to interact with the dark-bright soliton.

To test the analytical predictions against the numerical outcomes, we plot the center of mass oscillation frequency ω_{DB} of the dark-bright soliton vs. the trapping frequency Ω in Figure 5.6. The analytical results are obtained by evolving the nonlinear ODEs and performing a Fourier transform. These scale almost linearly together showing they are nearly

but not quite proportional for weak trapping. For small trapping frequencies, as shown in Figure 5.2, the internal frequency is also nearly independent of the trap. This is an indication that the internal oscillation of the two components does not couple with the oscillation of the dark-bright soliton in the weak trapping case. In contrast, our coupled GPE simulations show that for stronger trapping the internal degree of freedom is strongly dependent on the trap frequency, see Figure 5.2. In this regime, the analytical result diverges to zero, but the numerical result increases. We interpret these results further in Sec. 5.4.

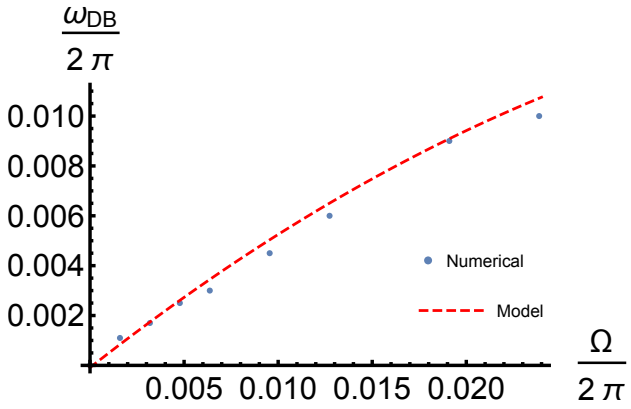

Figure 5.6 The oscillation of the dark-bright soliton for different values of the trap oscillation of the harmonic potential. We compare the analytical predictions to numerical results of the oscillation of dark-bright soliton, $\omega_{\mathrm{DB}}/2\pi$, for a wide range of trap frequencies, $\Omega/2\pi$.

5.3.2 Robustness of dark-bright soliton oscillations

In this section, we address the question of experimental observability. How stable are the dominant frequencies of dark-bright soliton motion in a harmonic trap? To answer this questions, we add white noise to the system in the spatial Fourier transform of the initial condition at the 5% level, then reverse Fourier transform to obtain a noisy initial state. Propagating this noisy initial state, we plot two cases for the same harmonic potential trap frequency, $\Omega/2\pi = 0.0064$ in Figure 5.8, Figure 5.9, Figure 5.10 and Figure 5.11. The free parameters are again taken to match our test case used throughout this paper, although we also examined other cases to find similar features. In Figure 5.8 and Figure 5.9 we plot the density of the bright component and the dark component, respectively. The dark-bright

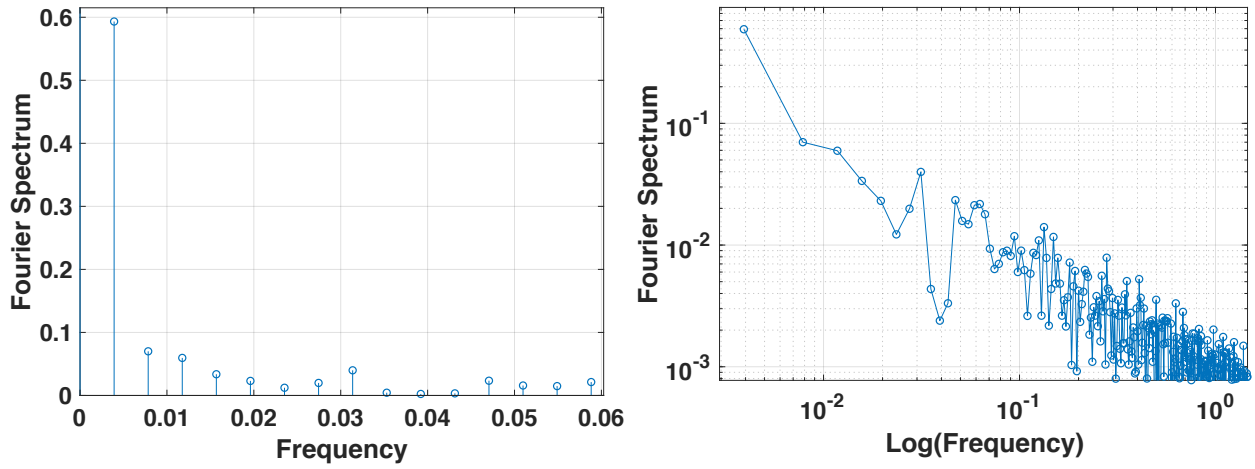

Figure 5.7 Oscillation frequencies of the dark-bright soliton in harmonic potential. A Fourier transform of our numerical results allows us to pick out the important frequencies in the problem. We show here a sample case of $\Omega/2\pi = 0.0064$. The first dominant frequency is located at $\omega/2\pi = 0.0039$ which corresponds to the center of mass oscillation of the dark-bright soliton in the harmonic potential. The second dominant frequency is located at $\omega/2\pi = 0.032$, and corresponds to the internal oscillation between the two components. Overall the dynamics is in fact quite rich, with many aspects to the motion, as observed in the dense Fourier tail.

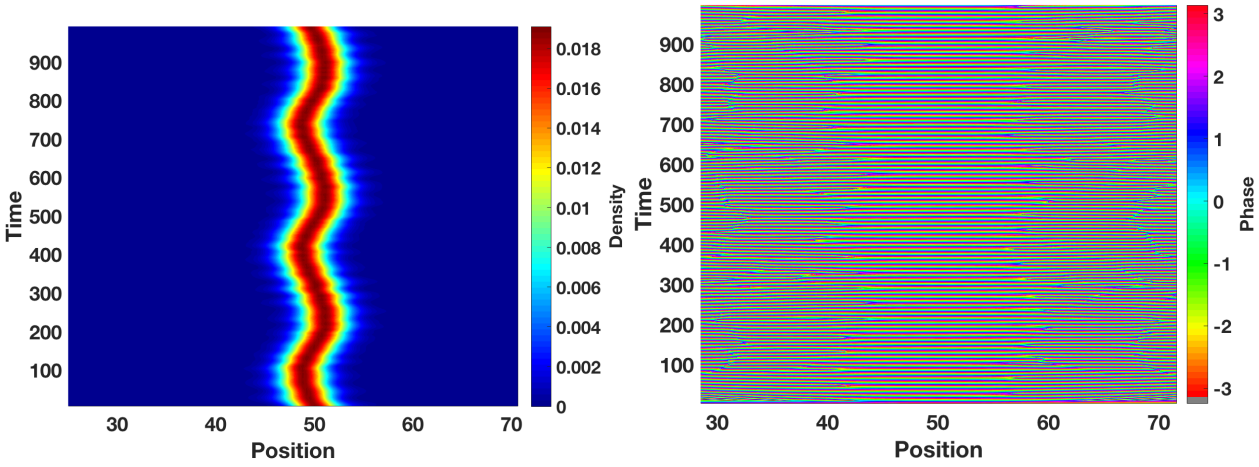

Figure 5.8 Oscillation of bright component in a harmonic potential. We plot the density (phase) in the upper (lower) panel for the bright component in dark-bright soliton with harmonic potential frequency, $\Omega/2\pi = 0.0064$, $g_1 = 2$, $g_2 = 2.6$ and $g = 2.6$.

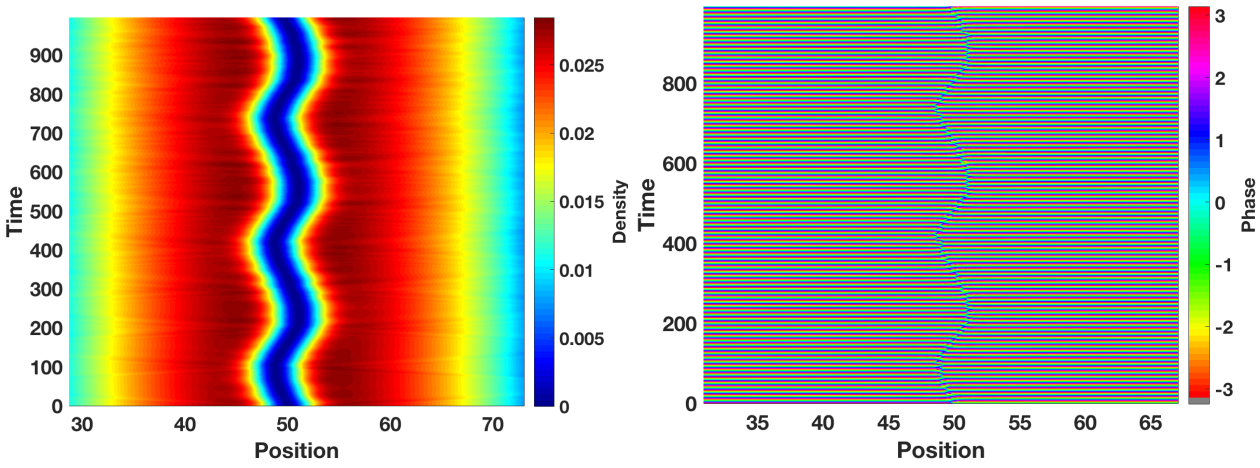

Figure 5.9 Oscillation of dark component in a harmonic potential. We plot the density (phase) in the upper (lower) panel for the dark component in dark-bright soliton with harmonic potential frequency, $\Omega/2\pi = 0.0064$, $g_1 = 2$, $g_2 = 2.6$ and $g = 2.6$.

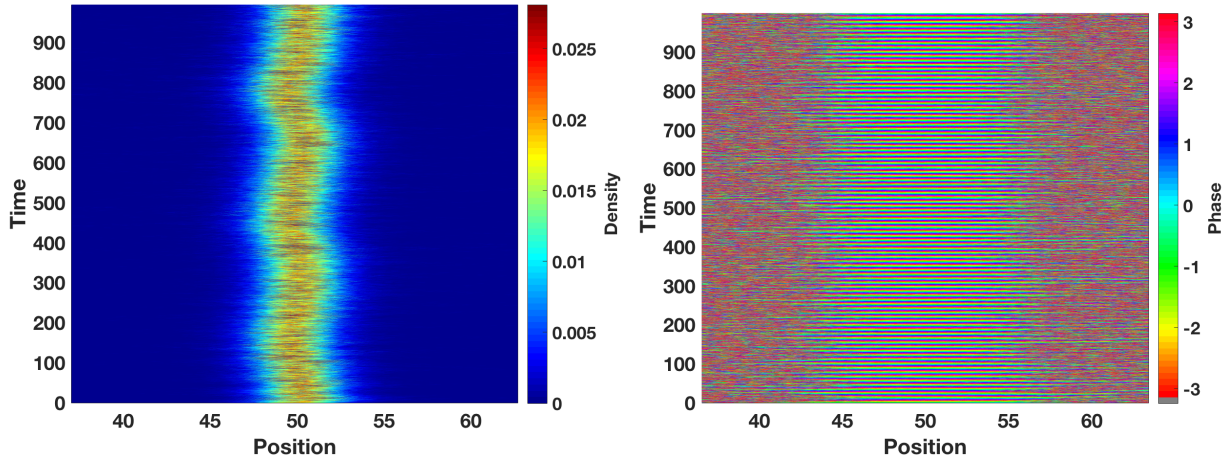

Figure 5.10 Oscillation of bright component in a harmonic potential when white noise added. We plot the density (phase) in the upper (lower) panel for the bright component in dark-bright soliton for the same parameters in Figure 5.8 with 5% noise added to the initial wave function at $t = 0$. The bright component oscillate with the same frequency in Figure 5.8 but with less oscillation amplitude.

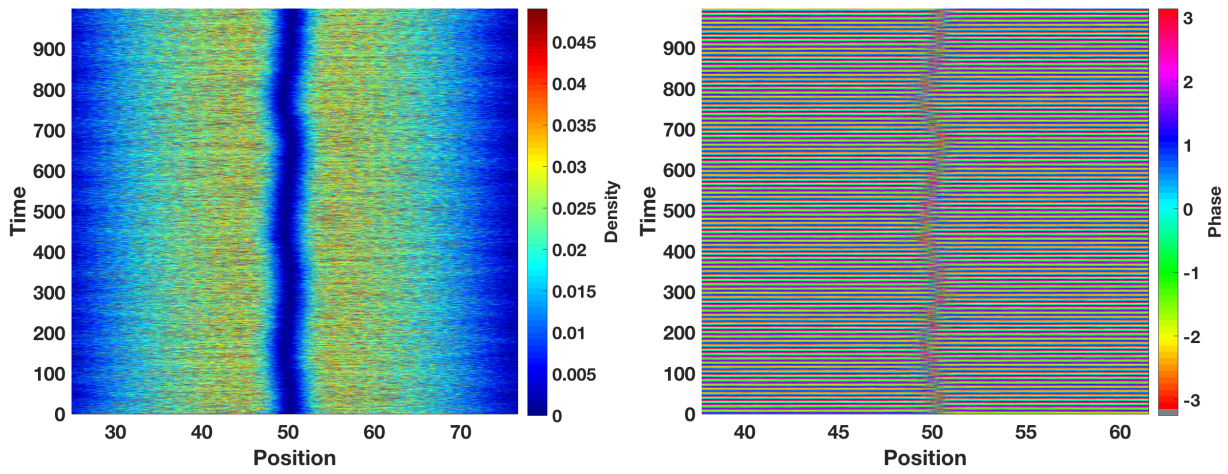

Figure 5.11 Oscillation of dark component in a harmonic potential with white noise added. Shown are density (phase) in the upper (lower) panel for the dark component in a dark-bright soliton for the same parameters in Figure 5.9 with 5% noise added to the initial wave function at $t = 0$. The dark component oscillates with the same frequency in Figure 5.9 but with a slightly smaller oscillation amplitude.

soliton oscillates with $\omega_{\rm DB}/2\pi = 0.0039$ and the internal oscillation in this case is $\omega_{\rm internal} = 0.032$. The noisy case is found to oscillate with the same frequency but with a slightly reduced oscillation amplitudeas can be seen in Figure 5.10 for the bright component and in Figure 5.11 for the dark component. Thus we expect our predictions to be experimentally observable.

5.4 Conclusions

We obtained a system of equation of motions for a dark-bright soliton in a harmonic potential. We used a variational method with a hyperbolic tangent for the dark component and a hyperbolic secant for the bright component. The harmonic potential modifies the background of the dark component according to the well-known Thomas-Fermi background approximation. A perturbation method was needed to include the effect of the harmonic potential, which amounts to restricting our analytical treatment cigar-shaped traps, also common in experiments.

The decoupling of relative and center of mass degrees of freedom for the harmonic case occurs for the classical two-body problem as well as its quantum extension, including to more than two particles, with relative coordinates appropriately generalized. It is not immediately obvious this decoupling should also occur for a two-body bound state of two emergent features, a bright and a dark soliton. For example, spontaneous symmetry breaking often causes such emergent properties to not respect underlying symmetries. In previous work, we showed that for a uniform system the decoupling in fact does hold [65]. For a weak trap, this property nearly holds, but as the trapping strength is increased, internal oscillations and external motion are strongly coupled. The effective potential, consisting of a sum between the potential and the mean field, may well be responsible for this effect, as found for example in non-exponential tunneling decay out of quasibound states in the scalar case [79–81]. As the trap is tightened the edges of the condensate are deformed by approach of the dark-bright soliton during its oscillations. Because we treat a purely repulsive condensate in both components, the effective potential is larger than the bare potential, leading to a higher effective trapping frequency. Moreover, the edges of the trap now impinge on the dark-bright soliton internal oscillations, shortening the internal oscillation time and therefore leading to a higher frequency. The result is a coupling between center of mass motion deforming the effective potential, and internal oscillations being sped up by the deformation.

Future work could be the study of the internal oscillation of the two-component dark-bright soliton in a harmonic potential with an impurity at the center to look at the damping of a dark-bright soliton under periodic interaction with an impurity. Other works have investigated the interaction of a dark-bright soliton in a harmonic potential with an impurity, but they did not take into account internal modes. Thus we suggest adding one more degree of freedom, namely, a relative coordinate for the position of the dark and bright solitons, which as we have shown is vital to understand and predict harmonic motion.

5.5 Matrix elements

The matrix elements in Eq. (5.19) are,

$$
\begin{aligned}
A_{11} &= i\omega, \\
A_{12} &= \frac{8gu_0^2}{15g_1 \mathrm{w}_{\mathrm{fp}}^2} - \frac{g\pi^2\Omega^2}{45g_1}, \\
A_{13} &= -\frac{8gu_0^2}{15g_1 \mathrm{w}_{\mathrm{fp}}^2} - \Omega^2 + \frac{2g\Omega^2}{3g_1} + \frac{g\pi^2\Omega^2}{45g_1}, \\
A_{22} &= \frac{4gu_0^2}{15g_2 \mathrm{w}_{\mathrm{fp}}^2} - \frac{\Omega^2(2 + u_0^2 \mathrm{w}_{\mathrm{fp}}^2)}{6u_0^2 \mathrm{w}_{\mathrm{fp}}}, \\
A_{23} &= -\frac{4gu_0^2}{15g_2 \mathrm{w}_{\mathrm{fp}}^2}, \\
A_{24} &= i\omega, \\
A_{32} &= \frac{4iu_0^2\omega}{g_1}, \\
A_{34} &= -\frac{\pi^2 u_0^2 \mathrm{w}_{\mathrm{fp}}^3 \Omega^2}{6g_1}, \\
A_{45} &= \frac{16gu_0^4 \mathrm{w}_{\mathrm{fp}}}{3g_1 g_2}, \\
A_{46} &= -\frac{8u_0^4}{3g_1} + \frac{8gu_0^4}{3g_1 g_2} + \frac{4u_0^2}{3g_1 \mathrm{w}_{\mathrm{fp}}^2} \\
&\quad - \Omega^2\left(\frac{6 + (12 + \pi^2)u_0^2 \mathrm{w}_{\mathrm{fp}}^2}{6g_1}\right), \\
A_{47} &= -\frac{4u_0^2}{3g_1 \mathrm{w}_{\mathrm{fp}}} - \frac{8u_0^4 \mathrm{w}_{\mathrm{fp}}}{g_1} + \frac{8gu_0^4 \mathrm{w}_{\mathrm{fp}}}{3g_1 g_1} \\
&\quad - \Omega^2\left(\frac{6 + (12 + \pi^2)u_0^2 \mathrm{w}_{\mathrm{fp}}^3}{6g_1}\right),
\end{aligned}
\tag{5.29}
$$

$$
\begin{aligned}
A_{55} &= 2i\mathrm{w}_{\mathrm{fp}}\omega, \\
A_{56} &= i\omega, \\
A_{61} &= \mathrm{w}_{\mathrm{fp}}, \\
A_{63} &= i\mathrm{w}_{\mathrm{fp}}\omega, \\
A_{65} &= \mathrm{w}_{\mathrm{fp}}\phi_{1fp}, \\
A_{66} &= \phi_{1fp}, \\
A_{75} &= -\frac{4(g_1-g_2)u_0^2}{3g_1g_2\mathrm{w}_{\mathrm{fp}}} - \frac{4(3g_1+g_2)u_0^4\mathrm{w}_{\mathrm{fp}}}{3g_1g_2} + \Omega^2\left(\frac{2(\pi^2-6)\mathrm{w}_{\mathrm{fp}}}{9g_1}\right. \\
&\quad \left. + \frac{u_0^2\mathrm{w}_{\mathrm{fp}}^3}{18g_1g_2}\left[-6(g+2g_2)+\pi^2(-5g+6g_1+3g_2)\right]\right), \\
A_{76} &= -\frac{4(g_1-g_2)u_0^4}{3g_1g_2} + \frac{4(g_1+g_2)u_0^2}{3g_1g_2\mathrm{w}_{\mathrm{fp}}^2} + \Omega^2\left(\frac{12-2\pi^2+27u_0^2\mathrm{w}_{\mathrm{fp}}^2}{9g_1}+\right. \\
&\quad \left.\frac{(2g_1-g_2)\pi^2u_0^2\mathrm{w}_{\mathrm{fp}}^2}{2g_1g_2} - \frac{g(6+5\pi^2)u_0^2\mathrm{w}_{\mathrm{fp}}^2}{6g_1g_2}\right),
\end{aligned}
\tag{5.30}
$$

$$
A_{77} = \frac{8u_0^2}{3g_1\mathrm{w}_{\mathrm{fp}}}(-1+2u_0^2\mathrm{w}_{\mathrm{fp}}^2) + \Omega^2\left(-\frac{2(-6+\pi^2)\mathrm{w}_{\mathrm{fp}}(2+3u_0^2\mathrm{w}_{\mathrm{fp}}^2)}{9g_1} + \frac{g(-6+\pi^2)u_0^2\mathrm{w}_{\mathrm{fp}}^3}{9g_1g_2}\right),
\tag{5.31}
$$

$$
\begin{aligned}
A_{85} &= -\frac{2u_0^2}{3g_1g_2\mathrm{w}_{\mathrm{fp}}}(g_1+2gu_0^2\mathrm{w}_{\mathrm{fp}}^2+12g_1u_0^2\mathrm{w}_{\mathrm{fp}}^2) + \Omega^2\left(\frac{g(12+\pi^2)u_0^2\mathrm{w}_{\mathrm{fp}}^3}{18g_1g_2} - \frac{\pi^2u_0^2\mathrm{w}_{\mathrm{fp}}^3}{6g_2}\right), \\
A_{86} &= \frac{1}{2g_2g_2\mathrm{w}_{\mathrm{fp}}^2}(2g_1u_0^2-4gu_0^4\mathrm{w}_{\mathrm{fp}}^2-8g_1u_0^4\mathrm{w}_{\mathrm{fp}}) + \Omega^2\left(\frac{gu_0^2\mathrm{w}_{\mathrm{fp}}^2(12+\pi^2)}{6g_1g_2} - \frac{\pi^2u_0^2\mathrm{w}_{\mathrm{fp}}^2}{2g_2}\right), \\
A_{87} &= \frac{16gu_0^4\mathrm{w}_{\mathrm{fp}}}{3g_1g_2} - \Omega^2\left(\frac{2gu_0^2\mathrm{w}_{\mathrm{fp}}^3}{9g_1g_2}\right), \\
A_{88} &= -\frac{4iu_0^2\mathrm{w}_{\mathrm{fp}}\omega}{g_2}.
\end{aligned}
$$

The frequency coefficients are,

$$\alpha_1 = \frac{1}{27 g_1^3 g_2^3}\left[768 u_0^8 (3 g_2 (g_2 - g_1) + u_0^2 \mathrm{w}_{\mathrm{fp}}^2 (2 g (3 g_1 + g_2) - g_2 (19 g_1 + 25 g_2)) \right. \tag{5.32}$$
$$+2(-g_2(3g_1+g_2)+g(g_1+3g_2))u_0^4\mathrm{w}_{\mathrm{fp}}^4$$
$$-32u_0^6\mathrm{w}_{\mathrm{fp}}^2\{2g_2(27g_1+g_2(129-14\pi^2))$$
$$+g_2(-198g+126g_1+600g_2+(3g+39g_1)$$
$$-70g_2\pi^2)u_0^2\mathrm{w}_{\mathrm{fp}}^2+12(5g^2+32gg_2+3g_2(g_1+8g_2))+u_0^4\mathrm{w}_{\mathrm{fp}}^4(50g^2+3(61g_1-31g_2)g_2$$
$$-4g(15g_1+29g_2))\}\Omega^2$$
$$-4g_2u_0^4\mathrm{w}_{\mathrm{fp}}^4(6+(12+\pi^2)u_0^2\mathrm{w}_{\mathrm{fp}}^2)(4g_2(-6+\pi^2))$$
$$\left.+(-6(g+3g_2)+(-29g+30g_1+3g_2)\pi^2u_0^2)\mathrm{w}_{\mathrm{fp}}^2\Omega^4)\right],$$

$$\alpha_2 = \frac{u_0^2}{4860 g_1^4 g_2^4 \mathrm{w}_{\mathrm{fp}}^2}\{384 g g_2 u_0^4 + 8 u_0^2 \mathrm{w}_{\mathrm{fp}}^2 (90 g_1 g_2 \tag{5.33}$$
$$-2gg_2(30+\pi^2)+gg_1\pi^2u_0^2\mathrm{w}_{\mathrm{fp}}^2)\Omega^2$$
$$-5g_1g_2\pi^2\mathrm{w}_{\mathrm{fp}}^4(2+u_0^2\mathrm{w}_{\mathrm{fp}}^2)\Omega^4$$
$$\left[192u_0^4(3(g_1-g_2)g_2+(-2g(3g_1+g_2)\right.$$
$$\left.+g_2(19g_1+25g_2))u_0^2\mathrm{w}_{\mathrm{fp}}^2 2(g_2(3g_1+g_2)-g(g_1+3g_2))u_0^4\mathrm{w}_{\mathrm{fp}}^4)\right]$$
$$+8u_0^2\mathrm{w}_{\mathrm{fp}}^2(2g_2(27g_1$$
$$+g_2(129-14\pi^2))+g_2(-198g+126g_1$$
$$+600g_2+(3g+39g_1-70g_2)\pi^2)u_0^2\mathrm{w}_{\mathrm{fp}}^2+(12(5g^2-32gg^2+3g_2(g_1+8g_2)+(50g^2+3(61g_1-31g_2)g_2$$
$$-4g(15g_1+29g_2))\pi^2)u_0^4\mathrm{w}_{\mathrm{fp}}^4)\Omega^2$$
$$+g_2\mathrm{w}_{\mathrm{fp}}^4(^+(12+\pi^2)u_0^2\mathrm{w}_{\mathrm{fp}}^2)(4g_2(-6+\pi^2)+(-6(g+3g_2)+(-29g+30g_1+3g_2)\pi^2)u_0^4\mathrm{w}_{\mathrm{fp}}^4)\Omega^4)\},$$

$$\alpha_3 = \frac{\pi^2 u_0^2 \Omega^4}{43740 g_1^4 g_2^4}(24 g u_0^2(2g_2 + (2g - 3g_1 + g_2)u_0^2 \mathrm{w}_{\mathrm{fp}}^2) \tag{5.34}$$
$$- g_2(-45g_1 + g(30 + \pi^2))\mathrm{w}_{\mathrm{fp}}^2(2 + u_0^2 \mathrm{w}_{\mathrm{fp}}^2)\Omega^2)$$
$$(192u_0^4(3(g_1 - g_2)g_2 + (-2g(3g_1 + g_2)$$
$$+ g_2(19g_1 + 25g_2))u_0^2 \mathrm{w}_{\mathrm{fp}}^2$$
$$+ 2(g_2(3g_1 + g_2) - g(g_1 + 3g_2))u_0^4 \mathrm{w}_{\mathrm{fp}}^4) + 8u_0^2 \mathrm{w}_{\mathrm{fp}}^2(2g_2(27g_1 + g_2(129 - 14\pi^2))$$
$$+ g_2(-198g + 126g_1$$
$$+ 600g_2 + (3g + 39g_1 - 70g_2)\pi^2)u_0^4 \mathrm{w}_{\mathrm{fp}}^4 + (12(5g^2 - 32gg_2 + 3g_2(g_1 + 8g_2)) + (50g^2$$
$$+ 3(61g_1 - 31g_2)g_2 - 4g(15g_1 + 29g_2))\pi^2)u_0^4 \mathrm{w}_{\mathrm{fp}}^4)\Omega^2$$
$$g_2 \mathrm{w}_{\mathrm{fp}}^4(6 + (12 + \pi^2)u_0^2 \mathrm{w}_{\mathrm{fp}}^2)(4g_2$$
$$(-6 + \pi^2) + (-6(g + 3g_2)$$
$$+ (-29g + 30g1 + 3g_2)\pi^2)u_0^2 \mathrm{w}_{\mathrm{fp}}^2)\Omega^4).$$

CHAPTER 6

CONCLUSIONS AND OUTLOOK

A dark-bright soliton is a bound state of a bright component with positive kinetic energy and a dark component with negative kinetic energy. We can think of the exciton as an analogy to this system where we have a bound state of an electron and a hole which are attracted to each other by the electrostatic Coulomb force. This model where we have two such complementary existing objects in a bound state is ubiquitous in nature. Therefore, a detailed study of the dynamics of these models is needed. The ability to control, to a high degree of accuracy, the interactions between the particles in each component in the dark-bright soliton and the interaction between the two components in BECs makes dark-bright solitons an ideal platform to compare the analytical predictions of mathematical models to the outcomes of experiments. The general motivation in this thesis is to shed light on relevant quantities that needed to be identified to gain a better understanding of the nature of dark-bright soliton interactions in BECs such as the binding energy between the two components, internal excitations, etc. Another aspect that motivates us to work with dark-bright solitons in BECs is that it can only exist in multiple-component condensates. In this case, due to the intra-actions/interactions of particles in multiple components, richer phenomena can be found than would be possible in one-component BECs.

In this thesis, we have studied the behavior of the two-component dark-bright solitons in BECs analytically and numerically. We utilized different analytical methods like the variational method, perturbation theory, etc. It is a well-known fact that the efficiency of the variational approach depends on the choice of the trial function (i.e., the ansatz). To obtain an accurate description, we used hyperbolic functions in our calculations which is more accurate than the Gaussian function and more challenging to work with. We compare our findings with numerical simulations where we use a pseudospectral method.

In the first project, we studied the internal oscillation of the two components dark-bright soliton. We calculated the normal modes of the system where we used hyperbolic secant for the bright soliton component and hyperbolic tangent for the dark soliton component. The velocity of each component depends on the imprinted phase. In the case of the dark soliton, the velocity depends on the amplitude too, in case we include this as a variational parameter, as in the second which we do in the second project. We find that there are two modes of the oscillation of the dark-bright soliton. The first one is the famous Goldstone mode. This mode represents a moving dark-bright soliton without internal oscillation and is related to continuous translational symmetry of the underlying equations of motion in the uniform potential. The second mode is the one we are interested in, namely the oscillation of the two components relative to each other. We compared the results obtained from the variational method with numerical simulations. We studied the binding energy and found a critical value for the breakup of the dark-bright soliton. By imprinting a linear phase on the bright component only, we were able to impart a velocity relative to the dark component. If we imprint a small phase, we get an oscillation between the two components, similar to exciting a vibrational mode of a diatomic molecule. But if we imprint a large phase we break up the dark-bright soliton, similar to unbinding a diatomic molecule. By comparing the kinetic and mean-field energies of the two components that we got from the analytical calculations, we find the critical value for the unbinding or break up of the dark-bright soliton. We investigated this scenario also numerically. We found by numerical simulation that to get a bright component in a dark-bright soliton the density must be less than the density of the dark element. We obtain this result analytically too, where we noticed that to make the dark and bright components oscillate relative to each other we must meet this rule. Also, we found numerically that the oscillation frequency is independent of the imprinted phase on the bright soliton. This means that for a small phase kick we have a simple harmonic oscillation motion around the equilibrium point. A possibility to extend this work is by considering an oscillation between three-component solitons. Different platforms could host

such experiments. For example, we can have three-component solitons in different hyperfine states of BEC like ^{87}Rb in the $F = 1$,$m_F \in \{-1, 0, +1\}$ states or for different types of atoms. In multicomponent BECs produced from the same hyperfine manifold, the phase between various components is coherent and the norm is not separately conserved, only the total number of atoms. This additional feature must be accounted in the analytical calculations.

In the second project, we studied the propagation of two-component dark-bright solitons in the presence of impurities. Physically any small impurity, relative to the size of the soliton, can be represented by a delta function: for instance, a heavy impurity atom, or a potential perturbation made with an focused laser. The inclusion of a delta function potential affects the background of the dark component. Therefore, we approximate the effect by considering a well-known method, namely, the Thomas-Fermi background approximation where we also used the perturbation theory. The interaction of the dark-bright soliton with the potential excites different modes in the system. As a result, the dark-bright soliton emerges with a different velocity. Our analytical model capture two of these modes: the dominant feature of relative oscillation between the two components, as well as the oscillation in the widths. However, the analytical model requires these widths oscillate in sync. The numerical simulations allow further internal modes to enter the problem, starting with out-of-sync oscillations of the soliton widths, and including even shape deformations of various kinds. We identify regions for the transmission, reflection and inelastic scattering of the dark-bright soliton by the potential barrier. We present three case studies outline the basic kinds of dynamical outcomes. The many internal modes excited in this problem show the complexity of the nonlinear dynamical multicomponent problem. Our study points to different physical regimes, and one can follow up by applying our model to any particular experiment intending to pursue the scattering question. The scattering of a dark-bright soliton could also cause quantum fluctuations, as one might model, e.g., in dynamical Bogoliubov theory. In this case, the kinetic energy would go not only into internal mean-field modes but also into enhanced quantum fluctuations localized in and near the dark-bright soliton. If that is the case, then

a reduced velocity of a scattered dark-bright soliton beyond mean-field predictions will be a sign of quantum fluctuations. This is another strong reason to get the mean-field inelastic scattering correct, carefully understanding all internal modes created by interaction with the impurity. We also study in this project the velocity of the dark-bright soliton. The velocity of a one-component dark soliton is well understood. By adding another component, in this case, a bright soliton, the behavior of the dark soliton speed is changing. We found for a dark-bright soliton the maximum velocity is limited by the relative number of atoms in the bright component as compared to the size of the hole or density notch created by the dark component. Above this critical velocity the dark-bright soliton develops internal oscillations, and eventually unbinds and breaks apart. Future work may extend the investigation of the interaction of dark-bright solitons with an impurity to three components, where the dynamics of internal excitations may become much more complex. We might rip apart the dark-bright soliton with the proper resonance condition, as found for exciton transport. In this sense the barrier can be used to reflect, transmit, excite, or even destroy the dark-bright soliton. In addition, by solving this single impurity problem, we may extend the work for solving the disordered problem.

In the last project, we studied the internal oscillation of the two-component dark-bright soliton in a harmonic potential. We used a variational method with a hyperbolic tangent for the dark component and a hyperbolic secant for the bright component. The harmonic potential modified the background of the dark component according to the well-known Thomas-Fermi background approximation. Therefore, a perturbation method was needed to include the effect of the harmonic potential. The decoupling of relative and center of mass degrees of freedom for the harmonic case occurs for the classical two-body problem as well as its quantum extension, including to more than two particles, with relative coordinates appropriately generalized. In this project, we studied the decoupling for a two-body bound state of two emergent features, a bright and a dark soliton and found that for a weak trap the internal oscillation modes were nearly independent of center of mass motion of the dark-bright

soliton. But as the trapping strength increased, internal oscillations and external motion were strongly coupled. One reason for this effect could be the effective potential as found for example in non-exponential tunneling decay out of quasibound states in the scalar case [79–81]. The tightened trap deforms the edges of the condensate when the dark-bright soliton approaches during its oscillations. Therefore, the edges of the trap influence the internal oscillation of the dark-bright soliton and as a result a coupling between the internal oscillation modes and the center of mass motion occurs. Future work could be the study of the internal oscillation of the two-component dark-bright soliton in a harmonic potential with an impurity at the center to look at the damping of a dark-bright soliton under periodic interaction with an impurity. Other works have investigated the interaction of a dark-bright soliton in a harmonic potential with an impurity, but they did not take into account internal modes. Thus we suggest adding one more degree of freedom, namely, a relative coordinate for the position of the dark and bright solitons, which as we have shown is vital to understand and predict harmonic motion.

REFERENCES CITED

[1] T. Dauxois and M. Peyrard. *Physics of Solitons*. Cambridge University Press, 2006. ISBN 9780521143608. URL https://books.google.com/books?id=YKe1UZc_Qo8C.

[2] A. Osborne. *Nonlinear Ocean Waves and the Inverse Scattering Transform*, volume 97. 2010. ISBN 9780125286299. doi: 10.1016/S0074-6142(10)97029-0. URL http://scholar.google.com/scholar?hl=en&btnG=Search&q=intitle:Nonlinear+ocean+waves+and+the+inverse+scattering+transform#1.

[3] A. Hasegawa. Transmission of stationary nonlinear optical pulses in dispersive dielectric fibers. I. Anomalous dispersion. *Applied Physics Letters*, 23(3):142, 1973. ISSN 00036951. doi: 10.1063/1.1654836. URL http://link.aip.org/link/?APL/23/142/1&Agg=doi.

[4] L. F. Mollenauer, R. H. Stolen, and J. P. Gordon. Experimental observation of picosecond pulse narrowing and solitons in optical fibers. *Physical Review Letters*, 45(13):1095–1098, 1980. ISSN 00319007. doi: 10.1103/PhysRevLett.45.1095.

[5] A. M. Weiner, J. P. Heritage, R. J. Hawkins, and R. N. Thurston. experimental observation of the fundamental dark soliton in optical fibers. *Physical Review Letters*, 61(21):2445–2448, 1988. URL http://link.aps.org/doi/10.1103/PhysRevLett.61.2445.

[6] P. G. Kevrekidis, D. J. Frantzeskakis, R. Carretero-González, N. G. Parker, B. Jackson, A. M. Martin, and C. S. Adams. *Emergent Nonlinear Phenomena in Bose-Einstein Condensates*. Springer Series, 2008. ISBN 978-3-540-73590-8. doi: 10.1007/978-3-540-73591-5. URL http://www.springer.com/us/book/9783540735908.

[7] H. J. Metcalf and P. van der Straten. *Laser Cooling and Trapping*. Graduate Texts in Contemporary Physics. Springer New York, 2001. ISBN 9780387987286. URL https://books.google.com/books?id=i-40VaXqrj0C.

[8] L. D. Carr, J. Brand, S. Burger, and A. Sanpera. Dark soliton creation in Bose-Einstein condensates. *Physical Review A*, 63(5):051601, Nov 2001. doi: 10.1103/PhysRevA.63.051601. URL http://link.aps.org/doi/10.1103/PhysRevA.63.051601.

[9] P. G. Kevrekidis, D. J. Frantzeskakis, and R. Carretero-González. *The Defocusing Nonlinear Schrodinger Equation: From Dark Solitons to Vortices and Vortex Rings*. Society for Industrial and Applied Mathematics, 2015. ISBN 9781611973945. URL https://books.google.com/books?id=1BVoCgAAQBAJ.

[10] C. Becker, S. Stellmer, P. Soltan-Panahi, S. Dorscher, M. Baumert, E. Richter, J. Kronjager, K. Bongs, and K. Sengstock. Oscillations and interactions of dark and dark-bright solitons in Bose-Einstein condensates. *Nat Phys*, 4(6):496–501, jun 2008. ISSN 1745-2473. URL http://dx.doi.org/10.1038/nphys962.

[11] Th. Busch and J. Anglin. Dark-Bright Solitons in Inhomogeneous Bose-Einstein Condensates. *Physical Review Letters*, 87(1):2–5, jun 2001. ISSN 0031-9007. doi: 10.1103/PhysRevLett.87.010401.

[12] C. Hamner, J. J. Chang, P. Engels, and M. A. Hoefer. Generation of Dark-Bright Soliton Trains in Superfluid-Superfluid Counterflow. *Physical Review Letters*, 106(6):65302, feb 2011. URL http://link.aps.org/doi/10.1103/PhysRevLett.106.065302.

[13] S. Rajendran, P. Muruganandam, and M. Lakshmanan. Interaction of dark-bright solitons in two-component Bose-Einstein condensates. *Journal of Physics B: Atomic, Molecular and Optical Physics*, 42(14):145307, jul 2009. ISSN 0953-4075. doi: 10.1088/0953-4075/42/14/145307. URL http://stacks.iop.org/0953-4075/42/i=14/a=145307?key=crossref.f6657ea2f6393059ff52eeadbf96ac1b.

[14] Xiao-Fei Zhang, Xing-Hua Hu, Xun-Xu Liu, and W. M. Liu. Vector solitons in two-component Bose-Einstein condensates with tunable interactions and harmonic potential. *Physical Review A*, 79(3):33630, mar 2009. URL http://link.aps.org/doi/10.1103/PhysRevA.79.033630.

[15] M. A. Hoefer, J. J. Chang, C. Hamner, and P. Engels. Dark-dark solitons and modulational instability in miscible two-component Bose-Einstein condensates. *Physical Review A*, 84(4):41605, oct 2011. URL http://link.aps.org/doi/10.1103/PhysRevA.84.041605.

[16] F. Kh. Abdullaev, A. Gammal, A. M. Kamchatnov, and L. Tomio. Dynamics of Bright Matter Wave Solitons in a Bose-Einstein Condensate. *International Journal of Modern Physics B*, 19(22):3415–3473, sep 2005. ISSN 0217-9792. doi: 10.1142/S0217979205032279. URL http://www.worldscientific.com/doi/abs/10.1142/S0217979205032279.

[17] V. Pérez-García and J. Beitia. Symbiotic solitons in heteronuclear multicomponent Bose-Einstein condensates. *Physical Review A*, 72(3):1–5, sep 2005. ISSN 1050-2947. doi: 10.1103/PhysRevA.72.033620. URL http://link.aps.org/doi/10.1103/PhysRevA.72.033620.

[18] Y. S. Kivshar and B. Luther-Davies. Dark optical solitons: physics and applications. *Physics Reports*, 298:81 – 197, 1998. URL http://www.sciencedirect.com/science/article/pii/S0370157397000732.

[19] T. Karpiuk, M. Brewczyk, S. Ospelkaus-Schwarzer, K. Bongs, M. Gajda, and K. Rzażewski. Soliton Trains in Bose-Fermi Mixtures. *Physical Review Letters*, 93 (10):100401, sep 2004. URL http://link.aps.org/doi/10.1103/PhysRevLett.93.100401.

[20] D. J. Kaup, B. A. Malomed, and R. S. Tasgal. Internal dynamics of a vector soliton in a nonlinear optical fiber. *Physical Review E*, 48(4):3049–3053, oct 1993. URL http://link.aps.org/doi/10.1103/PhysRevE.48.3049.

[21] B. A. Malomed. Polarization dynamics and interactions of solitons in a birefringent optical fiber. *Physical Review A*, 43(1):410–423, jan 1991. URL http://link.aps.org/doi/10.1103/PhysRevA.43.410.

[22] J. Scheuer and M. Orenstein. forces and equilibrium states between interacting vector solitons. *JOSA B*, 18(7):954–959, 2001. URL http://www.opticsinfobase.org/abstract.cfm?uri=josab-18-7-954.

[23] Y. V. Kartashov, V. A. Vysloukh, L. Torner, and B. A. Malomed. Self-trapping and splitting of bright vector solitons under inhomogeneous defocusing nonlinearities. *Optics letters*, 36(23):4587–9, dec 2011. ISSN 1539-4794. URL http://www.ncbi.nlm.nih.gov/pubmed/22139251.

[24] V. V. Afanasyev, Y. S. Kivshar, V. V. Konotop, and V. N. Serkin. Dynamics of coupled dark and bright optical solitons. *Optics letters*, 14(15):805–7, aug 1989. ISSN 0146-9592. URL http://www.ncbi.nlm.nih.gov/pubmed/19752974.

[25] D. J. Frantzeskakis. Dark solitons in atomic Bose-Einstein condensates: From theory to experiments. *Journal of Physics A: Mathematical and Theoretical*, 43(21):213001, may 2010. ISSN 1751-8113. doi: 10.1088/1751-8113/43/21/213001. URL http://stacks.iop.org/1751-8121/43/i=21/a=213001?key=crossref.5abffdb4faea7a9d58cbcb2019b4ba0e.

[26] R. Carretero-Gonzlez, D. J. Frantzeskakis, and P. G. Kevrekidis. Nonlinear waves in Bose-Einstein condensates: physical relevance and mathematical techniques. *Nonlinearity*, 21(7):R139, 2008. ISSN 0951-7715. URL http://stacks.iop.org/0951-7715/21/i=7/a=R01.

[27] Xunxu Liu, Han Pu, Bo Xiong, W. M. Liu, and J. Gong. Formation and transformation of vector solitons in two-species Bose-Einstein condensates with a tunable interaction. *Physical Review A*, 79(1):13423, jan 2009. URL http://link.aps.org/doi/10.1103/PhysRevA.79.013423.

[28] L. Qiu-Yan, L. Zai-Dong, and Y. Shu-Fang. Formation of combined solitons in two-component Bose–Einstein condensates. *Chinese Physics B*, 19(8):080501, 2010. URL http://iopscience.iop.org/1674-1056/19/8/080501.

[29] Zhang Xiao-Fei, Zhang Pei, He Wan-Quan, and Liu Xun-Xu. Stability properties of vector solitons in two-component Bose–Einstein condensates with tunable interactions. *Chinese Physics B*, 20(2):020307, 2011. URL http://stacks.iop.org/1674-1056/20/i=2/a=020307.

[30] D. Yan, J. J. Chang, C. Hamner, M. Hoefer, P. G. Kevrekidis, P. Engels, V. Achilleos, D. J. Frantzeskakis, and J. Cuevas. Beating dark-dark solitons in Bose-Einstein condensates. *Journal of Physics B: Atomic, Molecular and Optical Physics*, 45(11):115301, 2012. URL http://stacks.iop.org/0953-4075/45/i=11/a=115301.

[31] S. Middelkamp, J. J. Chang, C. Hamner, R. Carretero-González, P. G. Kevrekidis, V. Achilleos, D.J. Frantzeskakis, P. Schmelcher, and P. Engels. Dynamics of darkbright solitons in cigar-shaped Bose-Einstein condensates. *Physics Letters A*, 375(3):642–646, jan 2011. URL http://dx.doi.org/10.1016/j.physleta.2010.11.025.

[32] S. Burger, K. Bongs, S. Dettmer, W. Ertmer, and K. Sengstock. Dark Solitons in Bose-Einstein Condensates. *Physical Review Letters*, 83(25):5198–5201, dec 1999. ISSN 0031-9007. doi: 10.1103/PhysRevLett.83.5198. URL https://secure.mines.edu/abstract/PRL/v83/i25/,DanaInfo=prl.aps.org,SSO=U+p5198_1.

[33] J. Denschlag, J. E. Simsarian, D. L. Feder, C. W. Clark, L. A. Collins, J. Cubizolles, L. Deng, E. W. Hagley, K. Helmerson, W. P. Reinhardt, S. L. Rolston, B. I. Schneider, and W. D. Phillips. Generating Solitons by Phase Engineering of a Bose–Einstein Condensate. *Science*, 287(5450):97–101, 2000. ISSN 0036-8075. doi: 10.1126/science.287.5450.97. URL http://science.sciencemag.org/content/287/5450/97.

[34] K. E. Strecker, G. B. Partridge, A. G. Truscott, and R. G. Hulet. Formation and propagation of matter-wave soliton trains. *Nature*, 417(6885):150–3, May 2002. ISSN 0028-0836. doi: 10.1038/nature747. URL http://www.ncbi.nlm.nih.gov/pubmed/11986621.

[35] L. Khaykovich, F. Schreck, G. Ferrari, T. Bourdel, J. Cubizolles, L. D. Carr, Y. Castin, and C. Salomon. Formation of a matter-wave bright soliton. *Science (New York, N.Y.)*, 296(5571):1290–3, may 2002. ISSN 1095-9203. doi: 10.1126/science.1071021. URL http://www.sciencemag.org/content/296/5571/1290.short.

[36] B. P. Anderson, P. C. Haljan, C. A. Regal, D. L. Feder, L. A. Collins, C. W. Clark, and E. A. Cornell. Watching Dark Solitons Decay into Vortex Rings in a Bose-Einstein Condensate. *Physical Review Letters*, 86(14):2926–2929, apr 2001. ISSN 0031-9007. doi: 10.1103/PhysRevLett.86.2926. URL http://link.aps.org/doi/10.1103/PhysRevLett.86.2926.

[37] F. Y. Lim and W. Bao. Numerical methods for computing the ground state of spin-1 Bose-Einstein condensates in a uniform magnetic field. *Phys. Rev. E*, 78(6):66704, dec 2008. doi: 10.1103/PhysRevE.78.066704. URL https://link.aps.org/doi/10.1103/PhysRevE.78.066704.

[38] Jen-Hao Chen, I-Liang Chern, and Weichung Wang. Exploring ground states and excited states of spin-1 Bose-Einstein condensates by continuation methods. *Journal of Computational Physics*, 230(6):2222–2236, 2011. ISSN 0021-9991. doi: https://doi.org/10.1016/j.jcp.2010.11.048. URL http://www.sciencedirect.com/science/article/pii/S0021999110006637.

[39] P. Bader, S. Blanes, and F Casas. Solving the schrdinger eigenvalue problem by the imaginary time propagation technique using splitting methods with complex coefficients. *The Journal of Chemical Physics*, 139(12):124117, 2013. doi: 10.1063/1.4821126. URL https://doi.org/10.1063/1.4821126.

[40] T. Ernst and J. Brand. Resonant trapping in the transport of a matter-wave soliton through a quantum well. *Physical Review A*, 81(3):1–11, mar 2010. ISSN 1050-2947. doi: 10.1103/PhysRevA.81.033614. URL http://link.aps.org/doi/10.1103/PhysRevA.81.033614.

[41] W. E. Schiesser. *The Numerical Method of Lines: Integration of Partial Differential Equations*. Academic Press, 1991. ISBN 9780126241303. URL https://books.google.com/books?id=1vLFQgAACAAJ.

[42] M. R. Andrews, M.-O. Mewes, N. J. van Druten, D. S. Durfee, D. M. Kurn, and W. Ketterle. Direct, Nondestructive Observation of a Bose Condensate. *Science*, 273 (5271):84–87, 1996. ISSN 0036-8075. doi: 10.1126/science.273.5271.84. URL http://science.sciencemag.org/content/273/5271/84.

[43] C. Myatt, E. Burt, R. Ghrist, E. Cornell, and C. Wieman. Production of Two Overlapping Bose-Einstein Condensates by Sympathetic Cooling. *Physical Review Letters*, 78(4):586–589, jan 1997. ISSN 0031-9007. doi: 10.1103/PhysRevLett.78.586. URL http://link.aps.org/doi/10.1103/PhysRevLett.78.586.

[44] D. Yan, J. J. Chang, C. Hamner, P. G. Kevrekidis, P. Engels, V. Achilleos, D. J. Frantzeskakis, R. Carretero-González, and P. Schmelcher. Multiple dark-bright solitons in atomic Bose-Einstein condensates. *Physical Review A*, 84(5):053630, nov 2011. ISSN 1050-2947. doi: 10.1103/PhysRevA.84.053630. URL http://link.aps.org/doi/10.1103/PhysRevA.84.053630.

[45] Th. Busch and J R Anglin. Dark-Bright Solitons in Inhomogeneous Bose-Einstein Condensates. *Physical Review Letters*, 87(1):10401, jun 2001. URL https://link.aps.org/doi/10.1103/PhysRevLett.87.010401.

[46] V. Achilleos, D. Yan, P. G. Kevrekidis, and D. J. Frantzeskakis. Dark–bright solitons in Bose–Einstein condensates at finite temperatures. *New Journal of Physics*, 14(5): 055006, 2012. URL http://stacks.iop.org/1367-2630/14/i=5/a=055006.

[47] Chao-Fei Liu, Min Lu, and Wei-Qing Liu. Dynamics of vector dark soliton induced by the Rabi coupling in one-dimensional trapped Bose-Einstein condensates. *Physics Letters A*, 376(3):188–196, jan 2012. ISSN 0375-9601. URL http://www.sciencedirect.com/science/article/pii/S0375960111013272.

[48] H. Li, D. N. Wang, and Y. Cheng. Dynamics of dark-bright vector solitons in a two-component Bose-Einstein condensate. *Chaos, Solitons Fractals*, 39(4):1988–1993, feb 2009. ISSN 09600779. doi: 10.1016/j.chaos.2007.06.063. URL http://linkinghub.elsevier.com/retrieve/pii/S0960077907004560.

[49] B. A. Malomed. Internal vibrations of a vector soliton in the coupled nonlinear Schrodinger equations. *Physical Review E*, 58(2):2564–2575, 1998. URL http://pre.aps.org/abstract/PRE/v58/i2/p2564.

[50] J. Goldstone. Field theories with Superconductor solutions. *Il Nuovo Cimento (1955-1965)*, 19(1):154–164, 2008. ISSN 1827-6121. URL http://inspirehep.net/record/12289?ln=en.

[51] L. D. Carr and M. A. Leung. Dynamics of the Bose-Einstein condensate: quasi-one-dimension and beyond. *Journal of Physics B: Atomic, Molecular and Optical Physics*, 33(19):3983, 2000. URL http://stacks.iop.org/0953-4075/33/i=19/a=312.

[52] Y. S. Kivshar and W. Królikowski. Lagrangian approach for dark solitons. *Optics communications*, 114:353 – 362, 1995. URL http://www.sciencedirect.com/science/article/pii/003040189400644A.

[53] T. Ueda and W. L. Kath. Dynamics of coupled solitons in nonlinear optical fibers. *Physical Review A*, 42(1):563–571, 1990. URL http://pra.aps.org/abstract/PRA/v42/i1/p563.

[54] A. Roy and D. Angom. Fluctuation- and interaction-induced instability of dark solitons in single and binary condensates. *Physical Review A*, 90(2):023612, aug 2014. ISSN 1050-2947. doi: 10.1103/PhysRevA.90.023612. URL http://link.aps.org/doi/10.1103/PhysRevA.90.023612.

[55] D. J. Griffiths. *Introduction to Quantum Mechanics*. Pearson international edition. Pearson Prentice Hall, 2005. ISBN 9780131118928. URL https://books.google.com/books?id=z4fwAAAAMAAJ.

[56] Y. S. Kivshar and B. A. Malomed. Dynamics of solitons in nearly integrable systems. *Reviews of Modern Physics*, 1989. URL http://rmp.aps.org/abstract/RMP/v61/i4/p763_1.

[57] A. M. Kosevich. Particle and wave properties of solitons. *Physica D: Nonlinear Phenomena*, 41(2):253–261, 1990. ISSN 01672789. doi: 10.1016/0167-2789(90)90126-A. URL http://linkinghub.elsevier.com/retrieve/pii/016727899090126A.

[58] C. Lee and J. Brand. Enhanced quantum reflection of matter-wave solitons. *Europhysics Letters (EPL)*, 73(3):321–327, feb 2006. ISSN 0295-5075. doi: 10.1209/epl/i2005-10408-4. URL http://stacks.iop.org/0295-5075/73/i=3/a=321?key=crossref.4f374a80b2971fa212982615b8ab2a70.

[59] D. Frantzeskakis, G. Theocharis, F. Diakonos, P. Schmelcher, and Y. S. Kivshar. Interaction of dark solitons with localized impurities in Bose-Einstein condensates. *Physical Review A*, 66(5):1–9, nov 2002. ISSN 1050-2947. doi: 10.1103/PhysRevA.66.053608. URL http://link.aps.org/doi/10.1103/PhysRevA.66.053608.

[60] J. Garnier. Transmission of matter-wave solitons through nonlinear traps and barriers 1. *Physical Review A*, 74:013604, 2006. doi: 10.1103/PhysRevA.74.013604.

[61] B. Seaman, L. D. Carr, and M. Holland. Effect of a potential step or impurity on the Bose-Einstein condensate mean field. *Physical Review A*, 71(3):1–10, mar 2005. ISSN 1050-2947. doi: 10.1103/PhysRevA.71.033609. URL http://link.aps.org/doi/10.1103/PhysRevA.71.033609.

[62] A. G. Sykes, M. J. Davis, and D. C. Roberts. Drag force on an impurity below the superfluid critical velocity in a quasi-one-dimensional Bose-Einstein condensate. *Physical Review Letters*, 103(8):1–4, 2009. ISSN 00319007. doi: 10.1103/PhysRevLett.103.085302.

[63] V. Achilleos, P. G. Kevrekidis, and V. M. Rothos. Statics and dynamics of atomic dark-bright solitons in the presence of impurities. *Physical Review A*, 053626:1–10, 2011. doi: 10.1103/PhysRevA.84.053626. URL http://pra.aps.org/abstract/PRA/v84/i5/e053626.

[64] A. Sykes. Exact solutions to the four Goldstone modes around a dark soliton of the nonlinear Schroedinger equation. *Journal of Physics A Mathematical and General*, 44: 135206, 2011. ISSN 1751-8113. doi: 10.1088/1751-8113/44/13/135206. URL http://arxiv.org/abs/1102.0587.

[65] M. O. D. Alotaibi and L. D. Carr. Dynamics of dark-bright vector solitons in Bose-Einstein condensates. *Phys. Rev. A*, 96(1):13601, jul 2017. doi: 10.1103/PhysRevA.96.013601. URL https://link.aps.org/doi/10.1103/PhysRevA.96.013601.

[66] Y. S. Kivshar and X. Yang. Perturbation-induced dynamics of dark solitons. *Physical Review E*, 49(2):1657, 1994. URL http://www.sciencedirect.com/science/article/pii/0960077994901082.

[67] D. J. Frantzeskakis. Dark solitons in atomic Bose-Einstein condensates: From theory to experiments. *Journal of Physics A: Mathematical and Theoretical*, 43(21):213001, 2010. ISSN 1751-8113. doi: 10.1088/1751-8113/43/21/213001. URL http://stacks.iop.org/1751-8121/43/i=21/a=213001.

[68] R. Carretero-Gonzlez, D. J. Frantzeskakis, and P. G. Kevrekidis. Nonlinear waves in Bose-Einstein condensates: physical relevance and mathematical techniques. *Nonlinearity*, 21(7):R139–R202, jul 2008. ISSN 0951-7715. doi: 10.1088/0951-7715/21/7/R01. URL http://stacks.iop.org/0951-7715/21/i=7/a=R01?key=crossref.1ccf5d2b9ed8a75036b62b7149e21a80.

[69] L. Salasnich and B. A. Malomed. Vector solitons in nearly one-dimensional Bose-Einstein condensates. *Physical Review A*, 74(5):1–6, nov 2006. ISSN 1050-2947. doi: 10.1103/PhysRevA.74.053610. URL http://link.aps.org/doi/10.1103/PhysRevA.74.053610.

[70] V. Achilleos, P. G. Kevrekidis, V. M. Rothos, and D. J. Frantzeskakis. Statics and dynamics of atomic dark-bright solitons in the presence of impurities. *Phys. Rev. A*, 84(5):53626, nov 2011. doi: 10.1103/PhysRevA.84.053626. URL https://link.aps.org/doi/10.1103/PhysRevA.84.053626.

[71] A. Álvarez, J. Cuevas, F. R. Romero, C. Hamner, J. J. Chang, P. Engels, P. G. Kevrekidis, and D. J. Frantzeskakis. Scattering of atomic dark–bright solitons from narrow impurities. *Journal of Physics B: Atomic, Molecular and Optical Physics*, 46 (6):065302, 2013. URL http://stacks.iop.org/0953-4075/46/i=6/a=065302.

[72] W. P. Reinhardt. Soliton dynamics in the collisions of Bose–Einstein condensates: an analogue of the Josephson effect. *of Physics B: Atomic, Molecular and*, 785:9, 1997. URL http://iopscience.iop.org/0953-4075/30/22/001.

[73] Xiaoning Zang, S. Montangero, L. D. Carr, and M. T. Lusk. Engineering and manipulating exciton wave packets. *Physical Review B*, 95(19):1–15, 2017. ISSN 24699969. doi: 10.1103/PhysRevB.95.195423.

[74] M. T. Lusk, C. A. Stafford, J. D. Zimmerman, and L. D. Carr. Control of exciton transport using quantum interference. *Physical Review B*, 92(24):241112, 2015. ISSN 1098-0121. doi: 10.1103/PhysRevB.92.241112. URL https://link.aps.org/doi/10.1103/PhysRevB.92.241112.

[75] C. J. Pethick and H. Smith. *Bose-Einstein Condensation in Dilute Gases*. Cambridge University Press, Cambridge, 2 edition, 2008. ISBN 9780521846516. doi: DOI:10.1017/CBO9780511802850. URL https://www.cambridge.org/core/books/boseeinstein-condensation-in-dilute-gases/CC439EAD70D78E47E9AF536DA7B203EC.

[76] K. E. Strecker, G. B. Partridge, A. G. Truscott, and R. G. Hulet. Formation and propagation of matter-wave soliton trains. *Nature*, 417(6885):150–3, May 2002. ISSN 0028-0836. doi: 10.1038/nature747. URL http://www.nature.com/nature/journal/v417/n6885/full/nature747.html.

[77] G. Filatrella, B. A. Malomed, and M. Salerno. Domain walls and bubble droplets in immiscible binary Bose gases. *Physical Review A*, 90(4):043629, oct 2014. ISSN 1050-2947. doi: 10.1103/PhysRevA.90.043629. URL http://link.aps.org/doi/10.1103/PhysRevA.90.043629.

[78] F. Kh. Abdullaev, A. Gammal, A. M. Kamchatnov, and L. Tomio. Dynamics of Bright Matter Wave Solitons in a Bose-Einstein Condensate. *International Journal of Modern Physics B*, 19(22):3415–3473, sep 2005. ISSN 0217-9792. doi: 10.1142/S0217979205032279. URL http://www.worldscientific.com/doi/abs/10.1142/S0217979205032279.

[79] Xinxin Zhao, D. A. Alcala, M. A. McLain, K. Maeda, S. Potnis, R. Ramos, A. M. Steinberg, and L. D. Carr. Macroscopic quantum tunneling escape of Bose–Einstein condensates. *Phys. Rev. A*, 96:063601, Dec 2017. doi: 10.1103/PhysRevA.96.063601. URL https://link.aps.org/doi/10.1103/PhysRevA.96.063601.

[80] S. Potnis, R. Ramos, K. Maeda, L. D. Carr, and A. M. Steinberg. Interaction-Assisted Quantum Tunneling of a Bose–Einstein Condensate Out of a Single Trapping Well. *Phys. Rev. Lett.*, 118:060402, Feb 2017. doi: 10.1103/PhysRevLett.118.060402. URL https://link.aps.org/doi/10.1103/PhysRevLett.118.060402.

[81] L. D. Carr, M. J. Holland, and B. A. Malomed. Macroscopic quantum tunnelling of Bose–Einstein condensates in a finite potential well. *Journal of Physics B: Atomic, Molecular and Optical Physics*, 38(17):3217, 2005. URL `http://stacks.iop.org/0953-4075/38/i=17/a=012`.

APPENDIX

MATHEMATICA CODE FOR DYNAMICS OF DARK-BRIGHT VECTOR SOLITONS IN BOSE-EINSTEIN CONDENSATES

The following Mathematica notebook used to generate the analytical results for the dynamics of dark-bright vector solitons in Bose-Einstein Condensates project.

Introduction:

The NLSE :

If $g_{12} = g_{21} = g$, then we have

$i\,\partial_t u(x,t) = -\frac{1}{2}\,\partial_{xx} u(x,t) + \left[g_{11}\,|u(x,t)|^2 - {u_0}^2 + 2\,g\,|v(x,t)|^2\right] u(x,t)$

$i\,\partial_t v(x,t) = -\frac{1}{2}\,\partial_{xx} v(x,t) + \left[2\,g\,|u(x,t)|^2 + g_{22}\,|v(x,t)|^2\right] v(x,t)$

The Ansatz :

$u(x,t) = \frac{u_0}{\sqrt{g_{11}}}\left(i\,A + c\tanh\left[\frac{(d(t)+x)}{w}\right]\right)\mathrm{Exp}\left[I\left(\theta 0 + (d[t]+x)\,\theta 1[t] + (d[t]+x)^2\,\theta 2\right)\right]$, where $A^2 + c^2 = 1$

$v(x,t) = \frac{u_0}{\sqrt{g_{22}}}\,F\ \mathrm{sech}\left[\frac{(b(t)+x)}{w}\right]\mathrm{Exp}\left[i\left(\phi_0(t) + (x+b(t))\,\phi_1(t) + (x+b(t))^2\,\phi_2(t)\right)\right]$

The Lagrangian density:

$\mathcal{L} = \frac{i}{2}\left[u^*\,\frac{\partial u}{\partial t} - u\,\frac{\partial u^*}{\partial t}\right]\left[1 - \frac{{u_0}^2}{g_{11}|u|^2}\right] - \frac{1}{2}\left|\frac{\partial u}{\partial x}\right|^2 - \frac{1}{2}\left[\sqrt{g_{11}}\ |u|^2 - \frac{{u_0}^2}{\sqrt{g_{11}}}\right]^2$

$+\ \frac{i}{2}\left[v^*\,\frac{\partial v}{\partial t} - v\,\frac{\partial v^*}{\partial t}\right] - \frac{1}{2}\left|\frac{\partial v}{\partial x}\right|^2 - \frac{g_{22}}{2}\,|v|^4$

$\quad -2\,g\,|u|^2\,|v|^2 + \frac{\mathrm{u0}^2}{2\,\mathrm{g11}}\,(2\,\theta 2\,(x + d[t]) + \theta 1[t])^2$

Units:

[x]=[L] ,

$[t] = \left[L^2\right]$

$[g] = \left[\frac{1}{L}\right]$, $[u0] = \left[\frac{1}{L}\right]$

[F] = [1] , [c] = [1] ,[A] = [1]

$[v] = \left[\frac{1}{\sqrt{L}}\right]$,$[u] = \left[\frac{1}{\sqrt{L}}\right]$

[b] = [L] , [w] = [L] ,

$[\phi_0] = [1]$, $[\phi_1] = \left[\frac{1}{L}\right]$, $[\phi_2] = \left[\frac{1}{L^2}\right]$

Lagrangian:

```
In[•]:= u[x_, t_] :=
          u0/g11^(1/2) (I A + c Tanh[(d[t] + x)/w]) Exp[I (θ0 + (d[t] + x) θ1[t] + (d[t] + x)^2 θ2)];

In[•]:= v[x_, t_] := u0/g22^(1/2) F Sech[(b[t] + x)/w] Exp[I (ϕ0 + (b[t] + x) ϕ1[t] + (b[t] + x)^2 ϕ2)];

In[•]:= myassum = {{A, c, d[t], w, θ0, u0, g, g11, g22, 1/Sqrt[g11], 1/Sqrt[g22],
            F, b[t], ϕ0, ϕ1[t], θ1[t], ϕ2, x, t, l[t]} ∈ Reals, A^2 + c^2 == 1, w > 0};

In[•]:= φ_* := φ /. Complex[u_, v_] → Complex[u, -v]
```

Calculate:

$\mathcal{L}1 = \frac{i}{2}\left[u^*\,\frac{\partial u}{\partial t} - u\,\frac{\partial u^*}{\partial t}\right]\left[1 - \frac{{u_0}^2}{g_{11}|u|^2}\right]$

```
In[•]:= FullSimplify[ I/2 ((Evaluate[Simplify[u[x, t]*, Assumptions → myassum]]) ∂t u[x, t] -
          u[x, t] ∂t (Evaluate[Simplify[u[x, t]*, Assumptions → myassum]])) *
        (1 - u0^2 / (g11 u[x, t] (Evaluate[Simplify[u[x, t]*, Assumptions → myassum]])))],
       Assumptions → myassum]
```

$$\text{Out}[\bullet]= \frac{1}{g11\, w \left(A^2 + c^2 \tanh\left[\frac{x+d[t]}{w}\right]^2\right)}$$

$$c^2\, u0^2 \left(-1 + \tanh\left[\frac{x+d[t]}{w}\right]^2\right) \left(-w\,(2\,\Theta 2\,(x+d[t]) + \Theta 1[t])\,d'[t] - w\,(x+d[t])\,\Theta 1'[t] + c\,\text{Sech}\left[\frac{x+d[t]}{w}\right]^2 ((A + c\,w\,(2\,\Theta 2\,(x+d[t]) + \Theta 1[t]))\,d'[t] + c\,w\,(x+d[t])\,\Theta 1'[t])\right)$$

```
Integrate[%, {x, -∞, ∞}, Assumptions → myassum]
```

$$\text{eq1} = \frac{2\,u0^2\left(A\,c - \text{ArcTan}\left[\frac{c}{A}\right]\right)d'[t]}{g11} + \frac{2\,c^2\,u0^2\,w\,\Theta 1[t]\,d'[t]}{g11};$$

Calculate

$$\mathcal{L}2 = -\frac{1}{2}\left|\frac{\partial u}{\partial x}\right|^2 + \frac{2\,u0^2\,\Theta 2^2\,d[t]^2}{g11} + \frac{2\,u0^2\,\Theta 2\,d[t]\,\Theta 1[t]}{g11} + \frac{u0^2\,\Theta 1[t]^2}{2\,g11} + x\left(\frac{4\,u0^2\,\Theta 2^2\,d[t]}{g11} + \frac{2\,u0^2\,\Theta 2\,\Theta 1[t]}{g11}\right) + \frac{2\,u0^2}{g11}x^2\,\Theta 2^2$$

$$\& - \frac{1}{2}\left[\sqrt{g_{11}}\,\left|u\right|^2 - \frac{{u_0}^2}{\sqrt{g_{11}}}\right]^2$$

```
In[•]:= -1/2 ∂x u[x, t] Simplify[(Evaluate[∂x u[x, t]])*, Assumptions → myassum] + (2 u0^2 Θ2^2 d[t]^2)/g11 +
  (2 u0^2 Θ2 d[t] Θ1[t])/g11 + (u0^2 Θ1[t]^2)/(2 g11) + x ((4 u0^2 Θ2^2 d[t])/g11 + (2 u0^2 Θ2 Θ1[t])/g11) + (2 u0^2)/g11 x^2 Θ2^2
```

$$\text{Out}[\bullet]= \frac{2\,u0^2\,x^2\,\Theta2^2}{g11}+\frac{2\,u0^2\,\Theta2^2\,d[t]^2}{g11}+\frac{2\,u0^2\,\Theta2\,d[t]\,\Theta1[t]}{g11}+\frac{u0^2\,\Theta1[t]^2}{2\,g11}+$$
$$x\left(\frac{4\,u0^2\,\Theta2^2\,d[t]}{g11}+\frac{2\,u0^2\,\Theta2\,\Theta1[t]}{g11}\right)-\frac{1}{2\sqrt{g11}}e^{-i\left(\Theta0+\Theta2\,(x+d[t])^2+(x+d[t])\,\Theta1[t]\right)}$$
$$u0\left(\frac{c\,\text{Sech}\left[\frac{x+d[t]}{w}\right]^2}{w}-\left(A+i\,c\,\text{Tanh}\left[\frac{x+d[t]}{w}\right]\right)(2\,x\,\Theta2+2\,\Theta2\,d[t]+\Theta1[t])\right)$$
$$\left(\frac{c\,e^{i\left(\Theta0+\Theta2\,(x+d[t])^2+(x+d[t])\,\Theta1[t]\right)}\,u0\,\text{Sech}\left[\frac{x+d[t]}{w}\right]^2}{\sqrt{g11}\,w}+\right.$$
$$\left.\frac{i\,e^{i\left(\Theta0+\Theta2\,(x+d[t])^2+(x+d[t])\,\Theta1[t]\right)}\,u0\left(i\,A+c\,\text{Tanh}\left[\frac{x+d[t]}{w}\right]\right)(2\,\Theta2\,(x+d[t])+\Theta1[t])}{\sqrt{g11}}\right)$$

```
Integrate[%, {x, -∞, ∞}, Assumptions → myassum]

eq2 = -(2 c^2 u0^2)/(3 g11 w) + (c^2 π^2 u0^2 w^3 Θ2^2)/(3 g11) + (2 A c u0^2 Θ1[t])/g11 + (c^2 u0^2 w Θ1[t]^2)/g11 - (2 c^4 u0^4 w)/(3 g11);
```

Calculate

$\mathcal{L}3 = \frac{i}{2}\left[v^* \frac{\partial v}{\partial t} - v \frac{\partial v^*}{\partial t}\right]$

```
In[•]:= FullSimplify[
  I/2 ((Evaluate[Simplify[v[x, t]*, Assumptions → myassum]]) ∂t v[x, t] - v[x, t]
      ∂t (Evaluate[Simplify[v[x, t]*, Assumptions → myassum]])), Assumptions → myassum]
```

$$\text{Out}[\bullet]= -\frac{F^2\,u0^2\,\text{Sech}\left[\frac{x+b[t]}{w}\right]^2\left((2\,\phi2\,(x+b[t])+\phi1[t])\,b'[t]+(x+b[t])\,\phi1'[t]\right)}{g22}$$

```
Integrate[%, {x, -∞, ∞}, Assumptions → myassum]

eq3 = -(2 F^2 u0^2 w ϕ1[t] b'[t])/g22;
```

Calculate:

$\mathcal{L}4 = -\frac{1}{2}\left|\frac{\partial v}{\partial x}\right|^2 - \frac{g_{22}}{2}|v|^4$

```
In[•]:= Simplify[-1/2 ∂x v[x, t] (Evaluate[∂x v[x, t]])*, Assumptions → myassum] +
        Simplify[-g22/2 (v[x, t] (Evaluate[v[x, t]])*) (v[x, t] (Evaluate[v[x, t]])*),
         Assumptions → myassum]
```

$$\text{Out[•]=}\quad -\frac{F^4\,u0^4\,\text{Sech}\left[\frac{x+b[t]}{w}\right]^4}{2\,g22}-\frac{1}{2\,g22\,w^2}$$

$$F^2\,u0^2\,\text{Sech}\left[\frac{x+b[t]}{w}\right]^2\left(2\,w\,x\,\phi 2+2\,w\,\phi 2\,b[t]-i\,\text{Tanh}\left[\frac{x+b[t]}{w}\right]+w\,\phi 1[t]\right)$$

$$\left(2\,w\,x\,\phi 2+2\,w\,\phi 2\,b[t]+i\,\text{Tanh}\left[\frac{x+b[t]}{w}\right]+w\,\phi 1[t]\right)$$

```
Integrate[%, {x, -∞, ∞}, Assumptions → myassum]
```

```
eq4 = -F^2 u0^2/(3 g22 w) - 2 F^4 u0^4 w/(3 g22) - F^2 π^2 u0^2 w^3 ϕ2^2/(3 g22) - F^2 u0^2 w ϕ1[t]^2/g22;
```

Calculate:

$\mathcal{L}5 = -2\,g\,|\,u\,|^2\,|\,v\,|^2$

```
In[•]:= Simplify[-2 g (u[x, t] u[x, t]*) (v[x, t] v[x, t]*), Assumptions → myassum]
```

$$\text{Out[•]=}\quad -\frac{2\,F^2\,g\,u0^4\,\text{Sech}\left[\frac{x+b[t]}{w}\right]^2\left(1+c^2\left(-1+\text{Tanh}\left[\frac{x+d[t]}{w}\right]^2\right)\right)}{g11\,g22}$$

```
Integrate[%, {x, -∞, ∞}, Assumptions → myassum]
```

```
eq5 = 4 (-1 + c^2) F^2 g u0^4 w/(g11 g22) - 2 c^2 F^2 g u0^4/(g11 g22) Csch[(b[t] - d[t])/w]^2
      (w (3 + Cosh[2 (b[t] - d[t])/w]) + 4 Coth[(b[t] - d[t])/w] (-b[t] + d[t]));
```

The Average Lagrangian is:

```
eq1 + eq2 + eq3 + eq4 + eq5
```

$$-\frac{2\,c^2\,u0^2}{3\,g11\,w}-\frac{F^2\,u0^2}{3\,g22\,w}-\frac{2\,c^4\,u0^4\,w}{3\,g11}-\frac{2\,F^4\,u0^4\,w}{3\,g22}+\frac{4\left(-1+c^2\right)F^2\,g\,u0^4\,w}{g11\,g22}+$$
$$\frac{c^2\,\pi^2\,u0^2\,w^3\,\Theta 2^2}{3\,g11}-\frac{F^2\,\pi^2\,u0^2\,w^3\,\phi 2^2}{3\,g22}-\frac{1}{g11\,g22}2\,c^2\,F^2\,g\,u0^4\,\text{Csch}\left[\frac{b[t]-d[t]}{w}\right]^2$$
$$\left(w\left(3+\text{Cosh}\left[\frac{2\,(b[t]-d[t])}{w}\right]\right)+4\,\text{Coth}\left[\frac{b[t]-d[t]}{w}\right](-b[t]+d[t])\right)+$$
$$\frac{2\,A\,c\,u0^2\,\Theta 1[t]}{g11}+\frac{c^2\,u0^2\,w\,\Theta 1[t]^2}{g11}-\frac{F^2\,u0^2\,w\,\phi 1[t]^2}{g22}-\frac{2\,F^2\,u0^2\,w\,\phi 1[t]\,b'[t]}{g22}+$$
$$\frac{2\,u0^2\left(A\,c-\text{ArcTan}\left[\frac{c}{A}\right]\right)d'[t]}{g11}+\frac{2\,c^2\,u0^2\,w\,\Theta 1[t]\,d'[t]}{g11}$$

$$\mathbf{L}=-\frac{2\,c^2\,u0^2}{3\,g11\,w}-\frac{F^2\,u0^2}{3\,g22\,w}-\frac{2\,c^4\,u0^4\,w}{3\,g11}-\frac{2\,F^4\,u0^4\,w}{3\,g22}+\frac{4\left(-1+c^2\right)F^2\,g\,u0^4\,w}{g11\,g22}+$$
$$\frac{c^2\,\pi^2\,u0^2\,w^3\,\Theta 2^2}{3\,g11}-\frac{F^2\,\pi^2\,u0^2\,w^3\,\phi 2^2}{3\,g22}-\frac{1}{g11\,g22}2\,c^2\,F^2\,g\,u0^4\,\text{Csch}\left[\frac{b[t]-d[t]}{w}\right]^2$$
$$\left(w\left(3+\text{Cosh}\left[\frac{2\,(b[t]-d[t])}{w}\right]\right)+4\,\text{Coth}\left[\frac{b[t]-d[t]}{w}\right](-b[t]+d[t])\right)+$$
$$\frac{2\,A\,c\,u0^2\,\Theta 1[t]}{g11}+\frac{c^2\,u0^2\,w\,\Theta 1[t]^2}{g11}-\frac{F^2\,u0^2\,w\,\phi 1[t]^2}{g22}-\frac{2\,F^2\,u0^2\,w\,\phi 1[t]\,b'[t]}{g22}+$$
$$\frac{2\,u0^2\left(A\,c-\text{ArcTan}\left[\frac{c}{A}\right]\right)d'[t]}{g11}+\frac{2\,c^2\,u0^2\,w\,\Theta 1[t]\,d'[t]}{g11};$$

EOMs:

Normalizations:

For Dark Soliton, $\int_{-\infty}^{\infty}dx\left(\frac{u_0^2}{g_{11}}-\left|u(x,t)\right|^2\right)=$ N1

```
Integrate[u0^2/g11 - u[x, t] (Evaluate[Simplify[u[x, t]*, Assumptions → myassum]]),
 {x, -∞, ∞}, Assumptions → myassum]
```

$$\frac{2\,c^2\,u0^2\,w}{g11}$$

For Bright Soliton, $\int_{-\infty}^{\infty}dx\ \left|v(x,t)\right|^2=$ N2

```
Integrate[v[x, t] (Evaluate[Simplify[v[x, t]*, Assumptions → myassum]]),
 {x, -∞, ∞}, Assumptions → myassum]
```

$$\frac{2\,F^2\,u0^2\,w}{g22}$$

For b(t)

$$\text{Expand}[\partial_{b[t]} L]$$

$$\frac{20\, c^2\, F^2\, g\, u0^4\, \text{Coth}\left[\frac{b[t]-d[t]}{w}\right]\, \text{Csch}\left[\frac{b[t]-d[t]}{w}\right]^2}{g11\, g22} +$$

$$\frac{1}{g11\, g22}\, 4\, c^2\, F^2\, g\, u0^4\, \text{Cosh}\left[\frac{2\,(b[t]-d[t])}{w}\right]\, \text{Coth}\left[\frac{b[t]-d[t]}{w}\right]\, \text{Csch}\left[\frac{b[t]-d[t]}{w}\right]^2 -$$

$$\frac{1}{g11\, g22\, w}\, 16\, c^2\, F^2\, g\, u0^4\, b[t]\, \text{Coth}\left[\frac{b[t]-d[t]}{w}\right]^2\, \text{Csch}\left[\frac{b[t]-d[t]}{w}\right]^2 -$$

$$\frac{8\, c^2\, F^2\, g\, u0^4\, b[t]\, \text{Csch}\left[\frac{b[t]-d[t]}{w}\right]^4}{g11\, g22\, w} +$$

$$\frac{1}{g11\, g22\, w}\, 16\, c^2\, F^2\, g\, u0^4\, \text{Coth}\left[\frac{b[t]-d[t]}{w}\right]^2\, \text{Csch}\left[\frac{b[t]-d[t]}{w}\right]^2\, d[t] +$$

$$\frac{8\, c^2\, F^2\, g\, u0^4\, \text{Csch}\left[\frac{b[t]-d[t]}{w}\right]^4\, d[t]}{g11\, g22\, w} - \frac{4\, c^2\, F^2\, g\, u0^4\, \text{Csch}\left[\frac{b[t]-d[t]}{w}\right]^2\, \text{Sinh}\left[\frac{2\,(b[t]-d[t])}{w}\right]}{g11\, g22}$$

$$\text{Expand}[\partial_{b'[t]} L]$$

$$-\frac{2\, F^2\, u0^2\, w\, \phi 1[t]}{g22}$$

Equation I:

$$\frac{16\, c^2\, F^2\, g\, u0^4\, \text{Csch}\left[\frac{b[t]-d[t]}{w}\right]^4\, (-b[t]+d[t])}{g11\, g22\, w} +$$

$$\frac{1}{g11\, g22\, w}\, 8\, c^2\, F^2\, g\, u0^4\, \text{Cosh}\left[\frac{2\,(b[t]-d[t])}{w}\right]\, \text{Csch}\left[\frac{b[t]-d[t]}{w}\right]^4\, (-b[t]+d[t]) +$$

$$\frac{12\, c^2\, F^2\, g\, u0^4\, \text{Csch}\left[\frac{b[t]-d[t]}{w}\right]^4\, \text{Sinh}\left[\frac{2\,(b[t]-d[t])}{w}\right]}{g11\, g22} - \partial_t\left(-\frac{2\, F^2\, u0^2\, w\, \phi 1[t]}{g22}\right) = 0$$

$$\frac{16\, c^2\, F^2\, g\, u0^4\, \text{Csch}\left[\frac{b[t]-d[t]}{w}\right]^4\, (-b[t]+d[t])}{g11\, g22\, w} +$$

$$\frac{1}{g11\, g22\, w}\, 8\, c^2\, F^2\, g\, u0^4\, \text{Cosh}\left[\frac{2\,(b[t]-d[t])}{w}\right]\, \text{Csch}\left[\frac{b[t]-d[t]}{w}\right]^4\, (-b[t]+d[t]) +$$

$$\frac{12\, c^2\, F^2\, g\, u0^4\, \text{Csch}\left[\frac{b[t]-d[t]}{w}\right]^4\, \text{Sinh}\left[\frac{2\,(b[t]-d[t])}{w}\right]}{g11\, g22} + \frac{2\, F^2\, u0^2\, w\, \phi 1'[t]}{g22} = 0$$

For d(t)

$$\text{Expand}[\partial_{d[t]} L]$$

$$-\frac{20\,c^2\,F^2\,g\,u0^4\,\text{Coth}\left[\frac{b[t]-d[t]}{w}\right]\,\text{Csch}\left[\frac{b[t]-d[t]}{w}\right]^2}{g11\,g22} -$$

$$\frac{1}{g11\,g22}\,4\,c^2\,F^2\,g\,u0^4\,\text{Cosh}\left[\frac{2\,(b[t]-d[t])}{w}\right]\,\text{Coth}\left[\frac{b[t]-d[t]}{w}\right]\,\text{Csch}\left[\frac{b[t]-d[t]}{w}\right]^2 +$$

$$\frac{1}{g11\,g22\,w}\,16\,c^2\,F^2\,g\,u0^4\,b[t]\,\text{Coth}\left[\frac{b[t]-d[t]}{w}\right]^2\,\text{Csch}\left[\frac{b[t]-d[t]}{w}\right]^2 +$$

$$\frac{8\,c^2\,F^2\,g\,u0^4\,b[t]\,\text{Csch}\left[\frac{b[t]-d[t]}{w}\right]^4}{g11\,g22\,w} -$$

$$\frac{1}{g11\,g22\,w}\,16\,c^2\,F^2\,g\,u0^4\,\text{Coth}\left[\frac{b[t]-d[t]}{w}\right]^2\,\text{Csch}\left[\frac{b[t]-d[t]}{w}\right]^2\,d[t] -$$

$$\frac{8\,c^2\,F^2\,g\,u0^4\,\text{Csch}\left[\frac{b[t]-d[t]}{w}\right]^4\,d[t]}{g11\,g22\,w} + \frac{4\,c^2\,F^2\,g\,u0^4\,\text{Csch}\left[\frac{b[t]-d[t]}{w}\right]^2\,\text{Sinh}\left[\frac{2\,(b[t]-d[t])}{w}\right]}{g11\,g22}$$

$$\text{Expand}[\partial_{d'[t]} L]$$

$$\frac{2\,A\,c\,u0^2}{g11} - \frac{2\,u0^2\,\text{ArcTan}\left[\frac{c}{A}\right]}{g11} + \frac{2\,c^2\,u0^2\,w\,\Theta1[t]}{g11}$$

Equation II:

$$\frac{16\,c^2\,F^2\,g\,u0^4\,\text{Csch}\left[\frac{b[t]-d[t]}{w}\right]^4\,(b[t]-d[t])}{g11\,g22\,w} +$$

$$\frac{1}{g11\,g22\,w}\,8\,c^2\,F^2\,g\,u0^4\,\text{Cosh}\left[\frac{2\,(b[t]-d[t])}{w}\right]\,\text{Csch}\left[\frac{b[t]-d[t]}{w}\right]^4\,(b[t]-d[t]) -$$

$$\frac{12\,c^2\,F^2\,g\,u0^4\,\text{Csch}\left[\frac{b[t]-d[t]}{w}\right]^4\,\text{Sinh}\left[\frac{2\,(b[t]-d[t])}{w}\right]}{g11\,g22} -$$

$$\partial_t\left(\frac{2\,A\,c\,u0^2}{g11} - \frac{2\,u0^2\,\text{ArcTan}\left[\frac{c}{A}\right]}{g11} + \frac{2\,c^2\,u0^2\,w\,\Theta1[t]}{g11}\right) = 0$$

$$\frac{16\,c^2\,F^2\,g\,u0^4\,\text{Csch}\left[\frac{b[t]-d[t]}{w}\right]^4\,(b[t]-d[t])}{g11\,g22\,w}+$$

$$\frac{1}{g11\,g22\,w}8\,c^2\,F^2\,g\,u0^4\,\text{Cosh}\left[\frac{2\,(b[t]-d[t])}{w}\right]\text{Csch}\left[\frac{b[t]-d[t]}{w}\right]^4\,(b[t]-d[t])-$$

$$\frac{12\,c^2\,F^2\,g\,u0^4\,\text{Csch}\left[\frac{b[t]-d[t]}{w}\right]^4\,\text{Sinh}\left[\frac{2\,(b[t]-d[t])}{w}\right]}{g11\,g22}-\frac{2\,c^2\,u0^2\,w\,\theta1'[t]}{g11}=0$$

For $\phi_1(t)$,

```
Expand[∂ϕ1[t] L]
```

$$-\frac{2\,F^2\,u0^2\,w\,\phi1[t]}{g22}-\frac{2\,F^2\,u0^2\,w\,b'[t]}{g22}$$

```
Expand[∂ϕ1'[t] L]
```

```
0
```

Equation III:

$$-\frac{2\,F^2\,u0^2\,w\,\phi1[t]}{g22}-\frac{2\,F^2\,u0^2\,w\,b'[t]}{g22}=0$$

For $\theta_1(t)$,

```
Expand[∂θ1[t] L]
```

$$\frac{2\,A\,c\,u0^2}{g11}+\frac{2\,c^2\,u0^2\,w\,\theta1[t]}{g11}+\frac{2\,c^2\,u0^2\,w\,d'[t]}{g11}$$

```
Expand[∂θ1'[t] L]
```

```
0
```

Equation IV:

$$\frac{2\,A\,c\,u0^2}{g11}+\frac{2\,c^2\,u0^2\,w\,\theta1[t]}{g11}+\frac{2\,c^2\,u0^2\,w\,d'[t]}{g11}=0$$

EOMs:

```
b'[t] = -ϕ1[t] (* Eq A *)
```

$$d'[t] = -\frac{A}{c\,w} - \theta 1[t] \quad (* \text{ Eq B } *)$$

$$\phi 1'[t] = \frac{c^2\, g22}{F^2\, g11}\, \theta 1'[t]$$

$$\phi 1'[t] = \frac{2\, c^2\, g\, u0^2}{g11\, w^2} \left(\text{Csch}\left[\frac{b[t]-d[t]}{w}\right]^4 \left(2\left(2+\text{Cosh}\left[\frac{2\,(b[t]-d[t])}{w}\right]\right)(b[t]-d[t]) - 3\,w\,\text{Sinh}\left[\frac{2\,(b[t]-d[t])}{w}\right]\right)\right) \quad (* \text{ Eq C } *)$$

$$\theta 1'[t] = \frac{2\, F^2\, g\, u0^2}{g22\, w^2} \left(\text{Csch}\left[\frac{b[t]-d[t]}{w}\right]^4 \left(2\left(2+\text{Cosh}\left[\frac{2\,(b[t]-d[t])}{w}\right]\right)(b[t]-d[t]) - 3\,w\,\text{Sinh}\left[\frac{2\,(b[t]-d[t])}{w}\right]\right)\right) \quad (* \text{ Eq D } *)$$

Eq(C) and Eq(D) are identical. Except for a constant. So, it's better to choose b[t]-d[t] = l[t]
Re-write down the system of equations above.

$$b'[t] - d'[t] = -\phi 1[t] - \left(-\frac{A}{c\,w} - \theta 1[t]\right)$$

$$l'[t] = \frac{A}{c\,w} + \theta 1[t] - \phi 1[t] \quad (* \text{ Eq I } *)$$

$$\phi 1'[t] = \frac{2\, c^2\, g\, u0^2}{g11\, w^2}\, \text{Csch}\left[\frac{l[t]}{w}\right]^4 \left(2\left(2+\text{Cosh}\left[\frac{2\,l[t]}{w}\right]\right) l[t] - 3\,w\,\text{Sinh}\left[\frac{2\,l[t]}{w}\right]\right) \quad (* \text{ Eq II } *)$$

$$\theta 1'[t] = \frac{2\, F^2\, g\, u0^2}{g22\, w^2}\, \text{Csch}\left[\frac{l[t]}{w}\right]^4 \left(2\left(2+\text{Cosh}\left[\frac{2\,l[t]}{w}\right]\right) l[t] - 3\,w\,\text{Sinh}\left[\frac{2\,l[t]}{w}\right]\right) \quad (* \text{ Eq III } *)$$

Fixed Points:

From Eq A and Eq B we get

$$\phi 1fp = 0,\ \theta 1fp = -\frac{A}{c\,w}$$

Eq II and Eq III give the same results. Using FindRoot method.

$$\text{TrigReduce}\left[\text{Csch}\left[\frac{l[t]}{w}\right]^4 \left(2\left(2+\text{Cosh}\left[\frac{2\,l[t]}{w}\right]\right) l[t] - 3\,w\,\text{Sinh}\left[\frac{2\,l[t]}{w}\right]\right)\right]$$

$$-\frac{8\left(4\,l[t] + 2\,\text{Cosh}\left[\frac{2\,l[t]}{w}\right] l[t] - 3\,w\,\text{Sinh}\left[\frac{2\,l[t]}{w}\right]\right)}{-3 + 4\,\text{Cosh}\left[\frac{2\,l[t]}{w}\right] - \text{Cosh}\left[\frac{4\,l[t]}{w}\right]}$$

```
Numerator[%]
```

$$-8\left(4\,l[t]+2\,\text{Cosh}\left[\frac{2\,l[t]}{w}\right]\,l[t]-3\,w\,\text{Sinh}\left[\frac{2\,l[t]}{w}\right]\right)$$

```
ExpandAll[((4 l[t] + 2 Cosh[2 l[t]/w] l[t] - 3 w Sinh[2 l[t]/w]) 1/w)]
```

$$\frac{4\,l[t]}{w}+\frac{2\,\text{Cosh}\left[\frac{2\,l[t]}{w}\right]\,l[t]}{w}-3\,\text{Sinh}\left[\frac{2\,l[t]}{w}\right]$$

```
% /. {2 l[t]/w → y, 4 l[t]/w → 2 y}
```

$$2\,y+y\,\text{Cosh}[y]-3\,\text{Sinh}[y]$$

```
FullSimplify[2 y + y Cosh[y] - 3 Sinh[y]]
```

$$y\,(2+\text{Cosh}[y])-3\,\text{Sinh}[y]$$

Here we use FindRoot method,

```
y (2 + Cosh[y]) - 3 Sinh[y] = 0 → y = 3 Sinh[y]/(2 + Cosh[y])
```

```
FindRoot[y == 3 Sinh[y]/(2 + Cosh[y]), {y, 0}]
```

$$\{y\to 0.\}$$

So, the fixed point for $\frac{2\,l[t]}{w}=0$, that is

```
lfp = 0
```

We end up with the following fixed points

```
ϕ1fp = 0, ϑ1fp = -A/(c w), lfp = 0
```

Let's expand the system of ODE

System of ODEs,

```
expandaraoundFP = {ϑ1[t] → ϑ1fp + ϵ Δϑ1, ϕ1[t] → ϕ1fp + ϵ Δϕ1, l[t] → lfp + ϵ Δl};
```

```
insertExponential = { Δϑ1 → δϑ1 Exp[I ω t], Δϕ1 → δϕ1 Exp[I ω t], Δl → δl Exp[I ω t]};
```

```
fp = {ϕ1fp → 0, ϑ1fp → -A/(c w), lfp → 0};
```

```
l'[t] = A/(c w) + ϑ1[t] - ϕ1[t] (* Eq one *)
```

LHS,

```
l'[t] → d/dt (lfp + ϵ δl Exp[I ω t]) → d/dt (ϵ δl Exp[I ω t]) → i e^(i t ω) δl ω ϵ
```

RHS,

```
(A/(c w) + θ1[t] - ϕ1[t]) /. expandaraoundFP
```

$$\frac{A}{c\,w} + \Delta\theta 1\,\epsilon - \Delta\phi 1\,\epsilon + \theta 1\text{fp} - \phi 1\text{fp}$$

```
% /. fp
```

$$\Delta\theta 1\,\epsilon - \Delta\phi 1\,\epsilon$$

```
Series[Δθ1 ϵ - Δϕ1 ϵ, {ϵ, 0, 1}]
```

$$(\Delta\theta 1 - \Delta\phi 1)\,\epsilon + O[\epsilon]^2$$

```
Normal[(Δθ1 - Δϕ1) ϵ + O[ϵ]^2]
```

$$(\Delta\theta 1 - \Delta\phi 1)\,\epsilon$$

```
Collect[%, ϵ]
```

$$(\Delta\theta 1 - \Delta\phi 1)\,\epsilon$$

```
% /. insertExponential
```

$$\left(e^{i\,t\,\omega}\,\delta\theta 1 - e^{i\,t\,\omega}\,\delta\phi 1\right)\epsilon$$

We end up with,

```
-e^(i t ω) ϵ (δθ1 - δϕ1 - i δl ω) = 0
```

$$-e^{i\,t\,\omega}\,\epsilon\,(\delta\theta 1 - \delta\phi 1 - i\,\delta l\,\omega) = 0$$

```
ϕ1'[t] =
  (2 c^2 g u0^2)/(g11 w^2) Csch[l[t]/w]^4 (2 (2 + Cosh[(2 l[t])/w]) l[t] - 3 w Sinh[(2 l[t])/w]) (* Eq two *)
```

LHS,

$$\phi 1'[t] \to \frac{d}{dt}\,(\phi 1\text{fp} + \epsilon\,\delta\phi 1\,\text{Exp}[I\,\omega\,t]) \to \frac{d}{dt}\,(\epsilon\,\delta\phi 1\,\text{Exp}[I\,\omega\,t]) \to i\,e^{i\,t\,\omega}\,\delta\phi 1\,\omega\,\epsilon$$

RHS,

```
((2 c^2 g u0^2)/(g11 w^2) Csch[l[t]/w]^4 (2 (2 + Cosh[(2 l[t])/w]) l[t] - 3 w Sinh[(2 l[t])/w])) /.
  expandaraoundFP
```

$$\frac{1}{g11\,w^2}\,2\,c^2\,g\,u0^2\,\text{Csch}\left[\frac{\text{lfp} + \Delta l\,\epsilon}{w}\right]^4$$
$$\left(2\,(\text{lfp} + \Delta l\,\epsilon)\,\left(2 + \text{Cosh}\left[\frac{2\,(\text{lfp} + \Delta l\,\epsilon)}{w}\right]\right) - 3\,w\,\text{Sinh}\left[\frac{2\,(\text{lfp} + \Delta l\,\epsilon)}{w}\right]\right)$$

```
% /. fp
```

$$\frac{1}{g11\, w^2}\, 2\, c^2\, g\, u0^2\, \text{Csch}\left[\frac{\triangle l\, \epsilon}{w}\right]^4 \left(2\, \triangle l\, \epsilon \left(2 + \text{Cosh}\left[\frac{2\, \triangle l\, \epsilon}{w}\right]\right) - 3\, w\, \text{Sinh}\left[\frac{2\, \triangle l\, \epsilon}{w}\right]\right)$$

```
Series[%, {ϵ, 0, 1}]
```

$$\frac{16\, c^2\, g\, u0^2\, \triangle l\, \epsilon}{15\, g11\, w^2} + O[\epsilon]^2$$

```
Normal[16 c^2 g u0^2 △l ϵ / (15 g11 w^2) + O[ϵ]^2]
```

$$\frac{16\, c^2\, g\, u0^2\, \triangle l\, \epsilon}{15\, g11\, w^2}$$

```
% /. insertExponential
```

$$\frac{16\, c^2\, e^{i\, t\, \omega}\, g\, u0^2\, \delta l\, \epsilon}{15\, g11\, w^2}$$

We end up with,

```
i e^(i t ω) ϵ (16 i c^2 g u0^2 δl + 15 g11 w^2 δϕ1 ω) / (15 g11 w^2) == 0
```

```
θ1'[t] =
 2 F^2 g u0^2 / (g22 w^2) Csch[l[t]/w]^4 (2 (2 + Cosh[2 l[t]/w]) l[t] - 3 w Sinh[2 l[t]/w]) (* Eq three *)
```

LHS,

```
θ1'[t] → d/dt (θ1fp + ϵ δθ1 Exp[I ω t]) → d/dt (ϵ δθ1 Exp[I ω t]) → i e^(i t ω) δθ1 ω ϵ
```

RHS,

```
(2 F^2 g u0^2 / (g22 w^2) Csch[l[t]/w]^4 (2 (2 + Cosh[2 l[t]/w]) l[t] - 3 w Sinh[2 l[t]/w])) /.
 expandaraoundFP
```

$$\frac{1}{g22\, w^2}\, 2\, F^2\, g\, u0^2\, \text{Csch}\left[\frac{lfp + \triangle l\, \epsilon}{w}\right]^4 \left(2\, (lfp + \triangle l\, \epsilon) \left(2 + \text{Cosh}\left[\frac{2\, (lfp + \triangle l\, \epsilon)}{w}\right]\right) - 3\, w\, \text{Sinh}\left[\frac{2\, (lfp + \triangle l\, \epsilon)}{w}\right]\right)$$

```
% /. fp
```

$$\frac{1}{g22\, w^2}\, 2\, F^2\, g\, u0^2\, \text{Csch}\left[\frac{\triangle l\, \epsilon}{w}\right]^4 \left(2\, \triangle l\, \epsilon \left(2 + \text{Cosh}\left[\frac{2\, \triangle l\, \epsilon}{w}\right]\right) - 3\, w\, \text{Sinh}\left[\frac{2\, \triangle l\, \epsilon}{w}\right]\right)$$

```
Series[%, {ϵ, 0, 1}]
```

$$\frac{16\,F^2\,g\,u0^2\,\triangle l\,\epsilon}{15\,g22\,w^2}+O[\epsilon]^2$$

```
Normal[ 16 F^2 g u0^2 △l ϵ / (15 g22 w^2) + O[ϵ]^2 ]
```

$$\frac{16\,F^2\,g\,u0^2\,\triangle l\,\epsilon}{15\,g22\,w^2}$$

```
% /. insertExponential
```

$$\frac{16\,e^{i\,t\,\omega}\,F^2\,g\,u0^2\,\delta l\,\epsilon}{15\,g22\,w^2}$$

We end up with,

```
i e^(i t ω) ϵ (16 i F^2 g u0^2 δl + 15 g22 w^2 δθ1 ω) / (15 g22 w^2) == 0
```

Collect the Equations Above,

```
e^(i t ω) ϵ (-δθ1 + δϕ1 + i δl ω) == 0
```

```
e^(i t ω) ϵ (-16 c^2 g u0^2 / (15 g11 w^2) δl + i δϕ1 ω) == 0
```

```
e^(i t ω) ϵ (-16 F^2 g u0^2 / (15 g22 w^2) δl + i δθ1 ω) == 0
```

Form the Matrix,

$$\begin{pmatrix} -1 & 1 & i\,\omega \\ 0 & i\,\omega & -\frac{16\,c^2\,g\,u0^2}{15\,g11\,w^2} \\ i\,\omega & 0 & -\frac{16\,F^2\,g\,u0^2}{15\,g22\,w^2} \end{pmatrix} \begin{pmatrix} \delta\theta1 \\ \delta\phi1 \\ \delta l \end{pmatrix} = \begin{pmatrix} 0 \\ 0 \\ 0 \end{pmatrix}$$

```
Det[ {{-1, 1, i ω}, {0, i ω, -16 c^2 g u0^2 / (15 g11 w^2)}, {i ω, 0, -16 F^2 g u0^2 / (15 g22 w^2)}} ]
```

$$\left(240\,i\,F^2\,g\,g11\,u0^2\,w^2\,\omega-240\,i\,c^2\,g\,g22\,u0^2\,w^2\,\omega+225\,i\,g11\,g22\,w^4\,\omega^3\right)\Big/\left(225\,g11\,g22\,w^4\right)$$

```
Simplify[ (240 i F^2 g g11 u0^2 w^2 ω - 240 i c^2 g g22 u0^2 w^2 ω + 225 i g11 g22 w^4 ω^3) / (225 g11 g22 w^4) ]
```

$$\left(i\,\omega\left(16\,F^2\,g\,g11\,u0^2-16\,c^2\,g\,g22\,u0^2+15\,g11\,g22\,w^2\,\omega^2\right)\right)\Big/\left(15\,g11\,g22\,w^2\right)$$

```
Solve[% == 0, ω]
```

$$\left\{\{\omega \to 0\}, \left\{\omega \to -\frac{4\sqrt{-F^2\, g\, g11\, u0^2 + c^2\, g\, g22\, u0^2}}{\sqrt{15}\ \sqrt{g11}\ \sqrt{g22}\ w}\right\}, \left\{\omega \to \frac{4\sqrt{-F^2\, g\, g11\, u0^2 + c^2\, g\, g22\, u0^2}}{\sqrt{15}\ \sqrt{g11}\ \sqrt{g22}\ w}\right\}\right\}$$

Let's now do the calculations without using l[t], and use only b[t] and d[t]:

Use the following fixed points:

```
ϕ1fp = 0, Θ1fp = -A/(c w), bfp = 0, dfp = 0
```

And the system of ODEs are:

```
b'[t] = -ϕ1[t] (* Eq one-I *)
```

```
d'[t] = -A/(c w) - Θ1[t] (* Eq Two-II *)
```

```
ϕ1'[t] = (2 c^2 g u0^2)/(g11 w^2) (Csch[(b[t] - d[t])/w]^4 (2 (2 + Cosh[(2 (b[t] - d[t]))/w]) (b[t] - d[t]) -
    3 w Sinh[(2 (b[t] - d[t]))/w])) (* Eq Three-III *)
```

```
Θ1'[t] = (2 F^2 g u0^2)/(g22 w^2) (Csch[(b[t] - d[t])/w]^4 (2 (2 + Cosh[(2 (b[t] - d[t]))/w]) (b[t] - d[t]) -
    3 w Sinh[(2 (b[t] - d[t]))/w])) (* Eq Four-IV *)
```

```
expandfpNEW =
  {Θ1[t] → Θ1fp + ϵ ΔΘ1, ϕ1[t] → ϕ1fp + ϵ Δϕ1, b[t] → bfp + ϵ Δb, d[t] → dfp + ϵ Δd};

insertExponentialNEW =
  { ΔΘ1 → δΘ1 Exp[I ω t], Δϕ1 → δϕ1 Exp[I ω t], Δb → δb Exp[I ω t], Δd → δd Exp[I ω t]};

fp = {ϕ1fp → 0, Θ1fp → -A/(c w), bfp → 0, dfp → 0};
```

Eq one-I

```
b'[t] = -ϕ1[t]
```

LHS,

$$b'[t] \to \frac{d}{dt}(bfp + \epsilon\, \delta b\, Exp[I\, \omega\, t]) \to \frac{d}{dt}(\epsilon\, \delta b\, Exp[I\, \omega\, t]) \to i\, e^{i\, t\, \omega}\, \delta b\, \omega\, \epsilon$$

RHS,

```
(-ϕ1[t]) /. expandfpNEW
```

$$-\triangle\phi 1\,\epsilon - \phi 1fp$$

```
% /. insertExponentialNEW
```

$$-e^{i\,t\,\omega}\,\delta\phi 1\,\epsilon - \phi 1fp$$

```
Series[%, {ϵ, 0, 1}]
```

$$-\phi 1fp - e^{i\,t\,\omega}\,\delta\phi 1\,\epsilon + O[\epsilon]^2$$

```
Normal[-ϕ1fp - e^(i t ω) δϕ1 ϵ + O[ϵ]^2]
```

$$-e^{i\,t\,\omega}\,\delta\phi 1\,\epsilon - \phi 1fp$$

```
% /. fp
```

$$-e^{i\,t\,\omega}\,\delta\phi 1\,\epsilon$$

We end up with,

```
i e^(i t ω) δb ω ϵ  + e^(i t ω) δϕ1 ϵ = 0
```

```
Collect[i e^(i t ω) δb ω ϵ  + e^(i t ω) δϕ1 ϵ, ϵ e^(i t ω)]
```

$$e^{i\,t\,\omega}\,\epsilon\,(\delta\phi 1 + i\,\delta b\,\omega)$$

```
e^(i t ω) ϵ (δϕ1 + i δb ω) = 0
```

Eq Two-II

```
d'[t] = -A/(c w) - Θ1[t]
```

LHS,

```
d'[t] → d/dt (dfp + ϵ δd Exp[I ω t]) → d/dt (ϵ δd Exp[I ω t]) → i e^(i t ω) δd ω ϵ
```

RHS,

```
(-A/(c w) - Θ1[t]) /. expandfpNEW
```

$$-\frac{A}{c\,w} - \triangle\Theta 1\,\epsilon - \Theta 1fp$$

```
% /. insertExponentialNEW
```

$$-\frac{A}{c\,w} - e^{i\,t\,\omega}\,\delta\Theta 1\,\epsilon - \Theta 1fp$$

```
Series[%, {ϵ, 0, 1}]
```

$$\left(-\frac{A}{c\,w} - \Theta 1fp\right) - e^{i\,t\,\omega}\,\delta\Theta 1\,\epsilon + O[\epsilon]^2$$

```
Normal[((-A/(c w)) - θ1fp) - e^(i t ω) δθ1 ϵ + O[ϵ]^2]
```

$$-\frac{A}{c\,w} - e^{i\,t\,\omega}\,\delta\theta 1\,\epsilon - \theta 1 fp$$

```
% /. fp
```

$$-e^{i\,t\,\omega}\,\delta\theta 1\,\epsilon$$

We end up with,

```
e^(i t ω) ϵ (δθ1 + i δd ω) = 0
```

Eq Three-III

```
ϕ1'[t] = (2 c^2 g u0^2)/(g11 w^2) (Csch[(b[t] - d[t])/w]^4
    (2 (2 + Cosh[(2 (b[t] - d[t]))/w]) (b[t] - d[t]) - 3 w Sinh[(2 (b[t] - d[t]))/w]))
```

LHS,

```
ϕ1'[t] → d/dt (ϕ1fp + ϵ δϕ1 Exp[I ω t]) → d/dt (ϵ δϕ1 Exp[I ω t]) → i e^(i t ω) δϕ1 ω ϵ
```

RHS,

```
((2 c^2 g u0^2)/(g11 w^2) (Csch[(b[t] - d[t])/w]^4 (2 (2 + Cosh[(2 (b[t] - d[t]))/w]) (b[t] - d[t]) -
        3 w Sinh[(2 (b[t] - d[t]))/w]))) /. expandfpNEW
```

$$\frac{1}{g11\,w^2}\,2\,c^2\,g\,u0^2\,\text{Csch}\left[\frac{bfp - dfp + \triangle b\,\epsilon - \triangle d\,\epsilon}{w}\right]^4$$
$$\left(2\,(bfp - dfp + \triangle b\,\epsilon - \triangle d\,\epsilon)\,\left(2 + \text{Cosh}\left[\frac{2\,(bfp - dfp + \triangle b\,\epsilon - \triangle d\,\epsilon)}{w}\right]\right) -\right.$$
$$\left.3\,w\,\text{Sinh}\left[\frac{2\,(bfp - dfp + \triangle b\,\epsilon - \triangle d\,\epsilon)}{w}\right]\right)$$

```
% /. fp
```

$$\frac{1}{g11\,w^2}\,2\,c^2\,g\,u0^2\,\text{Csch}\left[\frac{\triangle b\,\epsilon - \triangle d\,\epsilon}{w}\right]^4$$
$$\left(2\,(\triangle b\,\epsilon - \triangle d\,\epsilon)\,\left(2 + \text{Cosh}\left[\frac{2\,(\triangle b\,\epsilon - \triangle d\,\epsilon)}{w}\right]\right) - 3\,w\,\text{Sinh}\left[\frac{2\,(\triangle b\,\epsilon - \triangle d\,\epsilon)}{w}\right]\right)$$

```
Series[%, {ϵ, 0, 1}]
```

$$\frac{16\,c^2\,g\,u0^2\,(\triangle b - \triangle d)\,\epsilon}{15\,g11\,w^2} + O[\epsilon]^2$$

```
Normal[16 c^2 g u0^2 (Δb - Δd) ϵ / (15 g11 w^2) + O[ϵ]^2]
```

$$\frac{16\, c^2\, g\, u0^2\, (\Delta b - \Delta d)\, \epsilon}{15\, g11\, w^2}$$

```
% /. insertExponentialNEW
```

$$\frac{16\, c^2\, g\, u0^2\, \left(e^{i\, t\, \omega}\, \delta b - e^{i\, t\, \omega}\, \delta d\right)\, \epsilon}{15\, g11\, w^2}$$

We end up with,

$$i\, e^{i\, t\, \omega}\, \delta\phi 1\, \omega\, \epsilon \;=\; \frac{16\, c^2\, g\, u0^2\, \left(e^{i\, t\, \omega}\, \delta b - e^{i\, t\, \omega}\, \delta d\right)\, \epsilon}{15\, g11\, w^2}$$

Eq Four-IV

$$\theta 1'[t] = \frac{2\, F^2\, g\, u0^2}{g22\, w^2}\left(\text{Csch}\left[\frac{b[t] - d[t]}{w}\right]^4 \left(2\left(2 + \text{Cosh}\left[\frac{2\,(b[t] - d[t])}{w}\right]\right)(b[t] - d[t]) - 3\, w\, \text{Sinh}\left[\frac{2\,(b[t] - d[t])}{w}\right]\right)\right)$$

LHS,

$$\theta 1'[t] \to \frac{d}{dt}\,(\theta 1 fp + \epsilon\, \delta\theta 1\, \text{Exp}[I\, \omega\, t]) \to \frac{d}{dt}\,(\epsilon\, \delta\theta 1\, \text{Exp}[I\, \omega\, t]) \to i\, e^{i\, t\, \omega}\, \delta\theta 1\, \omega\, \epsilon$$

RHS,

```
(2 F^2 g u0^2 / (g22 w^2) (Csch[(b[t] - d[t])/w]^4 (2 (2 + Cosh[2 (b[t] - d[t])/w]) (b[t] - d[t]) -
      3 w Sinh[2 (b[t] - d[t])/w]))) /. expandfpNEW
```

$$\frac{1}{g22\, w^2}\, 2\, F^2\, g\, u0^2\, \text{Csch}\left[\frac{bfp - dfp + \Delta b\, \epsilon - \Delta d\, \epsilon}{w}\right]^4 \left(2\,(bfp - dfp + \Delta b\, \epsilon - \Delta d\, \epsilon)\left(2 + \text{Cosh}\left[\frac{2\,(bfp - dfp + \Delta b\, \epsilon - \Delta d\, \epsilon)}{w}\right]\right) - 3\, w\, \text{Sinh}\left[\frac{2\,(bfp - dfp + \Delta b\, \epsilon - \Delta d\, \epsilon)}{w}\right]\right)$$

```
% /. fp
```

$$\frac{1}{g22\, w^2}\, 2\, F^2\, g\, u0^2\, \text{Csch}\left[\frac{\Delta b\, \epsilon - \Delta d\, \epsilon}{w}\right]^4 \left(2\,(\Delta b\, \epsilon - \Delta d\, \epsilon)\left(2 + \text{Cosh}\left[\frac{2\,(\Delta b\, \epsilon - \Delta d\, \epsilon)}{w}\right]\right) - 3\, w\, \text{Sinh}\left[\frac{2\,(\Delta b\, \epsilon - \Delta d\, \epsilon)}{w}\right]\right)$$

```
Series[%, {ϵ, 0, 1}]
```

$$\frac{16\,F^2\,g\,u0^2\,(\Delta b-\Delta d)\,\epsilon}{15\,g22\,w^2}+O[\epsilon]^2$$

```
Normal[ 16 F^2 g u0^2 (Δb - Δd) ϵ / (15 g22 w^2) + O[ϵ]^2 ]
```

$$\frac{16\,F^2\,g\,u0^2\,(\Delta b-\Delta d)\,\epsilon}{15\,g22\,w^2}$$

```
% /. insertExponentialNEW
```

$$\frac{16\,F^2\,g\,u0^2\,\left(e^{i\,t\,\omega}\,\delta b-e^{i\,t\,\omega}\,\delta d\right)\,\epsilon}{15\,g22\,w^2}$$

We end up with,

$$i\,e^{i\,t\,\omega}\,\delta\theta 1\,\omega\,\epsilon \;=\; \frac{16\,F^2\,g\,u0^2\,\left(e^{i\,t\,\omega}\,\delta b-e^{i\,t\,\omega}\,\delta d\right)\,\epsilon}{15\,g22\,w^2}$$

Collect these equations:

$$e^{i\,t\,\omega}\,\epsilon\,(\delta\phi 1+i\,\delta b\,\omega)=0$$

$$e^{i\,t\,\omega}\,\epsilon\,(\delta\theta 1+i\,\delta d\,\omega)=0$$

$$e^{i\,t\,\omega}\,\epsilon\left(-\frac{16\,c^2\,g\,u0^2}{15\,g11\,w^2}\,\delta b+\frac{16\,c^2\,g\,u0^2}{15\,g11\,w^2}\,\delta d+i\,\delta\phi 1\,\omega\right)=0$$

$$e^{i\,t\,\omega}\,\epsilon\left(-\frac{16\,F^2\,g\,u0^2}{15\,g22\,w^2}\,\delta b+\frac{16\,F^2\,g\,u0^2}{15\,g22\,w^2}\,\delta d+i\,\delta\theta 1\,\omega\right)=0$$

Matrix,

$$e^{i\,t\,\omega}\,\epsilon\begin{pmatrix} i\,\omega & 0 & 1 & 0\\ 0 & i\,\omega & 0 & 1\\ -\frac{16\,c^2\,g\,u0^2}{15\,g11\,w^2} & \frac{16\,c^2\,g\,u0^2}{15\,g11\,w^2} & i\,\omega & 0\\ -\frac{16\,F^2\,g\,u0^2}{15\,g22\,w^2} & \frac{16\,F^2\,g\,u0^2}{15\,g22\,w^2} & 0 & i\,\omega \end{pmatrix}\begin{pmatrix}\delta b\\ \delta d\\ \delta\phi 1\\ \delta\theta 1\end{pmatrix}=\begin{pmatrix}0\\0\\0\\0\end{pmatrix}$$

```
Det[ { {i ω, 0, 1, 0}, {0, i ω, 0, 1}, {-16 c^2 g u0^2/(15 g11 w^2), 16 c^2 g u0^2/(15 g11 w^2), i ω, 0}, {-16 F^2 g u0^2/(15 g22 w^2), 16 F^2 g u0^2/(15 g22 w^2), 0, i ω} } ]
```

$$\left(240\,F^2\,g\,g11\,u0^2\,w^2\,\omega^2-240\,c^2\,g\,g22\,u0^2\,w^2\,\omega^2+225\,g11\,g22\,w^4\,\omega^4\right)\Big/\left(225\,g11\,g22\,w^4\right)$$

```
Simplify[(240 F^2 g g11 u0^2 w^2 ω^2 - 240 c^2 g g22 u0^2 w^2 ω^2 + 225 g11 g22 w^4 ω^4) / (225 g11 g22 w^4)]
```

$$\frac{1}{15}\omega^2\left(-\frac{16\,c^2\,g\,u0^2}{g11\,w^2}+\frac{16\,F^2\,g\,u0^2}{g22\,w^2}+15\,\omega^2\right)$$

```
Solve[% == 0, ω]
```

$$\left\{\{\omega\to 0\},\ \{\omega\to 0\},\ \left\{\omega\to -\frac{4\sqrt{-F^2\,g\,g11\,u0^2+c^2\,g\,g22\,u0^2}}{\sqrt{15}\ \sqrt{g11}\ \sqrt{g22}\ w}\right\},\right.$$
$$\left.\left\{\omega\to \frac{4\sqrt{-F^2\,g\,g11\,u0^2+c^2\,g\,g22\,u0^2}}{\sqrt{15}\ \sqrt{g11}\ \sqrt{g22}\ w}\right\}\right\}$$

```
FullSimplify[%]
```

$$\left\{\{\omega\to 0\},\ \{\omega\to 0\},\ \left\{\omega\to -\frac{4\sqrt{g\left(-F^2\,g11+c^2\,g22\right)\,u0^2}}{\sqrt{15}\ \sqrt{g11}\ \sqrt{g22}\ w}\right\},\ \left\{\omega\to \frac{4\sqrt{g\left(-F^2\,g11+c^2\,g22\right)\,u0^2}}{\sqrt{15}\ \sqrt{g11}\ \sqrt{g22}\ w}\right\}\right\}$$